Letter of Intent
for
the Experiments on Strangeness Nuclear Physics at the 50-GeV Proton Synchrotron

JHF Strangeness Nuclear Physics Group

K. Imai

Kyoto University

T. Nagae, M. Ieiri, H. Noumi, T. Fukuda, H. Outa

KEK

K. Nakazawa

Gifu University

K. Yamamoto, T. Yoshida

Osaka City University

O. Hashimoto, H. Tamura, T. Takahashi, Y. Fujii

Tohoku University

T. Kishimoto

Osaka University

K. Tanida

University of Tokyo

B. Bassalleck

University of New Mexico

Version 1.0

July 12, 2000

Contents

1 Introduction

K. Imai
Kyoto Univeristy, Sakyo-ku, Kyoto 606-8224, Japan

The world of hadron and nuclei can be expanded by adding strangeness quantum number. Discovery of a new type or new state of nuclei has often provided us new physics. The strangeness nuclear physics is a frontier of nuclear physics with a good chance of such discovery. High intensity and high quality kaon and pion beams at 50 GeV proton synchrotron will certainly provide us such opportunities.

Strangeness nuclear physics has attracted much attention for various reasons. First of all, a hyperon can penetrate deep inside a nucleus due to the lack of Pauli exclusion. Recent spectroscopy of heavy hypernuclei clearly demonstrated the s-shell structure in nuclei as heavy as Pb, which has only been seen by a probe such as a hyperon. Recently it was experimentally verified that an addition of a Λ hyperon shrinks the size of the Li nucleus. Even a single hyperon can change the properties of nuclei which provide a new playground for nuclear physics. Some nuclei become bound by a Λ and then one can study their electromagnetic properties by γ transitions, otherwise not possible.

One can also study the properties of hyperons in nuclear matter by studying hypernuclei. Hadrons in nuclei have been a big topics in nuclear and hadronic physics recently. Hypernuclei are unique in this context. Since a hyperon such as the Λ is stable in nuclei, one can study not only the energy of various states but also the lifetime, magnetic moment and etc. The hypernuclei give a unique place to study the nucleon-hyperon weak interaction. One of the motives for studying the non-mesonic weak decay of hypernuclei is to investigate the origin of the $\Delta I = 1/2$ rule in the hyperon decays.

Since the QCD was established, models such as the quark-cluster model were proposed to describe the nuclear force based on QCD and quark structure of the nucleon. The flavor SU(3) symmetry is well established in meson and baryon spectroscopy. It is natural to extend such studies in the frame of SU(3) to refine and verify these models. The experimental studies of hyperon-nucleon and hyperon-hyperon interaction, therefore become important. We can learn about the hyperon-nucleon interaction by the scattering experiments, though very difficult, and also by the study of hypernuclei. The recent observations of "fine structure" of hypernuclei with the Hyperball have clarified the $\Lambda-N$ spin-spin and spin-orbit interactions. The binding energy of a double Λ hypernucleus is a unique source of information on the $\Lambda-\Lambda$ interaction.

It should be noted that the hyperon-nucleon interaction is essential to understand the structure of hypernuclei. It is also important for the astrophysics of neutron stars, since

there can be a considerable amount of hyperons in the core of neutron stars depending on the interactions.

After QCD was accepted, the quark degree of freedom in a nucleus has been a major topic in nuclear physics. It was speculated that the partial deconfinement of quarks in nuclear matter may be seen in hypernuclei. So far there has been no such evidence in the case of Λ hypernuclei. However, in the case of S=-2, the 6-quark H-dibaryon has not been ruled out yet, and there is still the possibility of H-nuclei being the ground state of S=-2 nuclei. One can not deny the possibility that the strange quark matter is a QCD ground state rather than nuclei. The S=-2 nuclei are the first step toward multi-strangeness systems. The experimental studies of S=-2 nuclei are, therefore, extremely important in relation to this question.

Initial program of Strangeness Nuclear Physics

Since the discovery of a hyperfragment in nuclear emulsion in 1953, the strangeness nuclear physics has a long history. However, the recent progress (within a decade) is rather outstanding, motivated by the physics described in the introduction. The followings are some examples;

1) High resolution (π^+, K^+) spectroscopy at SKS showed fine structure such as core excited states by achieving 1.5 MeV resolution.

2) Lifetime of hypernuclei was measured up to Y and is saturated at C-nuclei. The branching ratio of the weak decay was also measured up to Y. Observed n/p ratio can not be explained by current theories.

3) Bound Σ hypernuclei were established in the case of ${}^{4}_{\Sigma}$He.

4) The cross sections of Σ^+-p elastic scattering were measured in the region of 400-700 MeV/c with a scintillating fiber detector.

5) The existence of double hypernuclei was established by their cascade weak decays.

6) The γ spectroscopy of hypernuclei became possible keV resolution by the Hyperball. The fine structures due to the spin-spin and spin-orbit interaction were observed.

7) The first evidence of Ξ-nucleus was observed.

For the intial program of the 50-GeV machine, feasibility of the experiment is an important factor as well as the physics. The technology in 5 years will be advanced relative

to now. At present, however, we have to rely on the technology well within reach. We have, therefore, chosen the following initial program in order to somewhat extend the above studies and to answer the questions. We have three phyics goals in this program. One is ultimate high resolution spectroscopy of hypernuclei, namely, keV for bound state and 100keV for unbound states for a systematic study of hypernuclei. The second is to determine the hyperon-nucleon interaction by the scattering experiments. A few observables are chosen to select the interaction models effectively. The third is the systematic study of S=-2 nuclei which becomes possible thanks to the high intensity kaon beams.

1) High resolution γ spectroscopy of hypernuclei with upgraded Hyperball.

2) Spectroscopy of hypernuclei with a high resolution (200 keV) (π, K) spectrometer.

3) Cross sections for Ξ-p elastic scattering and Ξ-p $\rightarrow \Lambda\Lambda$ reaction, and polarization of Λ-p and Σ^+-p elastic scattering.

4) Extensive study of S=-2 nuclei. Spectroscopy of Ξ hypernuclei with the SKS spectrometer via (K^-, K^+) reaction, and decay pion spectroscopy of double hypernuclei with use of both emulsion and solenoidal spectrometer.

2 Spectroscopic Study of S=−2 Systems

The high intensity K^- beam at ∼1.8 GeV/c available at the 50-GeV PS is quite unique to open a new frontier of strangeness nuclear physics in the spectroscopic studies of strangeness S=−2 systems; here, the S=−2 systems include Ξ-hypernuclei, double-Λ hypernuclei, and possibly H-hypernuclei. This is not only a step forward from the S=−1 systems as a natural extension, but also a significant step to explore the multi-strangeness hadronic systems; in the course of the limit, strange hadronic matter (S=-∞) in the core of a neutron star is our concern. Also, it is important to extract some information on ΞN and Λ-Λ interactions from the spectroscopic data, considering the fact that there exist almost no experimental data on these interactions at this moment. Hence, we can explore the SU(3) character of the strong forces of QCD.

The (K^-,K^+) reaction is one of the best tools to implant the S=−2 through an elementary process $K^-+p \rightarrow K^++\Xi^-$, the cross section of which in the forward direction has a broad maximum around this energy as shown in Fig 1. The angular distribution is backward peak in the center-of-mass (c.m.) system. Since no meson of strangeness two is known to exist, there is no meson exchange (t-channel) contribution and a baryon exchange (u-channel) mechanism is dominant. However, owing to kinematics, the cross section is still peaked to forward angles in the lab. frame, which makes experimental detection efficient.

At present, the experimental information on the S=−2 systems mainly comes from several emulsion data in limited statistics and with poor identifications.

As for the Ξ-hypernuclei, there exist some hints of emulsion events for the existence. However, it is still not conclusive. Some upper limits on the Ξ-nucleus potential have been obtained from the production rate in the bound region of a Ξ-hypernucleus via the (K^-,K^+) reaction.

Only the existence of double-Λ hypernuclei is firmly known from three emulsion events, among which the recent observation in KEK E176 in 1991 has clearly confirmed it. Unfortunately, the binding energy of the double-Λhypernucleus was not determined well because of two possible interpretations for the hypernuclear species. Consequently, we still do not know whether the Λ-Λ interaction is attractive or repulsive.

A lot of searches for H-dibaryon have been carried out from the late 1980s to 1990s. No evidence has been observed so far. The observation of weak decays from the double-Λ hypernuclei limits the allowed mass range of the H-dibaryon very close to $2\times m_\Lambda$. There are suggestions that the H-particle may exist as a resonance and/or the "H"-type configuration might be mixed in the S=−2 systems.

In Fig. 2, a typical energy spectrum and decay thresholds for Ξ- and double-Λ hyper-

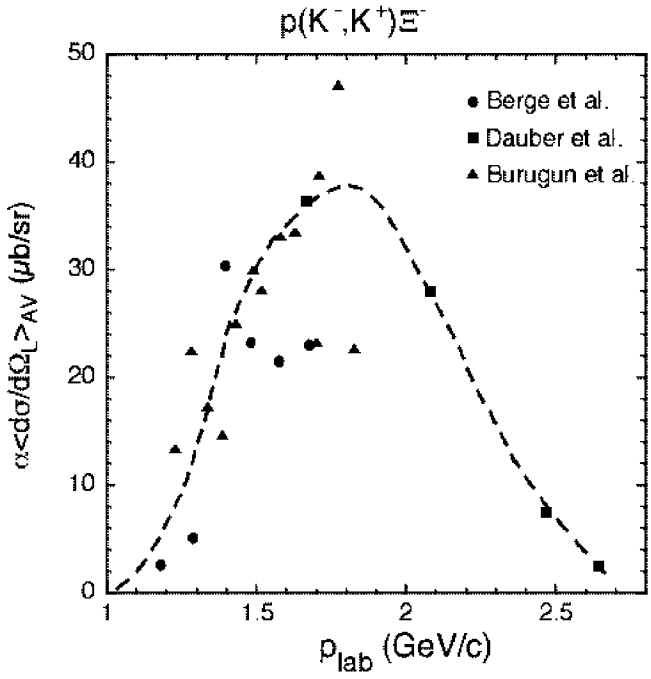

Figure 1: Incident momentum dependence of the production cross section of the K^-+p $\rightarrow$ K^++Ξ^- reaction.

nuclear configurations are shown. The energy difference between the (Ξ^-p) system and the ($\Lambda\Lambda$) system is only 28.3 MeV in free space. Therefore, a relatively large configuration mixing between Ξ^-+A and $\Lambda\Lambda$+(A-1) states is suggested. It should be noted that a mixing of the Σ component in Λ-hypernuclei is suggested to be several %, in which the energy difference between two states is $\sim$75 MeV. This mixing would be quite significant in heavy targets, because the Ξ^--hypernuclear levels are deeply bound with the aid of the large Coulomb potential. It is very interesting to investigate whether the single-particle picture of Ξ^- is valid or not in such a system.

In this letter of intent, we propose three experimental methods to explore the S=-2 systems:

1. Spectroscopy of Ξ-hypernuclei with the (K^-,K^+) reaction,
2. Study of double-Λ hypernuclei by sequential pionic decay,
3. Study of double-Λ hypernuclei by Hybrid-Emulsion Technique.

The first method investigates the entrance channel of the S=-2 world. Produced Ξ-hypernuclear states eventually decay into several forms of double-Λ systems through a strong

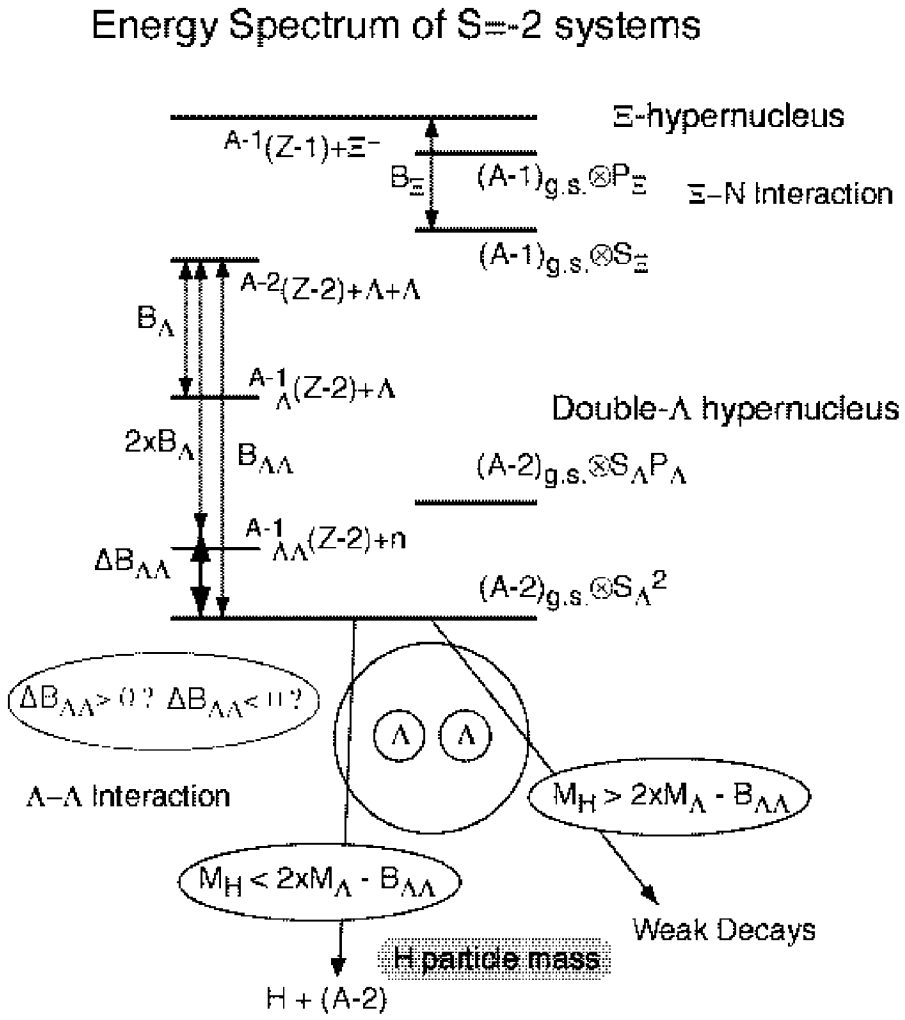

Figure 2: Typical energy spectrum and decay threshold for Ξ- and double-Λ hypernuclear configurations.

conversion process of $\Xi^- p \rightarrow \Lambda\Lambda$. The identification of the double-Λ hyper-fragment could be done by the second method if the pionic decay branch emitting a characteristic energy pion is large. This is the case for light hyper-fragments. The binding energy of the ground state of such light double-Λ hypernuclei can be measured.

The study of excited levels of double-Λ hypernuclei could be carried out via the same method as the first one, in principle, although we need further studies on the production mechanism to obtain much reliable estimation on the production rate. The measurement of the γ-ray transition of double-Λ hypernuclei is another way to investigate the excited levels. However, the energy range to be explored would be very much limited, because the population of double-Λ hypernuclei from the Ξ-hypernuclear formation in the (K^-,K^+) reaction tends to lower the neutron emission threshold close to the ground state. The study of

decay properties of double-Λ hypernuclei is another interesting subject to be investigated in the future: lifetime measurements of double-Λ hypernculei, non-mesonic weak decay modes of double-Λ hypernuclei, etc.

2.1 Spectroscopy of Ξ Hypernuclei

T. Nagae, T. Fukuda, H. Outa, H. Noumi
KEK, Tsukuba, Ibaraki 305-0801, Japan

2.1.1 Physics Interests

The Ξ-hypernuclei will play an essential role in our investigation of the S=−2 baryon-baryon interaction. Yet, at present, the existence of Ξ-hypernuclei cannot even be termed well established.

Unlike to Λ and double-Λ hypernuclear ground states which are long lived and decay via the weak interaction, Ξ-hypernuclei decay via the strong interaction through the Ξ^-p→ $\Lambda\Lambda(Q = 28.3MeV)$ conversion. In this sense, the situation is very similar to Σ-hypernuclei in which the strong conversion process ΣN→ ΛN ($Q \sim 75MeV$) exists and broaden the state. A naive semi-classical estimate of the spreading width for a Ξ^- single-particle state for an infinite nuclear matter gives us $\Gamma_\downarrow$ ∼13 MeV. However, for finite nuclei, the width would be reduced to be ≤1 MeV due to the reduction of phase space and overlap of wave functions, etc.

Therefore, it is expected that the spectroscopy of the Ξ-hypernuclei is promising. Here we use the (K^-,K^+) reaction in which we can use the same method for the (π^+,K^+) reaction in the Λ-hypernuclear spectroscopy. In fact, two reactions have a very similar characteristics of large recoil momentum of a produced hyperon: p_{Ξ^-} ∼500 MeV/c and p_Λ ∼350 MeV/c. Therefore, even for heavy targets well-separated peak structures are expected in spite of many possible excitations, because the spin-stretched configurations with $\ell_p + \ell_\Xi + J = even$ are strongly populated as in the case of the (π^+,K^+) reaction, or more strongly.

Convincing evidence for Ξ single-particle states would yield information on the Ξ single-particle potential and the effective ΞN interaction. Knowledge of the depth of the Ξ-nucleus potential is important also for estimating the existence of strange hadronic matter with Ξ's.

For the experimental targets, we propose three targets, ^{28}Si, ^{58}Ni, and ^{208}Pb, to get the information of Ξ single-particle states in a wide mass-number range.

2.1.2 Experimental Apparatus

For the spectroscopy of the (K^-,K^+) reaction, we need two spectrometers like in the (π^+,K^+) reaction: a beam line spectrometer for the incident K^- and a K^+ spectrometer.

At this moment, we propose to construct a new beam line with a good K^-/π^- ratio of ≥1 and a good momentum resolution of $\sim 5\times10^{-4}$(FWHM). As for the K^-/π^- ratio, the 2-GeV/c beam line at BNL-AGS is an excellent example. This is essential to handle such

a high intensity beam of 1×10^7/s. The momentum resolution in the beam line, however, is too poor to enable us to perform spectroscopic studies. The good momentum resolution better than 1×10^{-3} has been already achieved at the K6 beam line of the KEK 12-GeV PS. The last part of the beam line, after the mass separation, consists of a QQDQQ system to reconstruct the incident momentum. Thus, we need a combination of the two beam lines for the new K^- beam line.

K^- beam line

A 2-GeV/c kaon beam line for the JHF was designed by J. Doornbos [1]. In the design, he considered,

1) a good K/π separation,

2) a good resolution, and

3) a matching to a high-resolution pion line.

A schematic layout of the beam line is shown in Fig. 3.

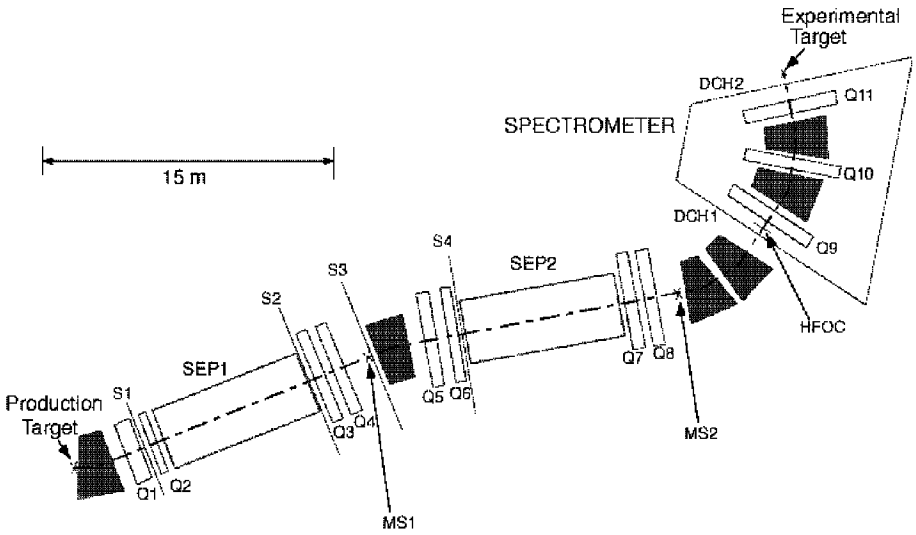

Figure 3: Schematic layout of the 2-GeV/c kaon beam line designed by J. Doornbos.

As for the K/π separation, two stage separator system is installed to attain K/π=2$\sim$5. The first stage acts like a preliminary clean up stage and defines a precise source for the second stage. In this way, the contamination due to cloud pions from neutral kaon decay near the production target and the contamination due to muons from pion decay in the channel can be reduced one order of magnitude. Contamination from pions directly produced in

the production target can be reduced by using multipoles to correct the aberrations which otherwise would cause long tails on the vertical pion distributions at the mass slits.

A beam line spectrometer is installed in the last part of the beam line. It consists of a QDQDQ system. Point to point focusing between DCH1 and DCH2 has the advantage that in the first order the momentum resolution becomes independent of multiple scattering in the DCH1. The momentum dispersion between DCH1 and DCH2 is 2.04 cm/%(Δp/p) and the magnification is 0.673. It is estimated that the momentum resolution of 2×10^{-4} could be achievable.

The first separation stage of the 2-GeV/c beam line could be shared by a high-resolution pion beam line proposed for the high-resolution (π^+,K^+) spectroscopy. For that purpose, a bending magnet is installed just after the first mass slit, where the kaon beam is bent to one side and the pion beam to the other side.

In this design, the beam line has an angle and momentum acceptance of 4.6 msr·% and is 42 m long. Compared to the D-line at BNL-AGS, it is about 10 m longer. The longer separators of 6 m versus 4.5 m give an extra length 3 m. The requirement that the first separation stage will be shared with a 1.2 GeV/c pion beam adds a further 2 m. Lastly, the beam line spectrometer lengthens the beam line by 5 m.

Table 1: Characteristics of the bending magnets

Bending Magnets	Field (kG)	Length (m)	Bending Radius (m)	Bending Angle (deg.)	Polegap (cm)
B1	19.4	1.35	3.44	22.5	10.16
B2	9.7	1.35	6.88	11.25	10.16
B3	19.4	1.35	3.44	22.5	10.16
B4	19.4	1.35	3.44	22.5	10.16
B5	19.4	1.35	3.44	22.5	10.16
B6	19.4	1.35	3.44	22.5	10.16

Separators:
The two separators are each 6 m long and have a vertical gap of 10 cm. The field over the gap is 750 kV. The useful horizontal aperture for the beam is 30 cm. The separators have no magnetic field but are preceded and followed by 20 cm long correction magnets with a vertical gap of 10 cm and a useful horizontal aperture for the beam of 30 cm. The field is 3.86 kG.

Table 2: Characteristics of the Quadrupole and Sextupole magnets

Quadrupole Magnets	Pole Field (kG)	Length (m)	Pole Radius (cm)
Q1	9.87	0.75	12.70
Q2	-12.0	0.50	12.70
Q3	-6.64	0.5384	15.24
Q4	4.16	0.5384	15.24
Q5	6.36	0.5384	15.24
Q6	-8.93	0.5384	15.24
Q7	-9.30	0.5384	15.24
Q8	8.78	0.5384	15.24
Q9	-7.53	0.60	15.24
Q10	8.62	0.60	15.24
Q11	-7.53	0.60	15.24

Sextupole Magnets	Pole Field (kG)	Length (m)	Pole Radius (cm)
S1	0.75	0.20	12.70
S2	-3.40	0.20	15.24
S3	1.50	0.20	15.24
S4	-0.60	0.20	15.24
S5	-0.25	0.60	15.24

K^+ spectrometer

For the K^+ spectrometer, we will use the existing SKS spectrometer with some modifications. In the (K^-,K^+) reaction, the K^+ momentum corresponding to the production of Ξ-hypernuclei is around 1.2 GeV/c. In the (π^+,K^+) reaction, the SKS magnetic field is 2.2 T for 0.72 GeV/c. Therefore, the SKS maximum magnetic field of $\sim$2.7 T does not allow us to put the central ray at 1.2 GeV/c. In Fig. 4, the setup of the SKS spectrometer for the (K^-,K^+) reaction is shown schematically.

Since the radius for the central momentum is larger than that for the (π^+,K^+) reaction, the target point is moved away from the magnet. So that, the acceptance of the spectrometer is reduced to be $\sim$50 msr.

The optical property and the acceptance could be improved by installing a small dipole magnet and/or a quadrupole magnet at the entrance of the SKS magnet. The design study is still underway.

The energy resolution for the Ξ-hypernuclear spectroscopy in the (K^-,K^+) reaction is

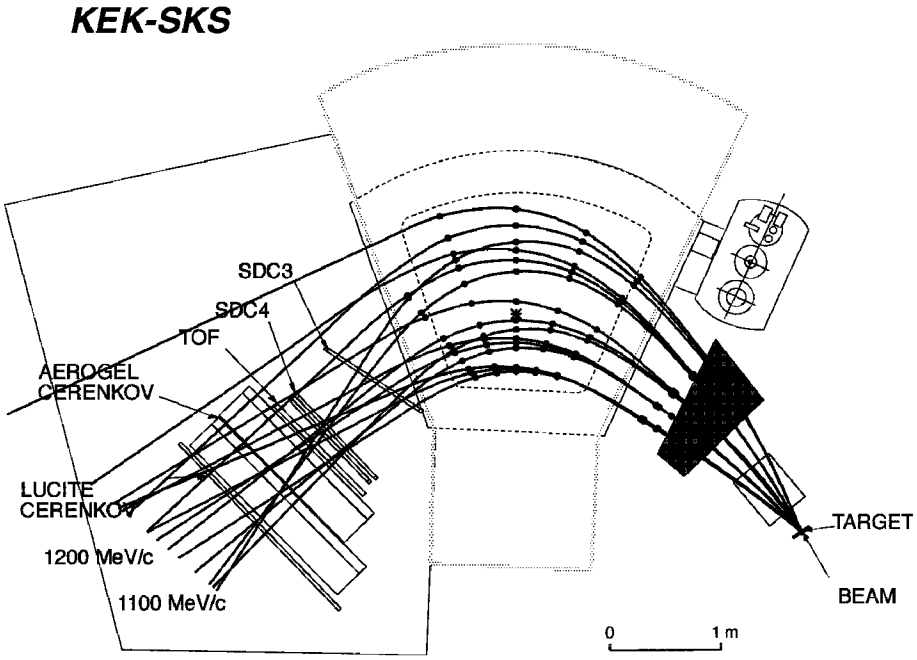

Figure 4: Schematic layout of the SKS spectrometer for the (K^-,K^+) reaction at 1.65 GeV/c.

estimated as follows;

$$\Delta E^2 = \beta_{K+}^2 \times \Delta {p_{K+}}^2 + \beta_{K-}^2 \times \Delta {p_{K-}}^2 + \Delta E_{straggling}^2,$$

where Δp's are momentum errors of two spectrometers, and the last term comes from the energy loss straggling in a target. In contrast to the (π^+,K^+) reaction, the difference of the mean energy losses between incident and out-going particles is negligible. For a 2 g/cm^2 target, $\Delta E_{straggling}$ ~0.5 MeV. The Δp/p of the beam line spectrometer is designed to be 2×10^{-4}. Thus, the second term is (0.31 MeV)^2. The momentum resolution of the SKS is know to be expressed as,

$$\frac{\Delta p}{p} = (0.96 \pm 0.13) \times 10^{-4} p_K + (0.092 \pm 0.007)(\%).$$

Assuming that the first term mainly determined by the optical property is same and the second term by the multiple scattering is proportional to 1/pβ, Δp/p for p_{K+}=1.2 GeV/c is 0.17%. Therefore, the overall energy resolution would be ΔE=$\sqrt{1.89^2 + 0.31^2 + 0.5^2}$= 2 MeV(FWHM).

2.1.3 Yield estimation

The production cross section of the Ξ-hypernuclei in the (K^-,K^+) reaction is calculated by Akaishi *et al.* [2] within the framework of the distorted-wave impulse approximation (DWIA) using the Green's function method. At present, we have very little information on the shape and the depth of Ξ^--nucleus potential. In the calculation, two types of the Ξ^--nucleus potential are used. One is Woods-Saxon type,

$$U_{\Xi^-}^{WS} = \frac{V_0 + iW_0}{1 + \exp\{(r-R)/a\}},$$

with V_0=-24 or 16 MeV, W_0=-1 MeV, R=1.1×$A^{1/3}$ fm and a=0.65 fm. The other one is the folding-type potential. As the effective ΞN potential, Shinmura's potential [3] equivalent to the Nijmegen model-D interaction is used. The result is shown in Fig. 5. As seen from the figure, we can expect the cross section to be ∼0.1 μb/sr/MeV around the middle of the bound region for all types of potentials calculated.

Then, the expected yield for the ^{208}Pb target with 2-g/cm^2 thickness could be calculated as follows;

$$\begin{aligned} Y &= I_{Beam} \times 2g/cm^2/208g \times N_A \times \frac{d\sigma}{d\Omega} \times \Delta\Omega \times f_{decay} \times f_{eff} \\ &= 10^7 \times (2/208) \times 6.02 \times 10^{23} \times 0.1 \times 10^{-30} \times 0.05 \times 0.5 \times 0.5 \; events/sec \\ &\simeq 6 \; events/day, \end{aligned}$$

where $\Delta\Omega$ is the spectrometer acceptance, f_{decay} is the survival rate for K^+ decay-in-flight, and f_{eff} is the overall detector efficiency. So, even for the heaviest case, we could get enough statistics within ∼20 days to obtain spectroscopic information. Several peak positions for Ξ-orbitals with high angular momenta would be measured within the precision of ≤1 MeV, so that we can accurately determine the potential depth of the Ξ^--nucleus potential. For lighter targets such as ^{28}Si and ^{58}Ni, the yields are several times higher with the normalized target thickness of 2 g/cm^2.

Production of Double-Λ hypernuclei with the (K^-,K^+) reaction

Production of double-Λ hypernuclei is possible directly through a second order process; $K^-p \rightarrow (\pi,\rho,\omega)\Lambda, (\pi,\rho,\omega)p \rightarrow K^+\Lambda$ and $K^-p \rightarrow K^+\Xi^-$, $\Xi^-p \rightarrow \Lambda\Lambda$. However, a theoretical estimation [4] suggests the cross section to discrete double-Λ hypernuclear states would be rather small, of the order of a few nb/sr. It is ∼1/100 of that for the Ξ-hypernuclear production. Thus, with a 2 g/cm^2 target of mass number ∼20, the production yield of ∼60 events/peak is expected for 100 days. This method has a unique advantage to allow us direct access to the spectroscopic information of excited states of double-Λ hypernuclei.

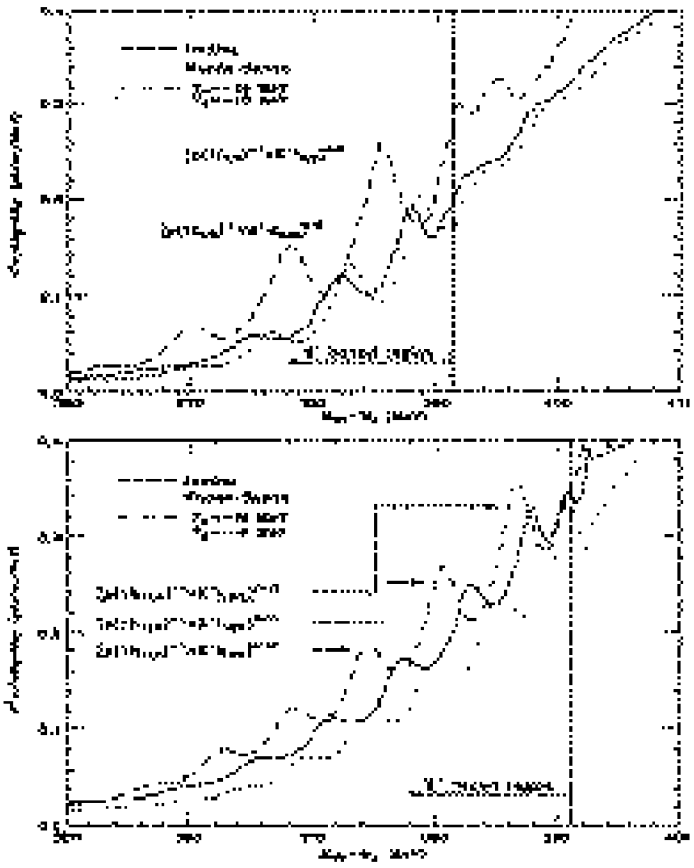

Figure 5: The Ξ^--hypernuclear spectra for the ^{58}Ni(K^-,K^+) and ^{208}Pb(K^-,K^+) reactions for p_{K^-}=1.65 GeV/c and θ_{K^+}=0° as a function of M_{HY}-M_A. The Ξ binding threshold is denoted by the vertical line. Spectrometer resolution is taken to be 2 MeV (FWHM).

2.2 Study of ΛΛ Hypernuclei by Sequential Pionic Decays

T. Fukuda, T. Nagae, H. Outa
KEK, Tsukuba, Ibaraki 305-0801, Japan
K. Imai
Kyoto Univeristy, Sakyo-ku, Kyoto 606-8224, Japan

Studies of double-Λ hypernuclei have attracted much interest, especially in connection with the existence of a predicted stable dibaryon, H , and the so far unsuccessful searches of H are certainly telling us something about quark systems in the non-perturbative regime. But the study of double-Λ hypernuclei also provides hitherto unavailable information concerning the Λ-Λ force, which is important in order to understand the baryon-baryon interaction in a unified way, and in particular its application to multi-strange systems, such as "strange matter ". At nuclear densities only twice or three times that of normal nuclear matter, it is theoretically predicted that systems of multiple strangeness will appear. If true, this means that the inner part of the neutron stars would be composed of nucleons, hyperons, and leptons. Also of obvious related interest, is the strangeness content of the quark-gluon plasma. Thus it is important to determine the equation of state of strange nuclear matter, and for this one needs effective hyperon-nucleon and hyperon-hyperon potentials. This can best be done by validating baryon-baryon potential models by studying S=-1 and -2 hypernuclei.

2.2.1 Introduction

Experimental studies on double-Λ hypernuclei are limited. In the 1960s two double-Λ hypernuclei were reportedly observed, showing sequential decay topologies in nuclear emulsion ($^{10}_{\Lambda\Lambda}$Be [5] and $^{6}_{\Lambda\Lambda}$He [6]). However the event in Ref. [6] is not convincing [7]. Recently a new observation was made by the KEK-E176 experiment using the emulsion-counter hybrid detector system [8], where Ξ^--particles were captured in emulsion with higher statistics than previously. The interpretation of this event is not unique, however; i.e. either $^{10}_{\Lambda\Lambda}$Be or $^{13}_{\Lambda\Lambda}$B, and accordingly the extracted Λ-Λ interaction energy is either -4.9 ± 0.7 MeV (repulsive Λ-Λ interaction) or $+4.9 \pm 0.7$ MeV (attractive Λ-Λ interaction). Currently a new experiment (E373) using the emulsion-counter hybrid detector system [9], which aims to increase statistics by one order of magnitude over that of E176, is under way.

Another new method to study double-Λ hypernuclei with much more statistics was proposed and accepted at BNL-AGS as E906 [10], and in 1998 the physics run was carried out. Preliminary analysis showed that we actually created and identified a few tens of $^{4}_{\Lambda\Lambda}$H by observing sequentially decaying two pions. Based on the result, we are going to propose an extensive study of the double-Λ hypernuclei by this technique.

2.2.2 Experimental principle

Several mechanisms have been tried in attempts to produce double-Λ hypernuclei (Fig. 6). In the simplest scenario, the double-Λ hypernuclei could be produced by stopping Ξ^- and allowing these hyperons to interact with the target nuclei. The Ξ can be made via a quasi-free process through the (K^-, K^+) reaction, and then brought to rest by ionization loss as they move through the production target. When essentially at rest a Ξ^- atom is formed, and the Ξ^- eventually absorbed by the nucleus, such that $\Xi^- p \rightarrow \Lambda\Lambda$, i.e. the Ξ^- and a proton in the nucleus are converted into two Λ's by the strong interaction. Then the double-Λ compound state is formed with a "sticking" probability of more than $\sim$10% [11]. It is also expected that the Ξ^- produced in the quasi-free process may be trapped in the same nucleus by the secondary reaction and, with some probability, two units of strangeness (eventually two Λ's) will be trapped in the same nucleus, albeit after emission of one or more nucleons, and form a double-Λ compound state. In any case, the compound state will subsequently decay into various hyperfragments containing one or two hyperons per fragment. Examples of such decays are ${}^{6}_{\Lambda\Lambda}\mathrm{He}$ and ${}^{4}_{\Lambda\Lambda}\mathrm{H}$, and they can be identified by detecting characteristic mesonic-decay pions, in analogy to conventional $\beta - \gamma$ spectroscopy.

The ${}^{4}_{\Lambda\Lambda}\mathrm{H}$ case serves as an example. Formation of the ${}^{4}_{\Lambda\Lambda}\mathrm{H}$ hypernucleus can be identified by observing two characteristic pions from the successive pion decays (${}^{4}_{\Lambda\Lambda}\mathrm{H} \rightarrow {}^{4}_{\Lambda}\mathrm{He} + \pi^-$ and ${}^{4}_{\Lambda}\mathrm{He} \rightarrow {}^{3}\mathrm{He} + \mathrm{p} + \pi^-$). In addition to this decay mode, ${}^{4}_{\Lambda\Lambda}\mathrm{H}$ will also decay to ${}^{3}_{\Lambda}\mathrm{H} + \mathrm{p} + \pi^-$ and then ${}^{3}_{\Lambda}\mathrm{H} \rightarrow {}^{3}\mathrm{He} + \pi^-$. The momentum of the π^-'s for the two-body decay mode will be monochromatic and that for three-body decay mode is also expected to be sufficiently narrow [12, 13]. From the momentum spectrum of pions in coincidence with pions of momentum $\sim$97 MeV/c (${}^{4}_{\Lambda}\mathrm{He} \rightarrow {}^{3}\mathrm{He} + \mathrm{p} + \pi^-$), we can determine the mass of ${}^{4}_{\Lambda\Lambda}\mathrm{H}$. For the other decay mode, we can determine the mass of ${}^{4}_{\Lambda\Lambda}\mathrm{H}$ by measuring the momentum of pions in coincidence with pions of momentum 114.3 MeV/c (${}^{3}_{\Lambda}\mathrm{H} \rightarrow {}^{3}\mathrm{He} + \pi^-$). Note that the branching ratios of pion decay rates $\Gamma_{\pi^-}/\Gamma_{\mathrm{tot}}$ are known or expected to be large enough ; ~ 0.25 to ~ 0.52 for the present case[12, 13].

In E906 decay pions were detected in the Cylindrical Detector System CDS, which surrounds the target region (Fig. 7). The momentum resolution and the solid angle of the CDS were about 7 MeV/c FWHM for 100 MeV/c pions, and 65% of 4π, respectively. We chose ${}^{9}\mathrm{Be}$ as the target to avoid the complexity because the double-Λ compound nucleus has $Z \leq 3$ and the possible species for the final hyperfragments are limited. We used a Be target sufficiently long in the beam direction so that there is a good chance for a quasi-free Ξ^- emitted in the forward direction to stop in the target material. According to a Monte Carlo simulation, we estimated about 4% of the Ξ^-'s will stop.

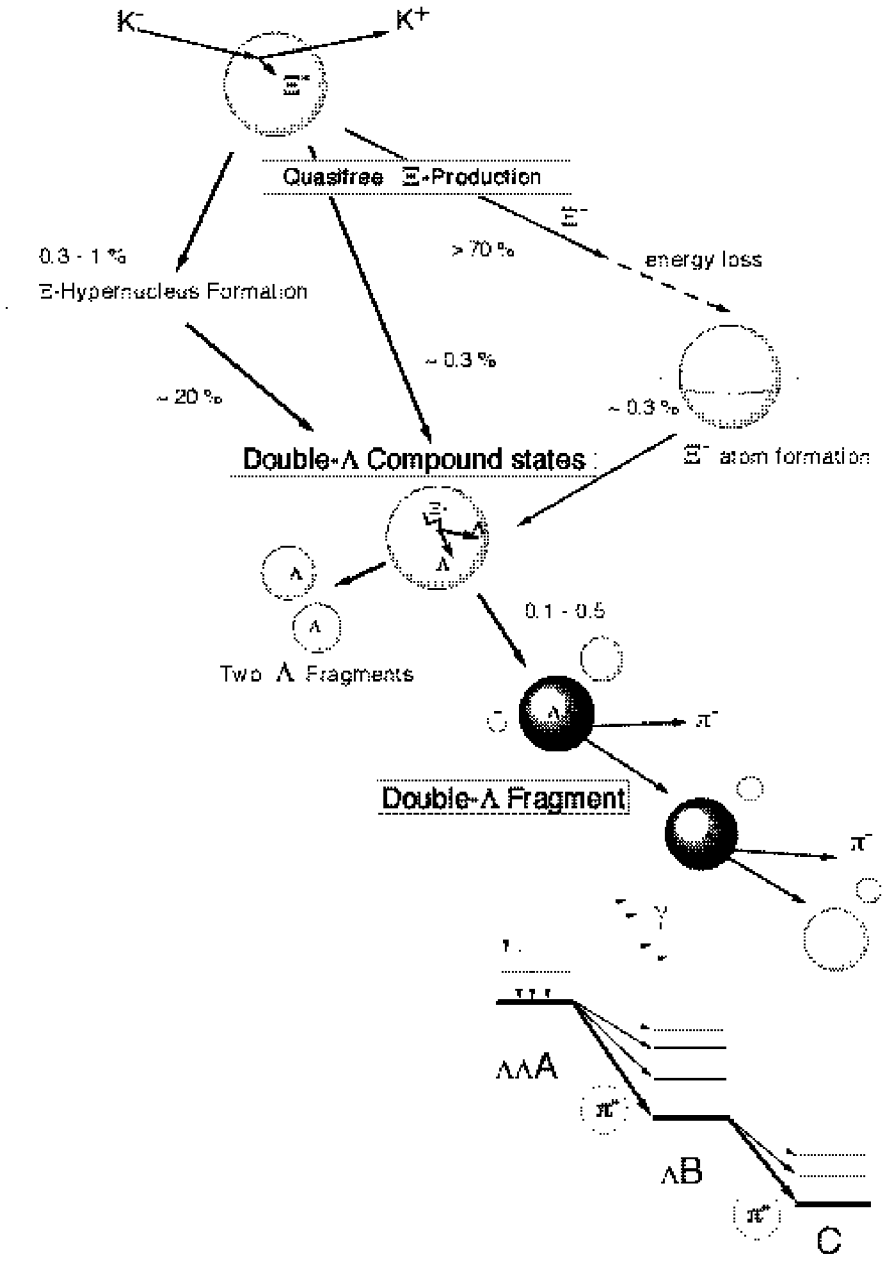

Figure 6: A possible scenario to produce and detect double-Λ hypernuclei in the (K^-, K^+) reaction.

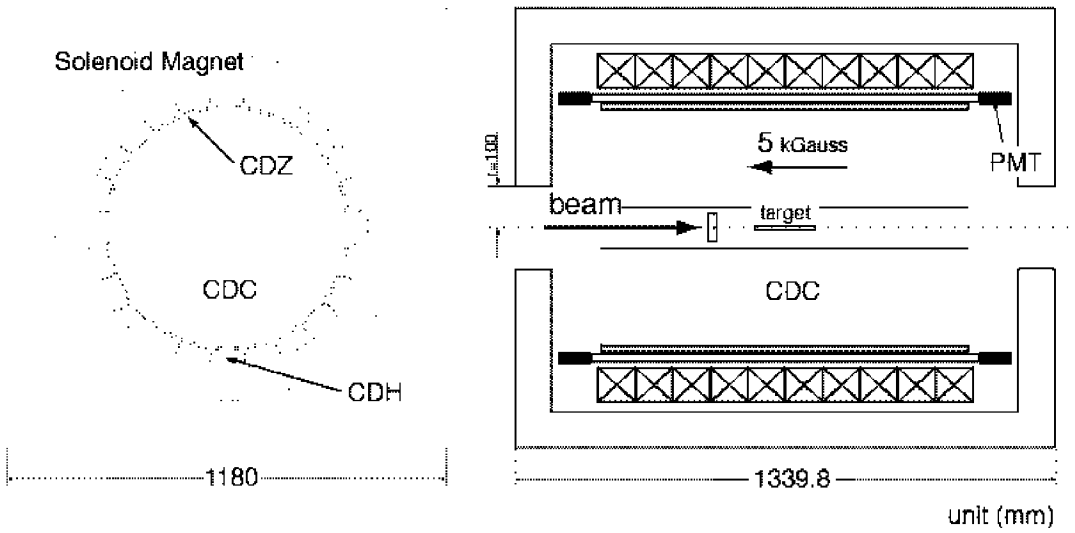

Figure 7: A schematic drawing of the Cylindrical Detector System (CDS).

The apparatus was installed at the 2 GeV/c K^- beam line(D6) at the AGS. This line typically delivers $(1-2)\times 10^6$ K^- /spill and a K/π ratio of about 0.72 at the momentum of 1.8 GeV/c with the usual beam-sharing conditions prevailing in fixed-target operation. The beam line and spectrometer drift chambers, particle ID detectors, and the trigger scintillators were used to identify (K^-, K^+) reaction.

The CDS is constructed of four main components; the cylindrical drift chamber, DC, a z-chamber, a timing hodoscope, and a solenoidal magnet. A ^{9}Be, 16 cm in beam length, 5 cm wide, and 1.27 cm high, was centered within the CDS. The size of the DC is 298mm in radius and 920mm long. It consists of twelve readout layers; six axial and six stereo. The total number of cells is 576. In order to reduce the effect of multiple scattering as much as possible, low Z materials are selected for use inside the chamber. We employ 80 μm Al for the field wires, 20 μm W for the sense wires and a 50-50 mixture of helium and ethane as the chamber gas. A z-chamber is placed outside the DC in order to get better vertex definition along the beam direction. An outer concentric hodoscope was used for timing and the trigger. As the hodoscope is inside the magnetic field, we employ a fine-mesh photomultiplier (Hamamatsu H6614) which is largely insensitive to this magnetic field. The size of the solenoid magnet is 1180 mm wide, 1180 mm high and 1280 mm long, and has a maximum field of 5 kGauss. The magnetic field has been checked with a NMR probe and the homogeneity of the field is within 0.5% for the entire DC volume.

2.2.3 Proposed experiments

Based on the result of E906, we are going to propose a study of the double-Λ hypernuclei by means of decay-pion spectroscopy. In E906, with a possible extension, we will identify

hundreds of ${}^{4}_{\Lambda\Lambda}$H by using a ^{9}Be target and a total number of K beam of $(2-3)\times10^{12}$ K^{-} ,and will determine the mass within 0.5 MeV accuracy. The reason why ${}^{4}_{\Lambda\Lambda}$H can be produced so copiously is now under investivation, but one naive consideration is that the Q-value of $\Xi + {}^{9}$ Be $\rightarrow {}^{4}_{\Lambda\Lambda}$ H + ^{6} He channel is small, resulting in a large overlap between the final and initial states. At the 50-GeV PS, we expect ∼10 times more K beams than AGS and therefore we will be able to identify several weaker channels than ${}^{4}_{\Lambda\Lambda}$H case, e.g. ${}^{6}_{\Lambda\Lambda}$He. Another interesting possibility is that the Ξ-hypernuclei produced in the (K^{-}, K^{+}) reaction on ^{7}Li will decay to ${}^{5}_{\Lambda\Lambda}$H with a large branching ratio of about 90% [14] (Fig. 8). When we

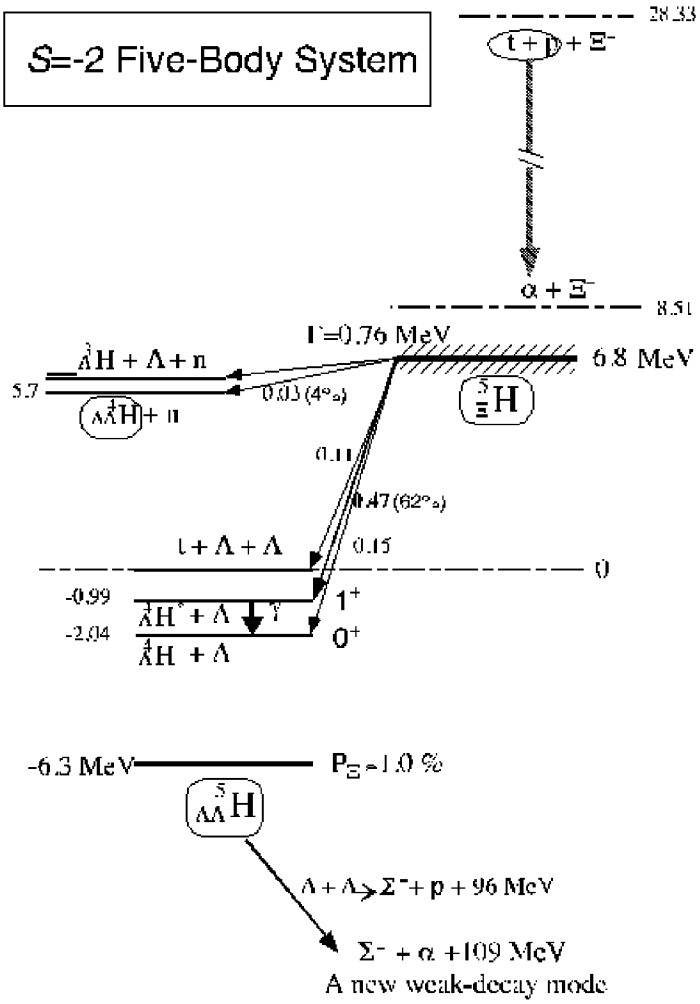

Figure 8: The energy levels of the S=−2 five-body system.

use heavier targets like ^{12}C, we can expect heavier double-Λ hypernuclei like ${}^{10}_{\Lambda\Lambda}$Be , which have relatively small Q-values for two- or three-body final states. Note that the many-body

final states have a small phase space, resulting in a small production rate.

From the systematic study of the ground state mass of double-Λ hypernuclei, we will be able to deduce the Λ-Λ interaction with less ambiguity on the nuclear structure problem. Moreover we can expect that a H-like structure, if any, will manifest itself in the structure of double-Λ hypernuclei. Another interesting subject is the weak decay of the double-Λ hypernuclei; what is the total decay rate ? What kind of the nonmesonic decay mode is available and what is the partial decay rate ? Are they affected by the co-existence of the H-like structure ? etc.

The detector to measure two pions will be an upgraded CDS, which can be a bit larger than the present one for a better momentum resolution and a better tracking capability. We will also install a vertex detector near the target (just above and below) to enable us to provide a much better vertex resolution in the target region. The overall momentum resolution will be better than 3 MeV/c for 100 MeV/c pions. The beam line system and the K^+ spectrometer will be the standard one for K1.8 beam line at the Joint Project.

2.3 Study of Double Strangeness Nuclei by an Emulsion-Counter Hybrid Method

K. Nakazawa

Gifu University, Japan

K. Imai

Kyoto Univeristy, Sakyo-ku, Kyoto 606-8224, Japan

K. Yamamoto and T. Yoshida

Osaka City University, Sumiyoshi-ku, Osaka 558-8585, Japan

2.3.1 Introduction

The primary purpose of the proposed experiment is to find double strangeness nuclei as many as possible and to determine their binding energies in nearly 100 samples. The first evidence of a double strangeness nucleus in the emulsion following Ξ^- capture at rest was reported thirty years ago[15]. At KEK, we carried out an emulsion-counter hybrid experiment (E176) to observe double strangeness nuclei and/or H-dibaryon. The hybrid method can greatly improve statistics and reliability than old emulsion experiments.

The recent E373 experiment at KEK started to solve the question about the $\Lambda\Lambda$ interaction given by the E176, confirm the findings of the E176 with better accuracy and provide new discoveries about double strangeness nuclei[16]. In the E373, the quasi-free 'p'(K^-, K^+)Ξ^- reaction occured in a diamond (^{12}C) target located upstream of the emulsion. Some of the Ξ^-s were stopped in the emulsion stack. The high precision tracking detector, micro fiber bundle tracker[17], is placed between the target and the emuslion to guide the Ξ^- tracks into the top emulsion plate. Since the ionization of the Ξ^-s with the momentum of $\sim$ 0.5 GeV/c is several times large camparing minimum ionizing particles, the scanning of the Ξ^- tracks is so easier and faster than K^+ track following done in the E176. The computer aided scanning system was developed and working well for Ξ^- track following. To detect the decay of the H particle and measure the energies of the doughter π^-s from sequential weak decay of double strangeness nuclei, large volume blocks of scintillating fibers were settled up- and downstream of the emulsion stack. Our main purpose of the E373 is to obtain 10^3 stopping Ξ^- events which is ten times larger number than that presented by the E176. The beam exposure is not finished, yet, but an event showing the decay topology of the twin single-Λ hypernucleus was already found in the analysis of 3 % data. The scanning and the analysis are going on.

In the proposed experiment, we will use almost pure K^- beam of 2 GeV/c K-beam line. The (K^-, K^+) reaction, K^-+'p'$\rightarrow K^+ + \Xi^-$, from a carbon target is detected with the

KURAMA spectrometer system. The target and the emulsion system is almost same as the E373. A new high position resolution detector, double-sided Si strip detector(DSSD), is placed between the target and the emulsion stack and tags the Ξ^- produced in the target and stopped in the emulsion. To condense events associated stopping Ξ^- in the emulsion, an additional DSSD is set just downstream of the emulsion. Scintillating fiber blocks which surround the emulsion is used to detect π^- from the hyperfragments and other particles. These detectors will reduce the amount of emulsion scanning and enable to analyze ten times more events than the E373 within a few years. The (K^-, K^+) reaction from the scintillating fiber block is also measured. The scintillating fiber detector worked quite successfully at the particle rate of $10^5 Hz$ in the KEK-E224. This proposal is based on the experience of KEK-E176, E224, E373 and BNL-E813, E885.

2.3.2 Physics

The proposed experiment expects to obtain 10^4 stopping Ξ^- events in the emulsion. From the E176, the probability of observing the weak decay of double strangeness nuclei is about 10% of all the stopping events[18]. If the mesonic decay branch is 10%, we can expect about 100 double strangeness nuclei to be identified. The $\Lambda\Lambda$ interaction energy should be confirmed in several nuclide, unambiguously. The more tight lower bound for the H-dibaryon mass may be given by observing other species (lighter mass) of double strangeness nuclei.

If we can expect 100 double strangeness nuclei to be identified, we could, at first, draw a nuclear chart for double strangeness on several nuclide. By obtaining 100 events, rare decay events such as $\Lambda\Lambda \to \Lambda N$ or ΣN are possibly observed and we could obtain the first information about the $\Lambda\Lambda$ weak interaction. These events also say something about the hyperon mixing based on the coupling of $\Lambda\Lambda - \Xi N - \Sigma\Sigma$ and the H.

As for the H-dibaryon study, the proposed experiment has a special sensitivity in the same range of lifetime by one order of magnitude as compared to the E373. Even if the H decays in the emulsion, we will trace back its daughter tracks into the emulsion guided by their hits on double-sided Si strip detectors. It is still important to confirm the H-dibaryon by observing its decay, if the E373 finds a positive evidence.

By observing one hundred times more events than the E176, we can study Ξ^- atomic and Ξ^- nuclear states more reliably. Following the Ξ^- nuclear capture, the Λ hyperon can be emitted. In the proposed experiment, the emulsion is surrounded by the scintillating fiber detectors. Therefore, the Λ hyperon can be detected by observing $\Lambda \to p + \pi^-$ decay in the scintillating fiber detectors. The sticking probability of strangeness to nuclei following the Ξ^- capture can be thus obtained. By using both the emulsion, double-sided Si strip detectors and the scintillating fiber detectors, the reaction mechanism following the Ξ^- atomic capture

can be extensively studied for the first time.

2.3.3 Experimental Method

We proposed an emulsion-counter hybrid method to detect double strangeness nuclei produced from Ξ^- stopping points in the emulsion. The double strangeness nuclei are identified by the characteristic cascade weak decay. Short tracks of hyperfragments and their decay vertices are extensively studied in the emulsion together with other decay particles. The emulsion is surrounded by scintillating fiber detectors which detect long tracks like π^- from hyperfragments.

The quasi-free reaction, $K^-+p \rightarrow K^++\Xi^-$, from a diamond target is detected with use of the KURAMA spectrometer system in KEK. Some of the Ξ^- s from the target are stopped in the emulsion stack placed downstream of the target. A high precision position detector, double-sided Si strip detector, placed between the target and the emulsion is used to identify the tracks of the Ξ^- in the emulsion. We will set an additinal double-sided Si strip detector to recognize that the Ξ^- doesn't go through out the emulsion, measure the energy of charged particles escaping from the emulsion and, if possible, locate some vertices in the emulsion by tracing back the tagged K^+ or other tracks. In the emulsion, the Ξ^- track is followed down to its stopping point, and the vertices of the stopping Ξ^- events are studied in detail under a microscope to find out double strangeness nuclei.

The emulsion is very expensive (1 $M\ Yen$ for 1 $liter$ including the fee for development) and the analysis is time and man-power consuming job. The proposed experiment is designed to save the amount of the emulsion and to make the analysis easier.

Setup of the experiment

The 1.8 GeV/c K^- beam is used for this experiment. We need only $1 \times 10^5 K^-/spill$ as an beam intensity but require a pure K^- beam with the K^-/π^- ratio of about 10. A schematic drawing of the experimental setup is shown in Fig. 9. The apparatus near the emulsion are also shown in Fig.10. The time-of-flight counters (T1 - T2) and an aerogel Cherenkov counter (BAC; n=1.03) are used to identify the K^- particles. A heavy metal slit is used to obtain a small sized beam ($5 \times 5\ mm^2$) at the target. For position callibartion between a double-sided Si strip detector and the emulsion, we will use tiny spot beam less than $1mm$ in diameter. A diamond target of $1.2cm$ in diameter and $3cm$ in length is placed upstream of the emulsion stack. It is used as the Ξ^- production target and as an energy degrader for the Ξ^-. A tracker for the Ξ^- is a double-sided Si strip detector (DSSD). It is placed between the target and the emulsion stack to measure the angle and position of the Ξ^- with

high precision instead of a fiber-bundle tracking detector which is employed in the E373.

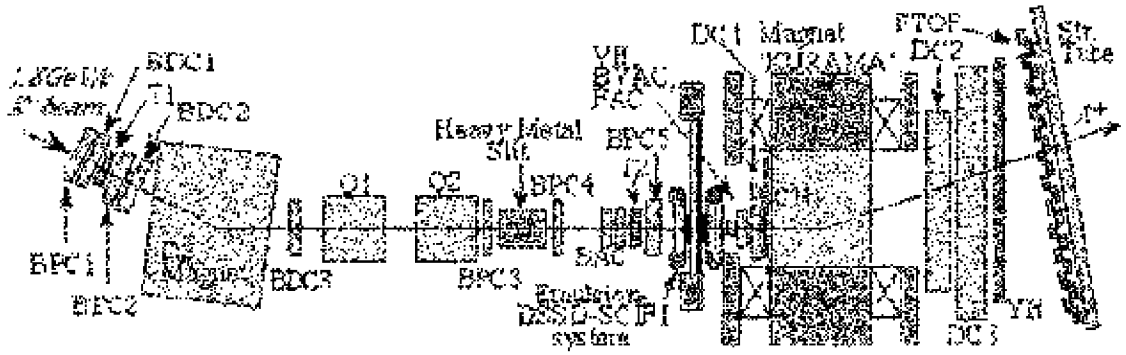

Figure 9: The The setup of the present experiment.

The scattered K^+ particles are detected with the KURAMA K^+ spectrometer system which consists of a magnet (KURAMA), time-of-flight counters (FTOF-T2), aerogel Cherenkov counters (BVAC, FAC), drift chambers (DC1-3) and trigger counters. The scintillating fiber detectors (SCIFI) are placed up- and downstream of the emulsion stack primarily to measure the energy of π^- from the hypernuclei, and also to search for the H-dibaryon and to detect Λ hyperons.

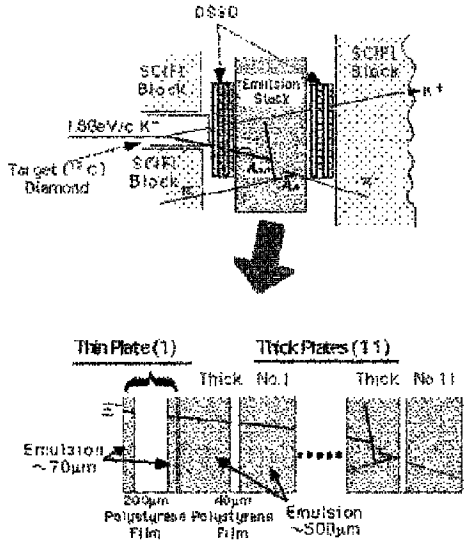

Figure 10: The apparatus around the emulsion and the emuslion stack.

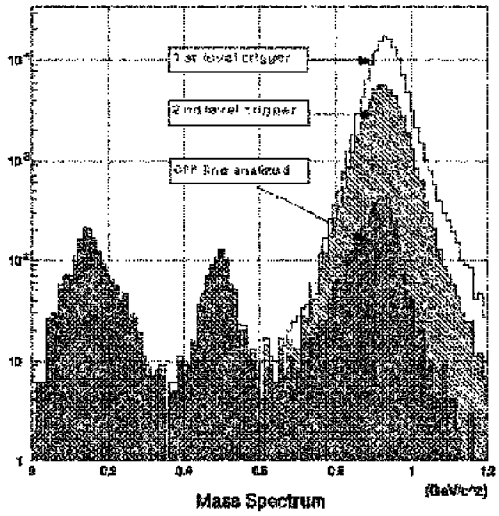

Figure 11: The mass spectrum obtained by the E373.

K^+ Spectrometer

The K^+ spectrometer is essentially the same as the one used for the E373. The K^+ particles are identified by the time-of-flight counters and the aerogel Chrenkov counters. The mass

spectrum obtained by the E373 is shown in Fig.11. The momentum of the K^+ particle is measured with the magnet (KURAMA) and DCs. The momentum resolution obtained by the E373 is good enough for the measurement of quasifree reaction from the carbon target. In order to get as many as events with a limited amount of the emulsion, as many as K^+ particles must be detected, keeping the integral beam flux constant. Therefore, we will use the KURAMA magnet in order to obtain larger acceptance($\sim$200 msr) for the K^+ particles, instead of the SKS magnet (100 msr). The TOF counters will be placed downstream of the DC3. The shorter distance for the TOF reduces the inefficiency due to the K-decay in the spectrometer and increases the acceptance.

Tracking detectors

a. double-sided Si strip detector (DSSD)

In the E373, we used micro fiber bundle tracking detector for the Ξ^- tracking from the target to the top of the emulsion stack. The detector consists of fine fibers as their diameter of $\sim 40\mu m$. By use of this reconstruction data, the mean number of the Ξ^- candidate tracks found in the emulsion was 4$\sim$5 even by such fine fibers, because the track image becomes broader than the size of one fiber.

To find the Ξ^- candidate track, unambigusly, we will employ double-sided Si strip detector (DSSD). This is an essential point to analyze the huge number of events, *i.e.* ten times more events than that of the E373. Two DSSDs are settled between the target and the emulsion to measure the angle and position of Ξ^-s, precisely. Since the resolution of charge deposit by charged particles is also very fine, Ξ^- particles can be separated from other protons or pions. We can reduce events to be scanned about one order of magnitude by using DSSD.

If we use this DSSD, the decay vertices such as the H in the emulsion can be located by following up the daughter tracks which are recorded in the DSSD. We will, therefore, set more two DSSDs downstream of the emulsion stack.

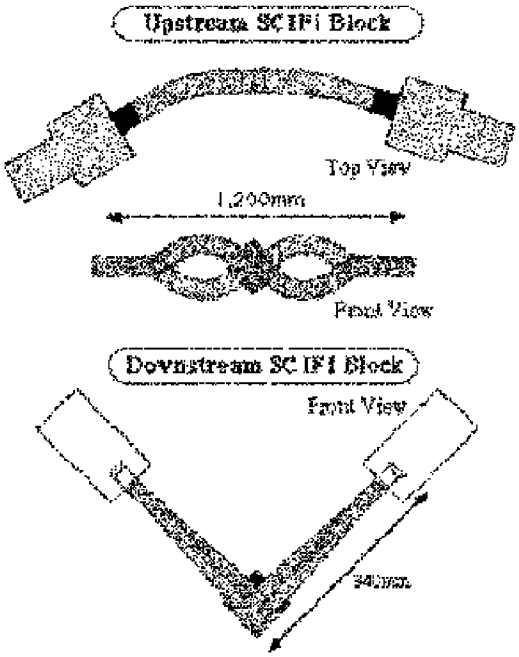

Figure 12: Schematic drawings of the SCIFI blocks.

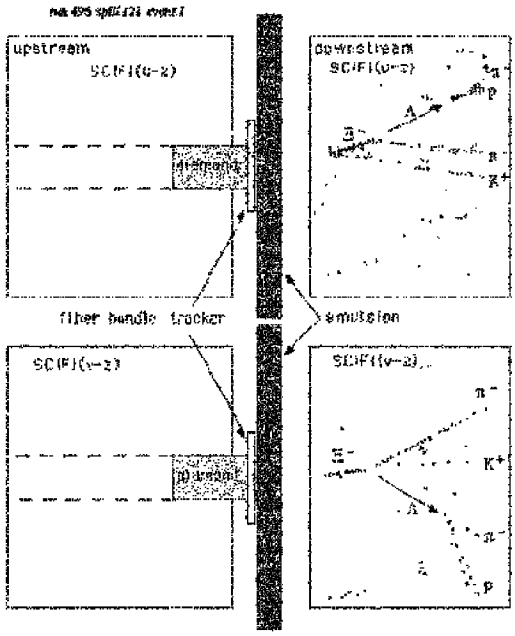

Figure 13: An image of Ξ^- decay sequence shown in SCIFI blocks of the E373.

b. scintillating fiber (SCIFI)

The scintillating fiber (SCIFI) detector had been developed as a live target to search for the H dibaryon about ten years ago. We employed SCIFI blocks settled up- and downstream of the emulsion to find the decay topologies of $H \rightarrow \Sigma + p$ and $\Lambda + p + \pi^-$ and to measure the energy of π^-s escaping from sequential weak decay of double strangeness nuclei produced in the emulsion. Schematic drawings are shown in Fig.12. The cross section of each fiber which we use is $0.3 \times 0.3 mm^2$. About one hundred fiber sheets are alternately packed in the u and v directions in order to reconstruct tracks in 3-dimension. To degrade π^- energy, Aluminum sheets with $0.3mm$ thickness are put between each SCIFI sheets. An image obtained by the E373 is displayed in Fig.13. The decay topology of Ξ^- is clearly understood with a tagged K^+ tracks.

In the present experiment, the SCIFI detector like the above can work effectively if the read out CCDs are changed to the faster ones.

Nuclear emulsion

The emulsion stack as shown in Fig.10 is constructed by 11 thick emulsion plates and one thin plate with each cross section of $24.5 \times 25.0 cm^2$. One thin plate has $70 \mu m$ thick emulsion on both sides of $200 \mu m$ polystyrene base. In this thin plate, the Ξ^- tracks are searched by the prediction of the Ξ^- tracking detector. This scanning will be done by the computer

aided scanning system developed in the E373. In a thick plate, emulsion of $500\mu m$ thickness is coated on both sides of also $40\mu m$ polystyrene base. These bases are preprocessed by us and more than one thousand plates were well prepared in the E373[19].

The emulsion crystal (AgBrI) has been developed to get better position resolution. In the present experiment, we use the emulsion with fine and uniform crystal of the size of $0.18\pm0.015\mu m$ which is different from that used in the E176 ($0.24\pm0.078\mu m$).

The emulsion stack is moving in x and y direction while the beam exposure. The emulsion mover drives it and provides the position accuracy about 10 μm. The coordinates between the DSSD and the emulsion is correlated by the exposure of narrow size beam less than $1mm^2$ in diameter.

Analysis

a. track reconstruction and event selection

The tracks are reconstructed in the DSSD and in the SCIFI of the down stream of the emulsion to select the Ξ^- stopped events. A π^- track reconstruction in the bottom SCIFI block is neccesary for rejection of Ξ^- decay events. Since the energy of this π^- particle is large enough rather than that of the π^- of decay product of hypernucleus, the high rejection reliability of Ξ^- decay events is expected. By a Monte Carlo simulation, the number of Ξ^- decay events is about 10 times larger than that of the Ξ^- stopping. This event selection is essential for us.

We also try to recognize Ξ^- candidates in the SCIFI block of down stream. This recognition is carried out by kinematical check between the candidate track and K^+ including the scattering effect. We can also reject such events because Ξ^- is passing through the emulsion stack without stopping.

b. emulsion, DSSD and SCIFI image scanning

We will follow the Ξ^- candidate track found in the top emulsion plate to its stop point. The scanning in the top plate can be done in one order faster speed as compared with the E373 by the $R\&D$ for hard- and soft-ware of the system. In the Ξ^- stop point, the decay topology is measured precisely. When we found (sequential) weak decay of a doble- or single-Λ hypernucleus, all decay products should be followed to those end points for measurement of those energies and for study of the characteritics of stop points. To be sure about the number of strangeness which are transferred in the nucleus, we will search for the decay products of missing strageness decay in the SCIFI.

2.3.4 Yield estimation to accumulate 10^4 Ξ^- stop events

Maximum number of exposed K^- particle for one stack :n_{K^-}

Since the emulsion stores all changed particles within exposure, the maximum number of exposed beames is limitted. That is given as follow;

$$n_{K^-} = n_e \cdot r_s \cdot s \cdot r_{K^-}$$

where n_e = maximum number of changed particles in emulsion to recognize thin tracks [$\Rightarrow 10^6/cm^2$], r_s = damage by shower particles produced in the diamond target [$\Rightarrow 1/1.14$ given by Monte Carlo], s = cross section of emulsion stack [$\Rightarrow 24 \times 24\ cm^2$] and $r_{K^-} = K^-$ ratio in beams [$\Rightarrow 0.9$ (assumed)]. It was found to be able to expose K^- of ($n_{K^-} =$) 4.55×10^8 to one emulsion stack.

Yield of Ξ^- stop in one emulsion stack : $y_{\Xi stop}$

We estimated the yield of the stopping Ξ^- event in the emulsion. This yield depends on the acceptance of the spectrometer. It depends also on the distance from the target to TOF counter. If the position of TOF is far from the target, the decay rate of K^+ becomes large. We are using the KURAMA sprectrometer, successfully, in the E373 experiment. The Ξ^- stopping yield is written by

$$y_{\Xi stop} = y_{K^+} \cdot \eta_\Xi \cdot R_{stop}$$

where $\eta_\Xi = \Xi^-$ escaping ratio from target nucleus (i.e. ^{12}C of diamond $\Rightarrow 0.8$ from the previous experiment[20]), $R_{stop} = \Xi^-$ stopping probability in the emultion stack (estimated by Monte Carlo $\Rightarrow 0.017$). The y_{K^+} is tagged K^+ number in one stack exposure which is shown as follow;

$$y_{K^+} = \frac{d\sigma}{d\Omega_L} \cdot \Delta\Omega \cdot N_p \cdot \eta_{abs} \cdot \eta_{K^+} \cdot \eta_{eff} \cdot n_{K^-}$$

where $\frac{d\sigma}{d\Omega_L}$ = the cross section of quasi-free 'p'$(K^-, K^+)\Xi^-$ reaction [$\Rightarrow 50 \times 10^{-30}\ cm^2/str.$], $\Delta\Omega$ = acceptance of the spectrometer [$\Rightarrow 0.20 sr.$], N_p = effective proton number of diamond target [$\Rightarrow 1.36 \times 10^{24}$], η_{abs} = beam absorption rate in $3cm$ long target [$\Rightarrow 0.947$], η_{K^+} = detecting rate of K^+ without decay before reaching the TOF [$\Rightarrow 0.735$] and η_{eff} = reconstruction efficiency of the tagged $K^+ \Rightarrow 0.85$ is assumed].

Finally, $y_{\Xi stop}$ is estimated to become 49.8 Ξ^- stops in one stack.

Emulsion volume and Beam time

To get 10^4 Ξ^- stop events, we need the emulsion volume of

$$0.650 \times 10000/49.8 = 130\ liters.$$

200 stacks are to be prepared. In our E373 experiment, 70 *liters* emulsion (100 stacks) were used. The total number of K^- is 0.91×10^{11}. If we get almost pure K^- beam with its intensity of 1×10^5 $K^-/spill$ $(3.42sec)$, we need 5 weeks' beam time by use of KURAMA spectrometer.

Emulsion handling

In the E373 experiment, we prepared 100 stacks of the emulsion for tatal 7 months by three people at Gifu Univ. This plate making speed is limited by the number of the drying machine after pouring of the emulsion gel. Since more than twice number of the emulsion plates for the E373 have to be prepared, the emulsion is exposed by cosmic rays and radiation from walls and air in a room for one year or more, if the plates of the proposed experiment are made at Gifu Univ. To minimize the plate making period, we need a room which has a space about 10×10 m^2, water and electric power supply to set three drying machines. If we are able to use such room, the plate making will be done very speedy, 3 times or more fast, even if the number of workers is the same as that of the E373.

We must develop the emulsion as soon as possible after the beam exposure, because the sensitive silver crytals by charged particles become insensitive to the development, month by month, *i.e.* fading. We certified there is no problem in scanning emulsion if we develop emulsion plates for 5 months later from the beam exposure. The emulsion plates of the E373 are developed at ICRR of Tokyo Univ. We are able to develop 4 stacks' emulsion at once in one week, so at least 50 weeks are necessary to develop all of the emulsion plates. This means we need one year even if we can occupied the development apparatus at ICRR. It is impossible, in principle, because there are own projects of ICRR. Therefore, the development facility have to be built up at JHF.

2.3.5 Summary

We propose an experiment to study nuclei with double strangeness by using a new emulsion-counter hybrid method. The emulsion is used to detect especially hyperfragments and counters are used to identify the (K^-, K^+) reaction and Ξ^-. About ten years ago, the KEK hybrid emulsion experiment, E176, found that double strangeness nuclei are efficiently produced through the Ξ^- nuclear capture at rest (stopping Ξ^- events in the emulsion). To analyze ten times more number of stopping Ξ^- events than those obtained by the E176, the experiment using an emulsion-scintillating fiber hybrid method, E373, is going on with data taking. The goal of the proposed experiment is to obtain 10^4 stopping Ξ^- events in the emulsion, which will provide one thousand events showing the formation of double starn-

geness nuclear system. Among them, we can expect one hundred nuclear fragments with double strangeness to be identified.

The E176 found one mesonic weak decay of a double strangeness nucleus which was interpreted as either ${}^{10}_{\Lambda\Lambda}$Be or ${}^{13}_{\Lambda\Lambda}$B with completely different binding energies. One gives repulsive $\Lambda\Lambda$ interaction and the other gives attractive $\Lambda\Lambda$ interaction. This problem will be resolved in the E373. The primary objective of the present experiment is to determine the $\Lambda\Lambda$ interaction energy, namely the binding energies of several double strangeness nuclei.

The present experiment can set more stringent lower bound for the mass of H-dibaryon by observing other species of double strangeness nuclei. Not only a ground state of double strangeness nuclei but excited states such as Ξ^- hypernuclei or H nuclei can also be studied. Since the number of Ξ^- stopping events is ten times more than E373, the sensitivity of the H-dibaryon search from Ξ^- atoms will be greatly improved. And also, rare decay modes of double strangeness nuclei can present rich information for the discussion about the hyperon mixing.

In order to improve statistics by ten times, we take advantage of almost pure K^- beam obtained at $1.8GeV/c$ line, compared to K/π =1/3 at KEK. We employ a new high position resolution detector, double-sided Si strip detector, to tag Ξ^- tracks done by the E373 in order to make the time-consuming emulsion scanning easier and faster, which is important to observe 10^4 stopping Ξ^- events. The scintillating fiber blocks which surround the emulsion are used to detect π^- and higher energy particles and the emulsion is used to detect mainly hyperfragments.

The present experiment can be carried out by ~5 weeks' beam and twice emulsion volume as compared with the E373, if it is available to use almost pure K^- beam ($1.8GeV/c$ K^- ; $1 \times 10^5 K^-/spill$ with K^-/π^- ~10), KURAMA spectrometer and emulsion handling facilities.

References

[1] J. Doornbos, KEK Report 97-5 (1997).

[2] T. Koike and Y. Akaishi, Genshikaku-Kenkyu 41 (19xx) 87.

[3] K.S. Myint and Y. Akaishi, Prog. Theor. Phys. Suppl. 117 (1994) 251.

[4] A.J. Baltz, C.B. Dover, and D.J. Millener, Phys. Lett. 123B (1983) 9.

[5] M. Danysz et al., Nucl. Phys. 49 (1963) 121.

[6] P.J. Prowse, Phys. Rev. Lett. 17 (1966) 782.

[7] R.H. Dalitz et al., Proc. R. Soc. Lond. A426 (1989) 1.

[8] S. Aoki et al., Prog. Theor. Phys. 85 (1991) 1287.

[9] K. Nakazawa, KEK proposal E373 (1993).

[10] T. Fukuda and R.E. Chrien, AGS proposal E906 (1994).

[11] K. Nakazawa, *in* Proc. of the 23rd INS Int. Symp. on Nuclear and Particle Physics with Meson Beams in the 1 GeV/c Region, eds. S. Sugimoto and O. Hashimoto (Universal Academy Press, Tokyo, 1995), p. 261.

[12] Izumi Kumagai-Fuse, Shigeto Okabe, and Yoshinori Akaishi, Phys. Rev. C54 (1996) 2843.

[13] Y. Yamamoto, M. Wakai, T. Motoba and T. Fukuda, Nucl. Phys. A625 (1997) 107;
Y. Yamamoto, Nucl. Phys. A639 (1998) 393c.

[14] I. Kumagai-Fuse and Y. Akaishi, Phys. Rev. 54 (1996) R24.

[15] M.Danysz et al., Phys. Rev. Lett. **11**(1963)29.

[16] K.Nakazawa, Nucl. Phys. A**585**(1995)75c, *ibid.* A**639**(1998)345c.

[17] A.Ichikawa et al., Nucl. Instr. & Mthod. A**417**(1998)220.

[18] K.Nakazawa, Proc. of the 23rd INS Symp., Univ. Academy Press. & INS. (1995)261,

[19] H.Akikawa et al., to be submitted to Nucl. Instr. & Mthod. A.

[20] S.Aoki, Nucl. Phys. A**644**(1995)365.

3 Hyperon Proton Scattering

M. Ieiri
KEK, Tsukuba, Ibaraki 305-0801, Japan
K. Imai
Kyoto University, Sakyo-ku, Kyoto 606-8224, Japan
B. Bassalleck
University of New Mexico, Albuquerque, NM 87131, U.S.A.

3.1 Introduction

Studies of the interactions among baryons are essential in understanding "QCD-inspired" pictures of strong interactions in nuclear physics. The nucleon-nucleon (NN) interactions have been extensively studied both theoretically and experimentally, but not much is known about the hyperon-nucleon (YN) interactions.

Nucleon-nucleon (NN) scattering was extensively studied in the 50's and 60's. The existence of a "hard-core" has been verified definitely by a phase-shift analysis, and the NN scattering data have been well described by one-boson exchange (OBE) models. The OBE models have been extended to include the YN sector to understand the NN interaction as the strong interaction between the baryon octet. The Nijmegen group took into account the flavor SU(3) symmetry [1] and the Bonn-Julich group developed a model based on SU(6) symmetry [2]. On the other hand, the short-range repulsive force of the strong interaction has been tried to be explained based on a more basic hierarchy, i.e., quarks and gluons. The quark-cluster model approach has been developed by groups from Tokyo, Tubingen and Kyoto-Niigata [3, 4, 5]. They successfully produced the "core" and predicted several interesting features such as strong isospin dependence of the interactions and the anti-symmetric spin-orbit force.

While we have thus seen a rapid theoretical progress in several pictures [1, 2, 3, 4, 5] of the baryon-baryon (BB) interaction, experimental investigations [6] for the YN interactions were very sparse and have fallen behind theory except for a present trial at KEK in the strangeness S=−1 YN system [7]. In order to scrutinize these models and to further understand the BB interaction, one has to extend his playground to the YN sector, since an additional degree of strangeness and the Pauli principle on the quark level are expected to give an important aspect. In the BB interaction, it seems to be difficult to incorporate both the boson exchange and the quark-gluon treatments due to the lack of the experimental effort. So, by getting reliable and accurate YN scattering data, one should like to settle a model based on QCD or SU(3) framework, especially for explaining the short range part and the l·s strength. And

if lucky, one can detect a "quark effects" as the limits of the conventional picture. YN scattering data will play a key role to get the right picture of the B-B interaction. Intense pion and kaon beam in 1$\sim$ 2 GeV/c region at the 50 GeV PS plays an important role for the progress of this subject.

3.2 Yp scattering

Hyperon-proton (Yp) scatterings are summarized in the table 3. For each hyperon, its production reactions, Yp scatterings and successive hyperon decays are displayed. As for Λp, Σ^+p, Σ^-p and Ξ^-p elastic scattering, charged particles take part in all the process, then these channels would be tractable. However, reaction channels such as $\Sigma^-\mathrm{p}\rightarrow \Sigma^0\mathrm{n}$, $\Xi^-\mathrm{p}\rightarrow \Xi^0\mathrm{n}$, might not be tangible, since more than one γ's and/or neutrons appear in the process. Channels, which are marked by star, can be reconstructed kinematically, if we detect all the charged particles in the production, scattering and decays.

In this letter of intent, we should like to propose two important experimental subjects as a first step; $\Xi^-\mathrm{p}\rightarrow \Lambda\Lambda$ reaction to study the interaction in the S=-2 sector directly, and asymmetry measurement in Λp and Σ^+p elastic scatterings to investigate the anti-symmetric spin-orbit strength.

3.3 $\Xi^-\mathrm{p}\rightarrow \Lambda\Lambda$ reaction

3.3.1 Physics interests

We propose to measure the energy dependence of the $\Xi^-\mathrm{p}\rightarrow \Lambda\Lambda$ reaction at the Ξ^- momenta below 1 GeV/c to study the $\Lambda\Lambda$ interaction by the $\Lambda\Lambda$ invariant mass and the differential cross section.

In the S=-2 sector, the H dibaryon was first predicted by Jaffe as a six-quark state bound by the color-magnetic interaction [8]. Although several experimental efforts have been made [9], the existence of the H is still an open question. The H-dibaryon is suggested to be very loosely bound, or unbound, relative to $2m_\Lambda$ by the observation of double Λ-hypernuclear events [10], or could be resonance by recent theoretical estimates [11]. In the theoretical frameworks, H particle can exist only in a quark picture, not in any OBE models. Thus, the characteristic features of a "core" region are different largely between the QCM and the OBE especially in S=-2. Since the direct production of the H-dibaryon seems to be very hard, Ξ^-p scattering experiment below 1 GeV/c will play an important role in the understanding of the short range part of the baryon-baryon interaction at S=-2.

The S=-2 baryon-baryon interaction can be studied also through the double Λ hypernuclei and Ξ-hypernuclei. The double Λ hypernuclei has been found in the KEK E176

	cτ (cm)	production reaction	[illegible]	outgoing particle	Y-p scattering		scattered particle		decay mode	α	decay particles	
Λ	7.89	[illegible]p → K⁰Λ	(700 [illegible] 1.0)	[illegible]	Λp	→ Λp		Λ	→ pπ⁻	−0.642	[illegible]	★
		[illegible]p → π⁰Λ	(350 [illegible] 0.9)	2γ					→ nπ⁰	+0.65	[illegible]	
						→ Σ⁰p	[illegible]	Σ⁰	→ Λγ		[illegible]	★
Σ⁺	2.396	[illegible]p → K⁺Σ⁺	(500 [illegible] 1.4)		Σ⁺p	→ Σ⁺p		Σ⁺	→ pπ⁰	[illegible]0.980	[illegible]	★
		[illegible]p → π⁻Σ⁺	(150 [illegible] 1.2)	[illegible]					→ nπ⁺	+0.068	[illegible]	★
Σ⁻	4.434	[illegible]p → K⁺Σ⁻	(250 [illegible] 1.5)		Σ⁻p	→ Σ⁻p		Σ⁻	→ nπ⁻	−0.068	[illegible]	★
		[illegible]p → π⁺Σ⁻	(150 [illegible] 1.0)	[illegible]		→ Λn	[illegible]	Λ	→ pπ⁻	−0.642	[illegible]	★
									→ nπ⁰	+0.65	[illegible]	
						→ Σ⁰n	[illegible]	Σ⁰	→ Λγ		[illegible]	
Σ⁰	2.22×10⁻⁹											
Ξ⁰	8.71	[illegible]p → K⁰Ξ⁰	[illegible]	[illegible]	Ξ⁰p	→ Ξ⁰p	[illegible]	Ξ⁰	→ Λπ⁰	−0.411	[illegible]	
Ξ⁻	4.91	[illegible]p → K⁺Ξ⁻	[illegible]		Ξ⁻p	→ Ξ⁻p	[illegible]	Ξ⁻	→ Λπ⁻	−0.456	[illegible]	★
						→ ΛΛ	Λ	Λ	→ pπ⁻	−0.642	[illegible]	★
									→ nπ⁰	+0.65	[illegible]	
						→ Ξ⁰n	[illegible]	Ξ⁰	→ Λπ⁰	−0.411	[illegible]	

Table 3: List of hyperon-proton scattering.

hybrid-emulsion experiment [8]. The event can be interpreted as either $_{\Lambda\Lambda}Be$ or $_{\Lambda\Lambda}B$. The assignment as $_{\Lambda\Lambda}B$ provides an attractive ΛΛ interaction like the old emulsion event, while the other assignment gives a repulsive interaction. The result is not conclusive still. The new emulsion-counter hybrid experiment has been approved at KEK as E373 [12] to obtain ten times more events than E176. The experiment to detect several hundreds double Λ hypernuclei by observing characteristic π^- mesonic decays [13] are also approved at BNL as E906. Two mesonic-decaying pions from a double Λ hypernuclei will be detected and the binding energy will be measured directly. This kind of double Λ hypernuclei study and the Ξ^-p scattering experiment proposed here are complementary each other in understanding of the baryon-baryon interaction at $S=-2$. A measurement of the Ξ^-p→ ΛΛ cross section is crucial in assessing the stability of Ξ quasi-particle states in the nucleus.

3.3.2 Experiment

The production cross section of the Ξ^- is ten times smaller than the Σ and Λ case, so intense K^- beam for its production is needed to obtain a sufficient number of scattering events for Ξ^-. Here, we expect the beam intensity of 10^7 K^-/sec with a good K/π ratio better than 1 at 1.7 GeV/c. We will use a "2 GeV/c kaon beam line" which is described in the "spectroscopic studies of S=−2" in Sect. 2 of this letter of intent.

The S=−1 YN scattering experiment at KEK utilized a plastic scintillating fiber block as a live target for the hyperon production and scattering (SCIFI detector) [7]. However, the maximum acceptable rate of the SCIFI detector at present is 10^5 Hz, which is limited by decay time of the phosphor of the first image intensifier tube (IIT). Therefore, at the 50 GeV PS, this SCIFI-IIT technique cannot be used in a Ξ^-pscattering experiment so far.

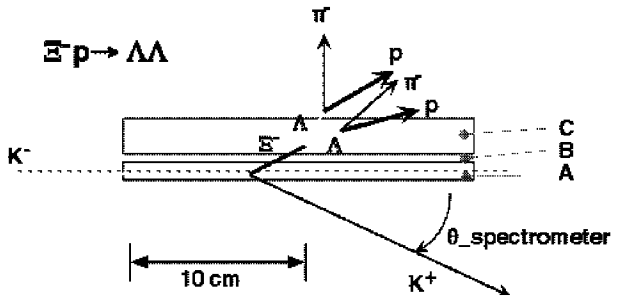

Figure 14: Schematic drawing of a traget region. A liquid hydrogen of 20 cm long, 5cm wide and 1 cm high is used as a production target of the Ξ^-. A: 10 mm thick liquid H_2, B: 5 mm thick tungsten degrader, C: 20 mm thick liquid H_2. The Ξ^- beam with wide kinetic energy range below 400 MeV is produced through the 5 mm thick tungsten energy-degrader. Another liquid hydrogen of 2 cm high is put on the tungsten as a scattering target of Ξ^-p interactions.

A schematic drawing around the target region is shown in Fig. 14. The shape of K^- beam is required to be thin (about 1 mm) in the vertical direction. A liquid hydrogen of 20 cm long, 5 cm wide and 1 cm high is used as a production target of the Ξ^- via the $K^-p \rightarrow K^+\Xi^-$ reaction. The produced Ξ^-'s are identified by tagging K^+'s in the forward K^+ spectrometer. The center of the K^+ spectrometer is located at 25 degrees beneath the K^- beam axis to produce the Ξ^- upwards in the production angle around 27 degrees in the laboratory frame as shown in Fig. 15. The Ξ^- beam with wide kinetic energy range below 400 MeV is produced through the 5 mm thick tungsten energy-degrader. Another liquid hydrogen of 2 cm high is put on the tungsten as a scattering target of Ξ^-p interactions.

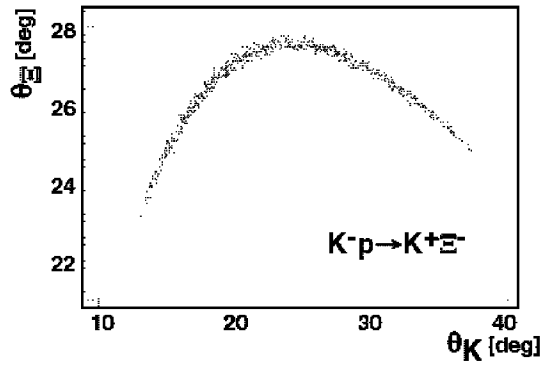

Figure 15: Ξ^- production angle vs K^+ outgoing angle. The center of the K^+ spectrometer is located at 25 degrees beneath the K^- beam axis to produce the Ξ^- upwards in the production angle around 27 degrees in the laboratory frame.

Fig. 16(a) shows a momentum distribution of Ξ^- just before its decay versus its vertical decay position. The kinetic energy of the Ξ^- beam after tungsten degrader is shown in Fig. 16(b), which covers below 400 MeV.

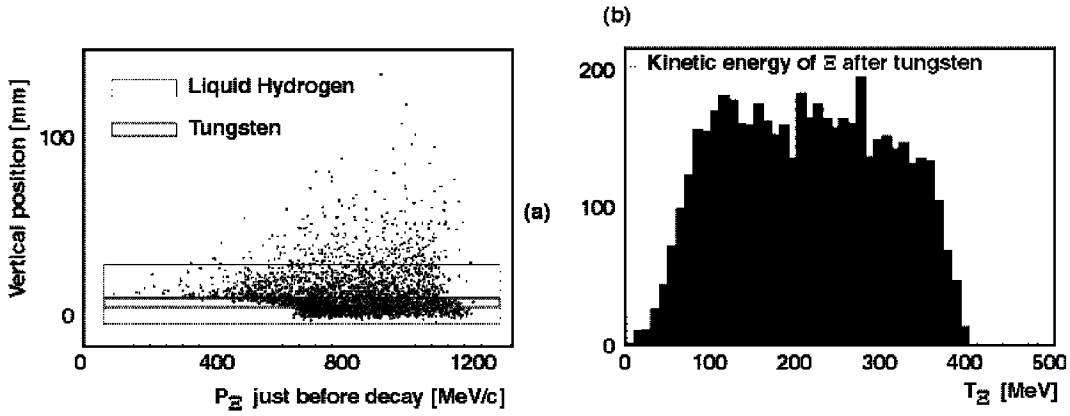

Figure 16: (a) Momentum distribution of Ξ^- just before its decay versus its vertical decay position. (b) The kinetic energy of the Ξ^- beam after tungsten degrader, which covers below 400 MeV.

A cylindrical drift chamber system (CDS), which is similar to the system of the BNL-AGS E906 [13], will be applied covering above a scattering target region to detect charged particles related to the Ξ^-p interactions as shown in Fig. 17. Some of Ξ^-'s interact with another proton in the liquid hydrogen scattering target. Both (A) elastic scatterings Ξ^-p→

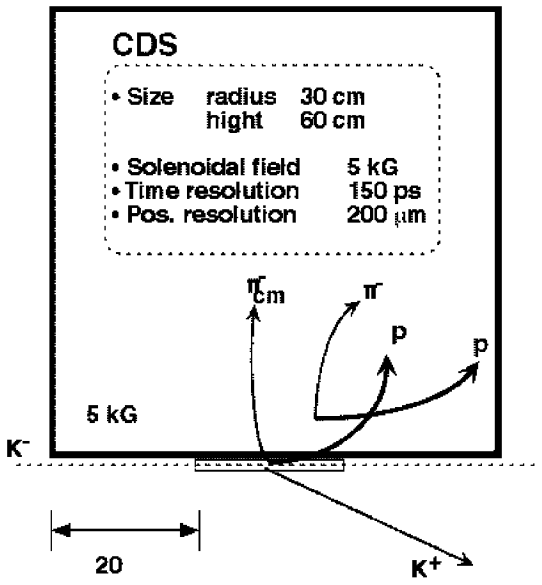

Figure 17: Schematic drawing of a cylindrical drift chamber system (CDS).

Ξ^-p (Isospin; T=0, 1) and (B) reaction Ξ^-p$\rightarrow \Lambda\Lambda$ (T=0) are available.

$$\begin{array}{lll} (A) & \Xi^- p \rightarrow \Xi^- \underline{p} \;\; ; \;\; \Xi^- \rightarrow \Lambda \underline{\pi}^- \, (100\%) & \Lambda \rightarrow \underline{p\pi}^- \, (64\%) \\ (B) & \Xi^- p \rightarrow \Lambda\Lambda \;\; ; \;\; \Lambda \rightarrow \underline{p\pi}^- \, (64\%) & \Lambda \rightarrow \underline{p\pi}^- \, (64\%) \end{array}$$

Charged-particles related to these Ξ^-p interactions (underlined particles in (A) and (B)) should be detected by the CDS to reconstruct its reaction kinematics. For both channels, final charged particles to be detected are two protons and two negative-pions.

Events, which have 4 charged-particles' trajectories by the CDS, are analyzed as Ξ^-p interaction candidates. Protons and π^-'s will be determined well by a mass analysis by tracking of their particle trajectories and TOF information from hodoscopes under a solenoidal magnetic field of 5 kG at the CDS. All 4 particles in this event will be identified as p or π^- by this mass analysis and their momentum can be obtained from trajectories in the CDS.

Next, Λ('s) will be identified by the "invariant mass" analysis for two "p" and "π^-" combinations. If single Λ is assigned from two protons and two π^-'s and then $\Xi^-$are identified with this Λ and a remaining π^-, this event is a candidate of the Ξ^-p$\rightarrow$ Ξ^-p elastic scattering. If two Λ's can be identified and a Ξ^- cannot be assigned from any combination with one of these Λ and π^-, the event is a candidate of the reaction Ξ^-p$\rightarrow \Lambda\Lambda$(Fig. 18). The kinematic fitting will be performed for these candidates of the Ξ^-p interaction to confirm the kinematics of (A) or (B).

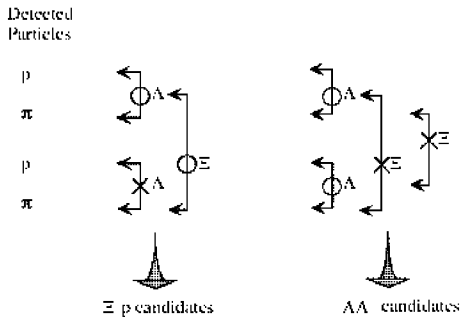

Figure 18: Procedure of assignment of the final state by the invariant mass analysis.

3.3.3 Identification efficiency of events

The identification rate in the analysis described here was evaluated in the work at the AGS proposal P928 [15]. We refer to values at that work, since we assume the similar CDS detector system for two protons and two negative-pions after the Ξ^-p scattering.

· Misidentification of "Λ" and "Ξ^-"

Events, with 4 charged-particles' trajectories by the CDS, will be analyzed. After the Ξ^-p interaction in the scattering target, 10% of the elastic scattering (A) and 8.8% of the reaction (B) will satisfy this condition.

As described in the previous section, the final state of the Ξ^-p interaction (Ξ^-p or $\Lambda\Lambda$) will be determined by the invariant mass analysis from 4 particles detected by the CDS. In the identification procedure of "Λ", some will be misidentified.

The average momentum resolution of the CDS is assumed to be 1% for π^- and 3% for p, respectively, in each kinematical region of the Ξ^-p interaction. For a miscombination, e.g. the combination of a recoil-proton and a decay- π^- from Ξ^-p after the elastic scattering (A) (Fig. 19), 32.9% of this combination will be assigned as "Λ" in the mass analysis (m_Λ-15 $< m < m_\Lambda$+15 [MeV/c^2]) under this momentum resolution. For the reaction (B), 31.1% of the combination by a Λ and a $\pi^-$are also misidentified as "Ξ^-" ($m_{\Xi^-}-15 < m < m_{\Xi^-}+15$ [MeV/c^2]).

After the invariant mass analysis of possible combinations of particles, the identification efficiencies of the final states are obtained as Table 4. Events which can be interpreted as both Ξ^-p and $\Lambda\Lambda$ will be discarded.

· Backgrounds from free Ξ^- decay

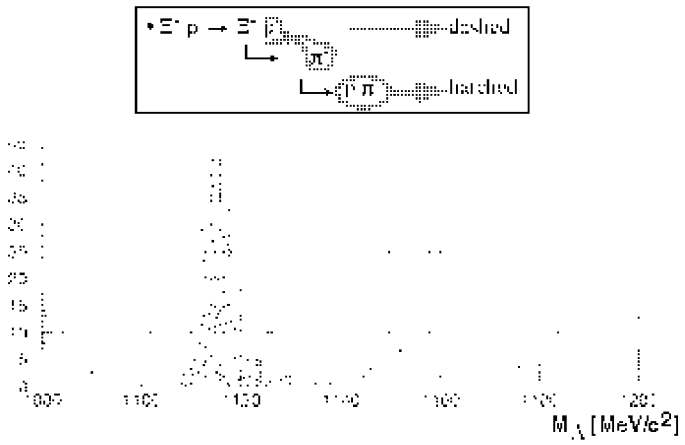

Figure 19: Invariant mass spectrum for the several combinations. "Λ" ; a correct combination, i.e. p and π^- from Λ decay (hatched), and a wrong combination of recoil-p and π^- from Ξ^- decay (dashed).

Final states	Real event [A] $\Xi^- p \to \Xi^- p$
Identified as $\Xi^- p$	65%
Both $\Xi^- p$ and are possible	35%
Final states	Real event [B] $\Xi^- p \to \Lambda\Lambda$
Identified as ΛΛ	50%
Both $\Xi^- p$ and are possible	50%

Table 4: Identification efficiencies of the final states for each reaction.

Almost all Ξ^-'s decay in flight in the target region, that is, 30% of produced Ξ^-'s decay to $\Lambda\pi^-$ in the target and 20% of these Λ's decay to $p\pi^-$ in the scattering liquid hydrogen target. If one of these decay products scatters elastically with proton in the target again, final particles of this event are two p's and two π^-'s same as Ξ^-p interactions as shown in Fig. 20. The rate of these elastic scatterings will be comparable to the Ξ^-p interaction in the liquid hydrogen target. Some of these events will also satisfy the analysis condition; 4 charged-particles' trajectories by the CDS. Therefore, these could be a source of backgrounds of this experiment.

(i) π^--p elastic scattering [Fig. 20 (a), (b)]

For a combination of π^- and p, we can try to calculate initial "π^-" mass from momenta of these $\pi^-$and p if we assume π^-p elastic scattering. However, for any combinations of π^-

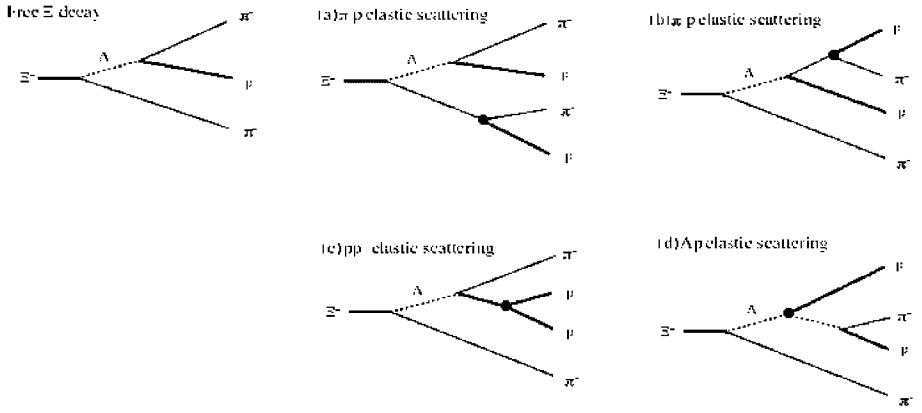

Figure 20: Possible sources of backgrounds: One of Ξ^- decay products scatters elastically with proton in the target, final particles of this event are two p's and two π^-'s same as Ξ^-p interactions.

and p resulting from Ξ^-p interactions (A) and (B), one cannot obtain this "π^-" mass (for these cases, the calculated $\langle$"π^-" mass$\rangle^2$ gives negative value for any combinations in this case). Then, events which will give the real "π^- mass" in this calculation come from π^-p elastic scattering in Fig. 20 (a) and (b). This check will eliminate events which include π^-p elastic scattering.

(ii) pp and Λp scattering [Fig. 20 (c), (d)]

As for (c) and (d) (also for (b)) in Fig. 20, decay π^- from Ξ^- goes out through the target without scattering. For these cases, mass of decay Λ from Ξ^- will be obtained by using the initial Ξ^- momentum from the (K^-,K^+) reaction and the momentum of one of π^- in the final particles detected by the CDS. For real Ξ^-p interactions, 25% of events satisfy this "Λ" mass (m_Λ-15 < m < m_Λ+15 [MeV/c^2]) which is calculated from initial Ξ^- and one of two π^- as shown in Fig. 20. After this procedure, 85% of real Ξ^-p interactions will survive.

Finally, 4.9% (= 10% $\times$ 65% $\times$ 75%) of the elastic scattering (A) and 3.3% (= 8.8% $\times$ 50% $\times$ 75%) of the reaction (B) will survive among all Ξ^-p interactions in the liquid hydrogen target.

3.3.4 Expected yield

The rate of the Ξ^-p hyperon production is expressed as:

$$Y_{\Xi^-} = n_{K^-} \cdot n_p \cdot \frac{d\sigma}{d\Omega}(K^- p \to K^+ \Xi^-) \cdot d\Omega_{Spectrometer} \cdot \eta_{K^+}$$

where,

n_{K^-}	number of incident K^- : 10^7 /sec
n_p	number of proton target
	8.5×10^{23}protons/cm^2 in the 20 cm liquid hydrogen
$\frac{d\sigma}{d\Omega}(K^- p \to K^+ \Xi^-)$	differential cross section for production [16]
$d\Omega_{Spectrometer}$	solid angle of the spectrometer
	40 cm wide and 20 cm high window at 1 m distance
η_{K^+}	survival rate of K^+ at TOF wall: 0.51 at 5 m

The production rate of Ξ^-, i.e. a rate of the (K^-,K^+) reaction, is 11 per second (9.7×10^7 Ξ^- in total of 100 days machine time). Next, the expected yields of the elastic scattering of Ξ^-p and the reaction Ξ^-p$\to \Lambda\Lambda$ in the 2 cm high liq. hydrogen target are expressed as:

$$Y_{\Xi^- p \to \Xi^- p, \Lambda\Lambda} = Y_{\Xi^-} \cdot n_{p-eff} \cdot \frac{d\sigma}{d\Omega}(\Xi^- p \to \Xi^- p, \Lambda\Lambda) \cdot d\Omega_{CDS-eff} \cdot Br$$

n_{p-eff}	effective number of proton target in Ξ^- flight length
$\frac{d\sigma}{d\Omega}(\Xi^- p \to \Xi^- p, \Lambda\Lambda)$	differential cross sections
	uniform angular distribution, but as for the incident momentum
	dependence, the Kyoto-Niigata model RGM-F is assumed [17]
	For example at 700 MeV/c, 21.9 mb for Ξ^-p $\to \Xi^-$p ,
	and 9.8 mb for Ξ^-p $\to \Lambda\Lambda$.
$d\Omega_{CDS-eff}$	effective solid angle of the CDS i.e. effective geometry for
	charged particles covered by the CDS,
	which is estimated by a simulation
Br	total branching ratio of decays to charged particles:
	$\cdot Br\,(\Xi^- \to \Lambda\pi^-) \times Br\,(\Lambda \to p\pi^-)$ for elastic scattering
	$\cdot [Br\,(\Lambda \to p\pi^-)]^2$ for$\Xi^- p \to \Lambda\Lambda$reactions

About 78000 Ξ^-p elastic scattering and 37000 Ξ^-p$\to \Lambda\Lambda$ reactions will occur in 100 days in the liquid hydrogen target. If we require that events should have 4 charged-particles' trajectories by the CDS as explained in the previous section, 10% of the Ξ^-p elastic scattering and 8.8% of Ξ^-p$\to \Lambda\Lambda$ reactions are remained. After the invariant mass analysis for the assignment of the final state and the elimination of backgrounds, we can expect 3650 elastic scatterings and 850 Ξ^-p$\to \Lambda\Lambda$ reactions. Fig. 22 shows a practical covered region by a simulation of this Ξ^-p experiment as a scatter plot for the Ξ^- incident momentum (just before scattering) vs. cosine of the scattering CM angle. If we assume 0.64 for the analysis efficiency (0.8 for the K^+ spectrometer side and 0.8 for the CDS side), the number of the Ξ^-p elastic scattering and the Ξ^-p$\to \Lambda\Lambda$ reaction will be finally about 2300 and 550, respectively.

As for the Ξ^-p$\to \Lambda\Lambda$ reaction, the covered region of the $\Lambda\Lambda$ invariant mass is from 2270 MeV/c^2 to 2410 MeV/c^2 as shown in Fig. 23. The positions of enhancement reported up to

now is also displayed in the figure. In the differential cross sections, statistical errors will be about 10% with $\Delta(\cos(\theta))= 0.2$ binning.

3.4 Asymmetry in Λp and Σ^+p elastic scatterings

3.4.1 Physics interests

In the hyperon-nucleon interaction, a remarkable feature is the existence of the anti-symmetric spin orbit (ALS) interaction, proportional to $\sigma_n^1 - \sigma_n^2$, in addition to the symmetric (LS) term. This ALS term is not present in the nucleon-nucleon case due to charge symmetry. The calculated spin-orbit strength shows difference between the OBE and the QCM [18]. Besides, large isospin dependence of the spin-orbit strength is expected for the Λ, Σ^+, and Σ^- -nucleon case [19]. In hypernuclei, both LS and ALS are important, since the spin-orbit strength in the folding model is proportional to the difference between the two (LS-ALS). A possible explanation of the observed small spin splitting of Λ-hypernuclei is a cancellation of LS and ALS strength, although each strength may not be so small [20].

An experimental study of the asymmetry measurement of 400 Σ^+p elastic scattering will start soon as KEK PS E452 [21]. This experiment will give information on the spin-orbit interaction as a first step to some extent, however, statistics will not be sufficient and one should measure several polarization observables to provide unique and quantitative understanding of the spin orbit interaction. Direct measurements of some sets of polarization observables in the YN elastic scattering will give a stringent constraint to the present BB interaction pictures and give a pivotal information on the study of hypernuclei.

3.4.2 Experiment

In the spin-scattering matrix [22], the ALS term $\mathbf{b} \cdot (\sigma_n^1 - \sigma_n^2)$ remains in the hyperon-nucleon system as follows:

$$M = a + c\left(\sigma_n^1 + \sigma_n^2\right) + b\left(\sigma_n^1 - \sigma_n^2\right) m\sigma_n^1\sigma_n^2 + g\left(\sigma_P^1\sigma_P^2 + \sigma_K^1\sigma_K^2\right) + h\left(\sigma_P^1\sigma_P^2 - \sigma_K^1\sigma_K^2\right)$$

Measurements of both the polarization (P_y) and the analyzing power with the polarized target (A_y^T) give the efficient information of the ALS strength $\mathbf{b}$, since P_y and A_y^T are given by the following equations (2) and (3), respectively:

$$\begin{array}{rcccccl} I_0 P_y & = & \frac{1}{4} Tr\left(M M^\dagger \sigma_n^1\right), & = & 2Re\left[(a+m)\, c^* + (a-m)\, \mathbf{b}^*\right] & = & I_0 A_y \\ I_0 A_y^T & = & \frac{1}{4} Tr\left(M \sigma_n^2 M^\dagger\right), & = & 2Re\left[(a+m)\, c^* - (a-m)\, \mathbf{b}^*\right] & = & I_0 P_y^T \end{array}$$

Since weak decays of Σ^+ and Λ tell us their polarization, we don't need any polarimeter, fortunately. Therefore, in Λ, Σ^+ -proton scattering experiment, it is not so difficult to measure the polarization and the polarization transfer.

In the Λ and Σ^+ production reaction, produced hyperons are ideally polarized when one detect K^+ meson at finite angles around 30 degrees [23]. So, the same experimental setup for the measurement of Ξ^-p can be used to produce the polarized Λ and Σ^+. For Σ^-, there is no polarization information of its production, since the decay asymmetry of Σ^- hyperon is almost zero. So one cannot measure the polarization for Σ^-p elastic scattering. However, A_y^T can be measured like the Λ and Σ^+. If produced Σ^-'s at finite angle are polarized, measurement of the analyzing power will be also possible. A design and simulation of the experiments for the polarization observables in the Yp elastic scattering is now in progress.

3.5 Summary

The coming 50 GeV machine will be unique facility to perform the Yp experiment, while there were a lot of places for pp and pn cases. So we should focus and select the experimental objectives to explore step by step certainly. Two important experimental subjects are proposed here; Ξ^-p$\rightarrow \Lambda\Lambda$ reaction to study the $\Lambda\Lambda$ interaction directly, and asymmetry measurement in Λp and Σ^+ p elastic scatterings to investigate the anti-symmetric spin-orbit strength. The hyperons in several hundred MeV/c have short lifetimes of a few centimeters. There are two tractable ways to perform the Yp scattering experiment. One is to detect all the charged particles from the scattering and decay at some distance with a cylindrical chamber surrounding the target region, which is described in this letter of intent. Another is to observe hyperon-proton scattering directly in a small region with a vertex detector such as a scintillating fiber or a bubble chamber. This technique will be very important when we measure the Yp scattering at low energy region. However, at present, data acquisition rate of this type of detectors is strongly limited by a repetition rate of an imaging device. To utilize these vertex detector under intense beam at 50 GeV, technical R & D such as the image delay tube [24] should be started as soon as possible. These above methods are typical approaches for Yp scattering experiments. At any rate, important points, when you proceed the Yp scattering experiments, are;

- one has to optimize between physics interest and technical feasibility.
- 'Triggers' would be a key of a design of Yp scattering experiments.

Many and vigorous data of pp and pn scattering experiments in 50s and 60s was really important and indispensable to get the picture of NN interaction. BB studies will give more elementary understanding of nuclear force and would reveal quark effect in hadronic phenomena.

References

[1] M. M. Nagels et al., Phys. Rev. D15 (1977) 2547; D20 (1979) 1633; P. M. Maessen et al., Phys. Rev. C40 (1989) 2226; Th. A. Rijken et al., Nucl. Phys. A547 (1992) 245c.

[2] B. Holzenkamp et al., Nucl. Phys. A500 (1989) 485; K. Holinde, Nucl. Phys. A547 (1992) 255c.

[3] M. Oka and K. Yazaki, Quarks and Nuclei, ed. W. Weise, Vol. 1 (World Scientific, 1984) 489; K. Yazaki, Nucl. Phys. A479 (1988) 217c; Perspectives of Meson Science, eds. T. Yamazaki, K. Nakai and K. Nagamine (Elsevier, The Netherlands, 1992) 795; K. Shimizu, Nucl. Phys. A547 (1992) 265c.

[4] U. Straub, Z. Y. Zhang, K. Bräuer, A. Faessler, S. B. Khadkikar, and G. Lübeck, Nucl. Phys. A483 (1988) 686; A508 (1990) 385c.

[5] Y. Fujiwara, C. Nakamoto, Y. Suzuki, Prog. Theor. Phys. 94 (1995) 214; 94 (1995)353; Phys. Rev. Lett. 76 (1996) 2242; Phys. Rev. C54 (1996) 2180.

[6] R. Engelmann et al. Phys. Lett. 21 (1966) 587; B. Sechi-Zorn et al. Phys. Rev. 175 (1968) 1735; G. Alexander et al. Phys. Rev. 173 (1968) 1452; J. A. Kadyk et al. Nucl. Phys. B27 (1971) 13; F. Eisele et al. Phys. Lett. 37B (1971) 204.

[7] J. K. Ahn et al., Nucl. Phys. A585 (1995)165c; A648 (1999) 263.

[8] R. L. Jaffe, Phys. Rev. Lett. 38 (1977) 195.

[9] A. S. Carroll et al., Phys. Rev. Lett. 41(1978) 777; H. Ejiri et al., Phys. Lett. B228 (1989) 24; B. A. Shahbazian et al., Phys. Lett. 235 (1990) 208; K. Imai et al., Nucl. Phys. A547 (1992) 199c; A. Rusek et al., Phys. Rev. C52 (1995) 1580; S. Aoki et al., Phys. Rev. Lett. 65 (1990) 1729; J. K. Ahn et al., Phys. Lett. B378 (1996) 53.

[10] S. Aoki et al., Prog. Theor. Phys. 85 (1991) 1287.

[11] S. V. Bashinsky, R. L. Jaffe, Nucl. Phys. A625 (1997) 167; S. D. Paganis, T. Udagawa, G. W. Hoffmann, R. L. Ray, Phys. Rev. C56 (1997) 570.

[12] E373 proposal at the KEK-PS (in Japanese).

[13] E906 proposal at the BNL-AGS.

[14] J. Nakano, Master Thesis (1996) unpublished.

[15] P928 proposal at the BNL-AGS.

[16] P. M. Dauber et al., Phys. Rev. 179 (1969) 1262.

[17] C. Nakamoto, private communication.

[18] A. Faessler, Nucl. Phys. A479 (1988) 3c; H. J. Pirner and B. Povh, Phys. Lett. 114B (1982) 308; A. Bouyssy, Nucl. Phys. A381 (1982) 445.

[19] K. Yazaki, Nucl. Phys. A479 (1988) 217c, K. Shimizu, Nucl. Phys. A547 (1992) 265c.

[20] C. Nakamoto, Y. Suzuki and Y. Fujiwara, Phys. Lett. B318 (1993) 587.

[21] E452 proposal at the KEK-PS.

[22] N. Hoshozaki, Suppl. Prog. Theo. Phys. 42 (1968) 107.

[23] Candlin et al., Nucl. Phys. B226 (1983) 1; Haba et al., Nucl. Phys. B299 (1988) 627; R. D. Baker et al., Nucl Phys. B141 (1980) 29; D. X. Saxson et al., Nucl Phys. B162 (1980) 522.

[24] A. Berkovski et al., Nucl. Instr. and Meth. A380 (1996) 537.

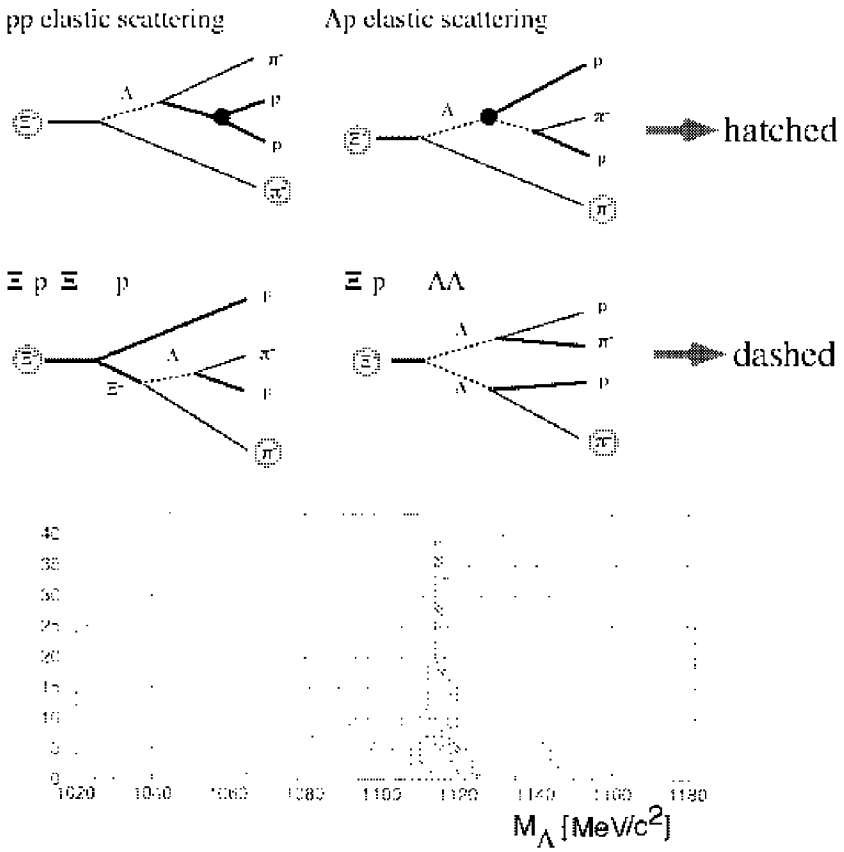

Figure 21: Mass spectrum of decay "Λ" from Ξ^- obtained by using the initial Ξ^- momentum from the (K^-,K^+) reaction and the momentum of one of π^- in the final particles detected by the CDS, under the assumption of Ξ^- free decay without scattering: (hatched) "Λ" mass obtained from Ξ^- free decay for (c) and (d) in Fig. 20, (dashed) "Λ" mass obtained from real Ξ^-p interactions.

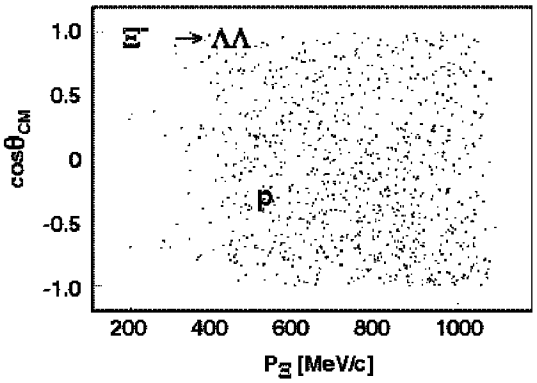

Figure 22: Practical covered region by a simulation of this Ξ^-pexperiment as a scatter plot for the Ξ^- incident momentum (just before scattering) vs. the scattering CM angle. The uniform angular distribution is used in the simulation.

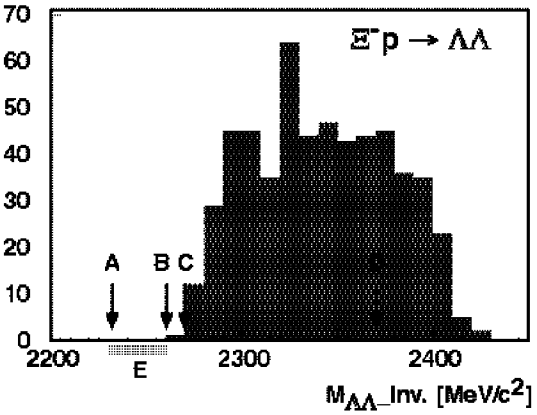

Figure 23: $\Lambda\Lambda$ invariant mass for the Ξ^-p$\rightarrow$ $\Lambda\Lambda$ reaction. It covers from 2270 MeV/c^2 to 2410 MeV/c^2. A$\sim$E in the figure represent the followings: A$\cdots$2231.4 MeV/c^2 ($2m_\Lambda$), B$\cdots$2259.6 MeV/c^2 ($m_{\Xi^-}+m_p$), Enhancements reported (as far as I know), C$\cdots$2270 MeV/c^2 B.A.Shahbazian et al., Lett. al Nuovo Cimento 6 (1973) 63 D$\cdots$2370 MeV/c^2 B.A.Shahbazian et al., Lett. al Nuovo Cimento 6 (1973) 63; P.Beilliere et al., Phys. Lett. 39B (1972) 671; not confirmed by G.Wilquet et al., Phys. Lett. 57B (1975) 97, E$\cdots$2230 - 2260 MeV/c^2 J. K. Ahn et al., Phys. Lett. B444 (1999) 267.

4 Hypernuclear γ-ray spectroscopy

H. Tamura
Tohoku University, Sendai, Miyagi 980-8578, Japan
K. Tanida
University of Tokyo, Hongo, Tokyo 113-0033, Japan
H. Outa
KEK, Tsukuba, Ibaraki 305-0801, Japan

4.1 Introduction

High-resolution γ-spectroscopy using germanium (Ge) detectors, which is one of the most powerful means to study nuclear structure, has recently been introduced in hypernuclear physics in order to drastically improve the energy resolution of hypernuclear levels from 1–2 MeV (FWHM) into a few keV (FWHM). We constructed Hyperball, a large-acceptance Ge detector array dedicated to hypernuclear γ-ray spectroscopy [1], and successfully observed hypernuclear γ transitions for the first time with Ge detectors [2, 3]. The results are shown in Fig. 24. We are presently investigating more p-shell hypernuclei for the purpose of experimentally determining ΛN spin-dependent (spin-spin, spin-orbit, and tensor) interactions(BNL E930).

These studies will be extended further and exciting new physics fields will be opened up at the 50 GeV PS. The following three subjects will be pursued.

(1) Baryon-baryon interactions

The ΛN interactions will be further studied from detailed hypernuclear level structures. The experimental information will be compared with theoretical models in order to understand the baryon-baryon interactions. In JHF, the ΛNN three-body force and charge symmetry breaking ΛN interaction will also be clarified with plenty data of hypernuclei. In addition, the $\Lambda\Lambda$ interaction will be studied from γ spectroscopy of double Λ hypernuclei, and ΞN and even ΩN interactions can be investigated by measuring X-rays from hyperon atoms.

(2) Impurity nuclear physics

Since hyperons are free from Pauli effect and feel nuclear forces different from those nucleons do in a nucleus, only one (or two) hyperon(s) introduced in a nucleus may give rise to drastic changes of the nuclear structure, such as changes of the size and the shape, change of the cluster structure, emergence of new symmetries, change of collective motions, etc. Level scheme and $B(E2)$ of Λ hypernuclei studied by γ spectroscopy will reveal such interesting phenomena, and a new field to be called "impurity nuclear physics" will be exploited.

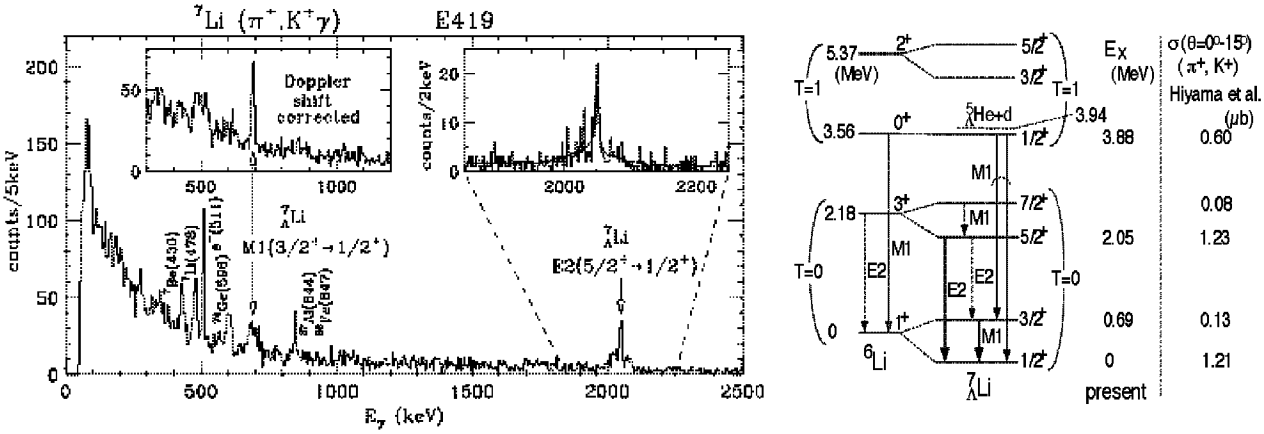

Figure 24: γ-ray spectrum of $^7_\Lambda$Li measured with Hyperball (KEK E419)(left) and the level scheme obtained from this experiment (right). We observed $M1(\frac{3}{2}^+\rightarrow\frac{1}{2}^+)$ and $E2(\frac{5}{2}^+\rightarrow\frac{1}{2}^+)$ transitions of $^7_\Lambda$Li at 692 keV and 2050 keV, respectively, and two M1 transitions from $\frac{1}{2}^+$,T=1 state to the ground state doublet. The observed $M1(\frac{3}{2}^+\rightarrow\frac{1}{2}^+)$ energy provides unambiguous information on the strength of the ΛN spin-spin interaction which was not well known. As for the $E2$ transition, the lifetime of the $\frac{5}{2}^+$ state was measured using Doppler shift attenuation method, as shown in the left inset, and $B(E2)$ was derived to be $3.6 \pm 0.5^{+0.5}_{-0.4}$ e^2fm^4. It indicates a shrinkage of the $^7_\Lambda$Li size from ^{6}Li by $19 \pm 4\%$.

(3) Medium effect of baryons

Using hyperons free from Pauli effect, we can investigate possible modification of baryons in nuclear matter, by deriving a magnetic moment of Λ from measurement of $B(M1)$ of a hypernuclei, for example.

In the following sections, we propose three types of experiments corresponding to these three physics motivations.

4.2 Spectroscopy of Light and Heavy Hypernuclei— ΛN Interactions

4.2.1 Motivation

Only some of light (mostly p-shell) hypernuclei will have been studied before the 50 GeV PS becomes available. At the 50 GeV PS, we will be able investigate almost all bound-state levels of various hypernuclei ranging, for example, from $^{12}_\Lambda$C to $^{208}_\Lambda$Pb. Measurements of γ-ray angular correlations and γ-ray polarizations allow us to assign their spin-parities. We can thus establish detailed level scheme of various hypernuclei as in the "Table of Isotopes"for normal nuclei.

The physics motivation here is to completely establish ΛN interactions and to reach complete understanding of hypernuclear structures. The ΛN effective two-body interaction may be expressed as;

$$V_{\Lambda N} = V_0(r) + V_\sigma \mathbf{s}_N \mathbf{s}_\Lambda + V_\Lambda \mathbf{l}_{N\Lambda} \mathbf{s}_\Lambda + V_N \mathbf{l}_{N\Lambda} \mathbf{s}_N + V_T[3(\boldsymbol{\sigma}_N \mathbf{r})(\boldsymbol{\sigma}_\Lambda \mathbf{r}) - \boldsymbol{\sigma}_N \boldsymbol{\sigma}_\Lambda] \quad (1)$$

The effective $s_\Lambda p_N$ (and $p_\Lambda s_N$) interactions have five radial integrals corresponding to each of these terms, denoted by V, Δ, S_Λ,S_N and T, respectively [4, 5]. These integrals can be determined phenomenologically from low-lying level structure of p-shell hypernuclei. Before we started the hypernuclear γ spectroscopy project with Hyperball, the spin-dependent terms (Δ, S_Λ,S_N and T) were not well known; the available hypernuclear data were not of sufficient quality (and quantity) to unambiguously extract them. The study of these ΛN spin-dependent interactions have recently been started using Hyperball. In KEK E419, we observed a spin-flip M1 transition between spin-doublet states in ${}^{7}_{\Lambda}$Li (see Fig. 24), which gives the strength of ΛN spin-spin interaction of Δ=0.5 MeV [2]. The subsequent experiment (E930), currently running at BNL, will determine all the other terms from γ spectroscopy of ${}^{9}_{\Lambda}$Be, ${}^{12}_{\Lambda}$C, ${}^{16}_{\Lambda}$O, etc.

However, the level energies of hypernuclei might not be able to be understood by those two body effective interactions because of the possible existence of the ΛNN three-body force. Many authors have discussed the three-body force due to intermediate Σ states (see Fig. 25) introduced by ΛN-ΣN couplings; examples include the discussion of effective ΛN spin-spin force by Gibson *et al.* [6] and Fetisov *et al.* [7], and of the ${}^{5}_{\Lambda}$He overbinding problem [8] by Akaishi [9].

Three body force caused by the diagram in Fig. 25 is expected to be stronger than the $3N$ force including the intermediate Δ states since the Σ particle in the intermediate state is only 80 MeV heavier than the Λ particle compared to the 300 MeV difference in the case of nucleon and Δ. In addition, since the ΛNN force is mediated by two pion exchange while one pion exchange between a Λ and a nucleon is forbidden by isospin conservation, relative importance of the ΛNN force to the ΛN force is expected to be large. It is also noted that the three body force cannot be studied by elastic ΛN scattering experiments.

The ΛNN force, if it is not renormalizable into two-body effective ΛN interaction, changes the level energies of hypernuclei so that they cannot be expressed with the five ΛN two body effective interactions in eq. (1). Therefore, the effect of the ΛNN force is expected to appear in inconsistency of the five parameters (Δ, S_Λ, S_N, and T) obtained from different hypernuclear states. To obtain information of the ΛNN force, plenty of hypernuclear data are required because it has larger degree of freedom than the ΛN force. Accumulation of various hypernuclear level energy data will also help us to discuss the two body interactions

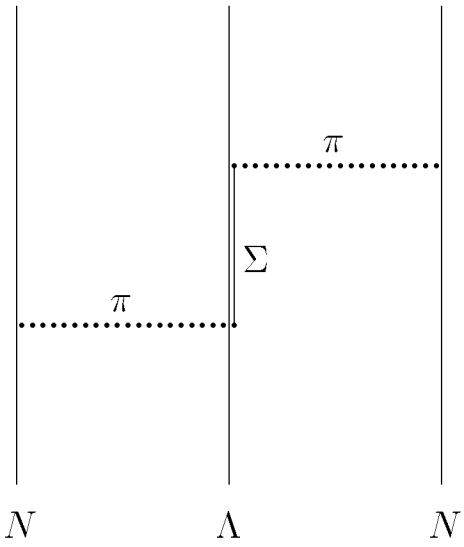

Figure 25: A diagram for the ΛNN three-body force due to intermediate Σ states introduced by ΛN-ΣN couplings.

more precisely, because it enables us to reduce uncertainties of structure of each nucleus, such as the shell-model oscillator parameter or a clustering feature.

Another very important subject in the study of ΛN interaction is the charge symmetry breaking (CSB) effect. This effect will not be able to be studied by ΛN scattering experiments, as Λn scattering experiment is almost impossible. Therefore, hypernuclei provide us with a unique laboratory to study the CSB effect in the ΛN interaction via the level energies of mirror hypernuclei.

Since the Λ has zero isospin and no charge, the Λp and Λn interactions are the same if the charge symmetry holds exactly. However, the Λ binding energies of the lightest mirror pair of hypernuclei, ${}^{4}_{\Lambda}$H and ${}^{4}_{\Lambda}$He, are

$$B_\Lambda({}^{4}_{\Lambda}\mathrm{H}) = 2.04 \pm 0.04\mathrm{MeV}, \quad \text{and}$$
$$B_\Lambda({}^{4}_{\Lambda}\mathrm{He}) = 2.39 \pm 0.03\mathrm{MeV}$$

for the ground (0^+) states and

$$B^*_\Lambda({}^{4}_{\Lambda}\mathrm{H}) = 1.00 \pm 0.06\mathrm{MeV}, \quad \text{and}$$
$$B^*_\Lambda({}^{4}_{\Lambda}\mathrm{He}) = 1.24 \pm 0.05\mathrm{MeV}$$

for the excited states (1^+) [10, 11], showing large differences of $\Delta B_\Lambda = 0.35 \pm 0.05$ MeV and $\Delta B^*_\Lambda = 0.24 \pm 0.06$ MeV for the ground and excited states, respectively. This means that the Λp interaction is more attractive than the Λn interaction, and the correction for the coulomb force makes the ΔB_Λ larger.

What is the origin of such large CSB? Several mechanisms such as Λ-Σ^0 mixing and ΛN-ΣN coupling are proposed, but still no conclusive remark is obtained yet. In order to answer the question, to investigate the spin-dependence of the CSB interaction is very important. For example, Λ-Σ^0 mixing model expects a CSB potential similar to that of the one-pion exchange, which includes spin-spin and tensor forces [12]. However, Bodmar and Usmani suggested that the CSB potential is almost spin independent based on the $A = 4$ hypernuclear data [13].

Another candidate for the origin of CSB is the ΛN-ΣN coupling effect; CSB occurs through the mass difference of the Σ's which is some 8 MeV or about 10% of the Σ-Λ mass difference. As described above, this mechanism also plays an essential role for the ΛNN three-body force. This fact implies that the CSB might appear in the ΛNN force as well as in the ΛN force. Therefore, systematic study of various mirror hypernuclei to investigate the spin dependence and possible three-body force components of CSB interaction is indispensable to understand the origin of the CSB interaction.

Such experimental information plays an essential role to discriminate and improve baryon-baryon interaction models, not only meson-exchange models but also those including quark-gluon degree of freedom, and to reach unified understanding of the baryon-baryon interactions.

Light Hypernuclei – An Example of ${}^{12}_{\Lambda}$C and ${}^{12}_{\Lambda}$B

In order to demonstrate possibilities and usefulness of hypernuclear γ-ray spectroscopy, we propose to study ${}^{12}_{\Lambda}$C and ${}^{12}_{\Lambda}$B, as the first sample, and to reveal the complete level structure of bound states. Then such studies will be extended to other hypernuclei, ${}^{13}_{\Lambda}$C, ${}^{11}_{\Lambda}$B, ${}^{15}_{\Lambda}$N, etc., and then to heavier hypernuclei.

In the case of ${}^{12}_{\Lambda}$C, a level at E_x=8.3 MeV, which is barely separated in the recent (π^+,K^+) spectrum (E369) (see Fig. 26 top) [15], is interpreted as a 2^+ state having a ${}^{11}\mathrm{C}(\frac{5}{2}^+) \otimes s_\Lambda$ ($d_N \otimes s_\Lambda$) configuration but with an admixture of ${}^{11}\mathrm{C}(J^-) \otimes p_\Lambda$ ($p_N^{-1} \otimes p_\Lambda$) configurations [16], as illustrated in Fig. 26 bottom. A small admixture of $p_N^{-1} \otimes p_\Lambda$ component makes the production cross section of this 2^+ state large. Due to such intershell coupling, a few positive parity states around 7 MeV are expected to be populated. Ref. [16] predicts the first 2^+ and 0^+ states at 7.4 and 6.7 MeV. Since they are particle bound (threshold is at 9.3 MeV), we can precisely determine their level energies from their γ transitions [1]. Their level energies contain information on the $p_\Lambda p_N$ interactions. We can also determine their spin-parities,

[1]The pure ${}^{11}\mathrm{C}(3/2^-)_{g.s.} \otimes p_\Lambda$ levels without the coupling exist at 10-11 MeV. Although these states have large production cross sections, they are above the particle emission threshold and precise energies cannot be determined from γ transitions.

which is essential because various levels with different spin-parities are expected to exist in this excitation energy region.

The level structure of ${}^{12}_{\Lambda}$B is expected to be in principle the same as that of ${}^{12}_{\Lambda}$C. By comparing the level energies of these mirror hypernuclei, we can obtain information on CSB in the ΛN interaction.

Heavy Hypernuclei – An Example of ${}^{208}_{\Lambda}$Pb

γ spectroscopy also enables us to investigate detailed low-lying level structures of medium and heavy hypernuclei. In heavy hypernuclei ($A > 150$), the energy spacing between single particle orbits of s_Λ and p_Λ is less than the nucleon emission threshold, and $p_\Lambda \rightarrow s_\Lambda$ E1 transitions can be observed. In ${}^{208}_{\Lambda}$Pb, the excitation energy of the p_Λ states was measured to be 4.5±0.6 MeV [17], being smaller than the proton/neutron separation energy of 6.7 MeV. Such E1($p_\Lambda \rightarrow s_\Lambda$) transitions are observable only in ${}^{13}_{\Lambda}$C and such heavy hypernuclei. Therefore, γ spectroscopy of heavy hypernuclei is particularly important to investigate hypernuclear structure including p_Λ levels in view of ΛN interactions.

Figure 27 shows expected low-lying level scheme and γ transitions of ${}^{208}_{\Lambda}$Pb. Here we assume one-hole configurations for ^{207}Pb core and weak coupling between a Λ and the core. γ transitions are characterized by many 4–5 MeV E1($p_\Lambda \rightarrow s_\Lambda$) transitions, some of which are followed by M1 or E2 core transitions. Here the E1 transitions for the $i_{13/2}$ hole state (1633 keV isomer of ^{207}Pb), production of which requires ΔL=7 and 5, are easily observed and identified by use of a large-momentum-transfer reaction.

4.2.2 Method and Setup

In order to produce Λ hypernuclei, we use (K^-,π^-) reaction at 1.1 GeV/c K^- in most cases. This reaction has a large spin-flip amplitude and allows population of various hypernuclear states including spin-flip states with unnatural parities. A schematic view of the setup is shown in Fig. 28.

We require a secondary beam line (K1.1) of which intensity is optimized to 1.1 GeV/c. It should have a double-stage mass separators to obtain pure K^- beams in order to minimize the counting rates of Ge detectors and tracking devices in the spectrometer. The beam intensity of 1.1 GeV/c K^- is expected to be 1.9×10^7 K^- per spill (2×10^{14} protons) in 3.4 sec cycle. We also use K1.8 beam line for the 1.8 GeV/c (K^-,π^-) reaction in order to study low-lying states of heavy hypernuclei such as ${}^{208}_{\Lambda}$Pb, which requires a larger momentum transfer to allow large ΔL transitions.

The momentum of the K^- beam is measured event-by-event with a beamline spectrom-

eter having < 0.2 % FWHM resolution. The outgoing π^- is measured with a spectrometer similar to SKS, which is required to have an acceptance of more than 50 msr and momentum resolution of < 0.2 % FWHM. The overall mass resolution better than 3 MeV is necessary. The tracking devices should be operated at a beam rate of 2×10^7 /sec, 5 times more than the present SKS case. We use scintillation fiber hodoscopes (0.5-1mm pitch) for the most upstream plane (BC1), 0.5mm pitch MWPC's for BC2-BC4 and SC1-SC2, and 3mm-pitch large-size drift chambers for SC3-SC4. The 0.5 mm-pitch MWPC's are under development at present. The other detectors are easily realized. A fast DAQ system has to be prepared which works at about 2000 trigger/sec $\times$ 1kB/event.

Around the target, we intall a Ge detector system, which is similar to the present Hyperball but has a much larger efficiency (Fig. 29). In the present design, we assume to use 14 sets of "Segmanted Super Clover Ge detectors", which has recently become commercially available. One detector set consists of four Ge crystals of 7cm$\phi\times$14 cm, and the electronode of each crystal is segmented into 4 readout channels. Such a fine segmentation is necessary for Doppler shift correction. The detectors are installed so that the crystal surface is located at least 20 cm from the target. This distance is necessary for counting rate of the detectors as well as for the Doppler shift correction. The Ge crystals cover about 40% of the total solid angle. The Ge detector system has a photo-peak efficiency of 12% at 1 MeV in total, as shown in Fig. 30. Each readout channels are connected with a transistor-reset type preamplifier and to fast readout electronics, realizing a counting-rate capability of more than 5 times higher than that of the present Hyperball. We have started developing such a readout system. Each of the Ge detector is surrounded by a set of BGO or GSO counters, which are used to veto Compton scattering and high-energy γ rays from π^0. These counters should be finely segmented to reduce the counting rate. The radiation damage of Ge detectors may be serious; according to our experience with the present Hyperball, the new Ge detectors will have to be annealed every a few weeks.

4.2.3 $^{12}_{\Lambda}$C – Yields and Expected Results

Yields

Figure 31 shows level energies, cross sections, and γ-ray branching ratios assumed in the simulation. The production cross sections of the $^{12}_{\Lambda}$C states (except for the first 2^+ state) were calculated by Itonaga *et al.* for 1.1 GeV/c (K^-,π^-) reaction [18]. The production yield of the 8.1 MeV state, assigned as the first 2^+ state, can be estimated from Fig. 26 (top) and the Itonaga's calculation, since the cross section ratio between the first 2^+ state (8 MeV) and the dominantly-populated 10–11 MeV two 2^+ states should be the same for the (K^-,π^-) and

(π^+,K^+) reactions. The energy levels are taken from the experimental values from E369 but the doublet spacing energies are taken from the new parameter set of the spin-dependent interactions by Millener [19]. The branching ratios are takes from Ref.[18] but corrected for the above excitation energies. The branching ratios from the 6 MeV 2^- state and 2^+ state are calculated assuming weak coupling limit[2]

In the yield estimation, we assumed the following values:

· K^- beam intensity: 1.9×10^7 /spill(2×10^{14}ppp)
· PS cycle: 3.4 sec
· Target: 10 g/cm^2 / A $\times6\times10^{23}$
· Effective spectrometer solid angle: $\Omega_{eff} = 0.03$ sr
· Spectrometer tracking efficiency: $\epsilon_{sp} = 0.4$
· Ge detector efficiency in Fig. 30
· Ge detector live time: $\epsilon_{Ge\ live} = 0.6$

We estimate the γ ray yields for 5 days' run as shown in Fig. 31.

Background and Simulation

In the hypernuclear γ-ray spectrum (γ spectrum after the hypernuclear bound state region is gated), the continuous background mainly comes from neutrons and π^0 emitted in hypernuclear weak decays, according to our analysis of E419 data. As we found in the E930 analysis, K^- decay in-flight also causes background in the (K^-,π^-) reaction, but after π^0 events are removed with the BGO counters, K^- decay is not a major part of the background. In addition, it can be completely removed by a kinematical cut using momentum and scattering angle of the outgoing particle.

Assuming the same continuous background level (γ-ray counts per gated event in the hypernuclear mass spectrum) as in the E419 experiment, we can simulate the spectrum for the ${}^{12}_{\Lambda}$C run. Figure 32 shows the simulated data for 5 days' run. Here the different energy dependence of the Ge detector efficiency is taken into account. We will be able to observe almost all the γ lines. Figure 33 shows some examples of γ-γ coincidence spectra. Those spectra enable us to completely reconstruct the level scheme as in Fig. 26.

[2]The 2^+ state was assumed to be coupled only to ^{11}C($\frac{5}{2}^+$), and the transition $2^+ \rightarrow 1^-_2$ is suppressed because the core transition is $\frac{5}{2}^+ \rightarrow \frac{1}{2}^-$(M2).

Angular correlations

When a hypernuclear state with spin J_1 is produced from a target nucleus with J by the (K^-,π^-) reaction with the orbital angular momentum transfer ΔL and the spin change ΔS, and then γ-decays into another state with J_2 via Eλ or Mλ transition:

$$ {}^{A}Z(J) \overset{(K^-,\pi^-)^{\Delta L,\Delta S}}{\longrightarrow} {}^{A}_{\Lambda}Z(J_1) \overset{\gamma(\lambda)}{\longrightarrow} {}^{A}_{\Lambda}Z(J_2), $$

the angular correlation exists between π^- and γ, as in the following form for ΔS=0 [3] [4]:

$$ W(\theta_{\pi\gamma}) = \sum_{M,M_1,M_2,m} \begin{pmatrix} \Delta L & J & J_1 \\ m & M & M_1 \end{pmatrix}^2 \left[\begin{pmatrix} \lambda & J_2 & J_1 \\ 1 & M_2 & M_1 \end{pmatrix}^2 + \begin{pmatrix} \lambda & J_2 & J_1 \\ -1 & M_2 & M_1 \end{pmatrix}^2 \right] |Y_m^{\Delta L}(\theta_{\pi\gamma})|^2 $$

In the case of hypernuclear productions of $\Delta L = 1$, such as productions of low-lying ($p_n^{-1}s_\Lambda$) levels of p-shell hypernuclei, the equation reduces to a simple from:

$$ W(\theta_{\pi\gamma}) \propto 1 + A cos^2\theta_{\pi\gamma}. $$

This angular correlation is much more sensitive to the spins of the states than the angular correlations between two γ's emitted in a cascade decay. In the case of ${}^{12}_{\Lambda}$C, $A = 0$, -1, 1, $-1/7$ for 0$\rightarrow$any, $1^- \rightarrow 0^-$, $1^- \rightarrow 1^-$, $1^- \rightarrow 2^-$ transitions, respectively, and $A = -27/53$ for the second γ ray in the cascade $1^- \rightarrow 2^- \rightarrow 1^-$.

Figure 34 shows simulated $\theta_{\pi\gamma}$ correlations for some of those transitions, indicating that these three types of transitions ($0^- \rightarrow 1^-$, $1^- \rightarrow 1^-$, and $1^- \rightarrow 2^-$) can be clearly discriminated in 5 days' beamtime. Combined with level scheme and γ-ray branching ratios, we can completely assign spins of all the bound states of ${}^{12}_{\Lambda}$C.

4.2.4 ${}^{12}_{\Lambda}$B – Yields and Expected Results

${}^{12}_{\Lambda}$B can be studied in a similar way as ${}^{12}_{\Lambda}$C. The difference in experimental method compared to the ${}^{12}_{\Lambda}$C case is that we use the ^{12}C(K^-,π^0) reaction instead of the ^{12}C(K^-,π^-) reaction to produce ${}^{12}_{\Lambda}$B. We require a high-resolution π^0 spectrometer, which consists of two clusters of CsI or GSO counters and sustains an effective solid angle of about 10 msr for 2γ's from π^0.

The production cross section for each of the ${}^{12}_{\Lambda}$B states by ^{12}C(K^-,π^0) is a half of the corresponding state of ${}^{12}_{\Lambda}$C by ^{12}C(K^-,π^-). By assuming the efficiency of the π^0 spectrometer to be one third of the π^- case, 30 day's beamtime is necessary to collect the number of γ-ray events as shown in Fig. 31. However, most of the other techniques equally apply to the ${}^{12}_{\Lambda}$B

[3] The spin-flip case (ΔS=1) is not calculated in Ref.[4].

experiment. As for the background, we can expect a similar or slightly lower level compared to the ^{12}C(K^-,π^-) case, since the main background source is the same and K^-in-flight decay does not contribute to the background in the (K^-,π^0) reaction.

4.2.5 $^{208}_{\Lambda}$Pb – Yields and Expected Results

We estimate γ-ray yields for $^{208}_{\Lambda}$Pb. We use the reaction ^{208}Pb$(K^-,\pi^-)^{208}_{\Lambda}$Pb at 1.8 GeV/c to efficiently populate p_Λ states coupled to the $i_{13/2}$ hole state (1633 keV isomer of ^{207}Pb). There are three possible non-spin-flip transitions, namely $i_{13/2} \rightarrow p_{1/2}$ and $i_{13/2} \rightarrow p_{3/2}$ with $\Delta L = 7$ and $i_{13/2} \rightarrow p_{3/2}$ with $\Delta L = 5$ (see Fig. 27). The cross sections of those states were calculated as shown in Fig. 35 [20].

Those populated states, $[(1i_{13/2})_n^{-1}(1p_{1/2})_\Lambda]_{7_2^-}[(1i_{13/2})_n^{-1}(1p_{3/2})_\Lambda]_{7_1^-,5^-}$, undergo 4 MeV E1$(1p_\Lambda \rightarrow 1s_\Lambda)$ transitions to the doublet (7^+, 6^+). By using the K$^-$ intensity at the K1.8 beamline (3.8×10^7/spill) and the other conditions same as in the $^{12}_{\Lambda}$C case, the expected yields for those transitions are obtained as 670 ($7_2^- \rightarrow 7^+, 6^+$ total), 390 ($7_1^- \rightarrow 7^+, 6^+$ total), and 1500 ($5^- \rightarrow 6^+$) events, respectively, for 5 days' beam time.

In the same way, other p_Λ states coupled to other hole states, $(3p_{1/2})_n^{-1}$, $(2f_{1/2})_n^{-1}$, and $(3p_{1/2})_n^{-1}$, corresponding to the ground, 570 keV, and 898 keV states of ^{207}Pb, can also be populated, and their E1$(p_\Lambda \rightarrow s_\Lambda)$ transitions can be observed (see Fig. 27). Since the production cross sections of different hole states are sensitive to the momentum transfer, we can identify initial states of γ transitions from π^--angular dependence of those γ-ray yields and/or using different (lower) incident K$^-$ momenta.

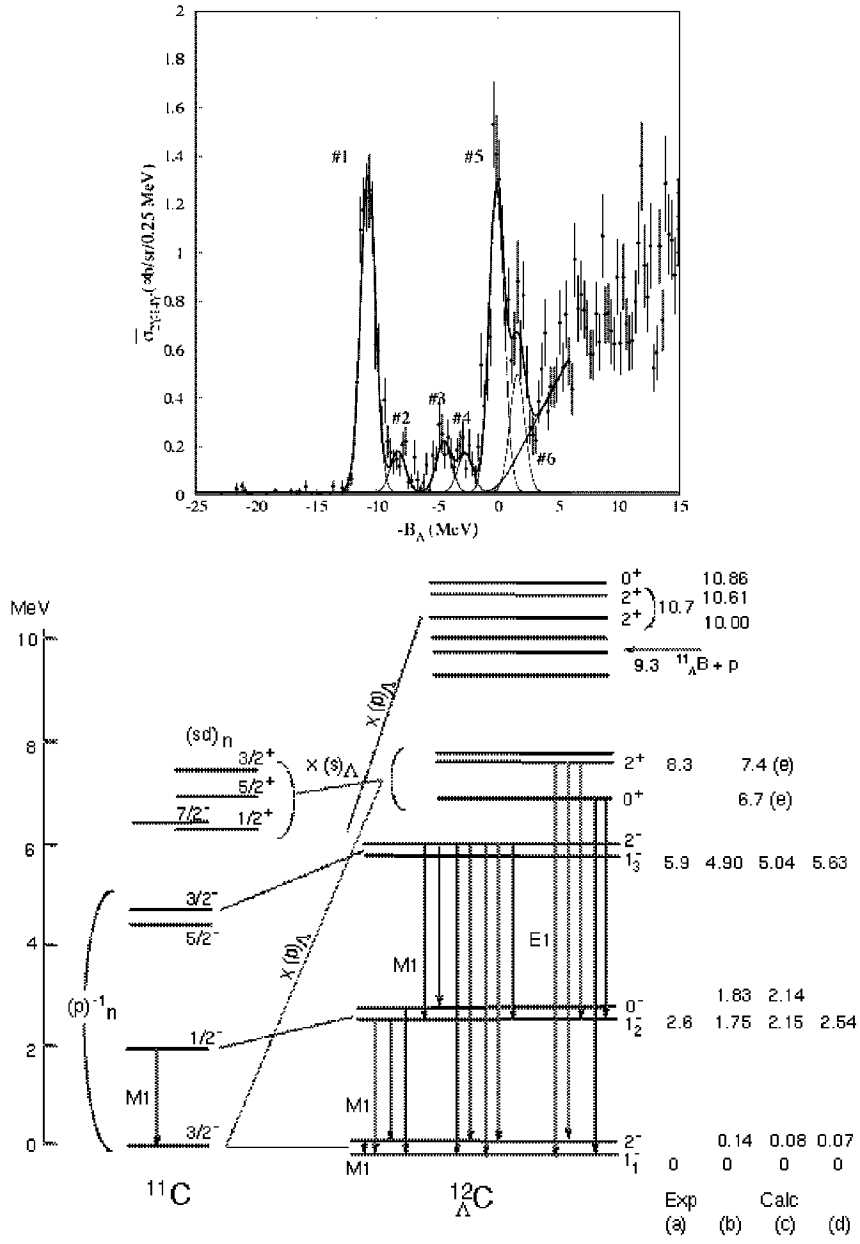

Figure 26: Top: ${}^{12}_{\Lambda}$C spectrum measured by the (π^+,K^+) reaction (KEK E369) [15]. The peaks #1, #2, #3, #4 are interpreted as 1^-_1, 1^-_2, 1^-_3, and 2^+_1 states. Bottom: Level scheme and expected γ transitions of ${}^{12}_{\Lambda}$C hypernucleus. (a) shows experimental level energies (E369), and (b), (c), (d) are calculated energies by Itonaga *et al.* [18], Fetisov *et al.* [21], and Millener *et al.* [19], respectively.

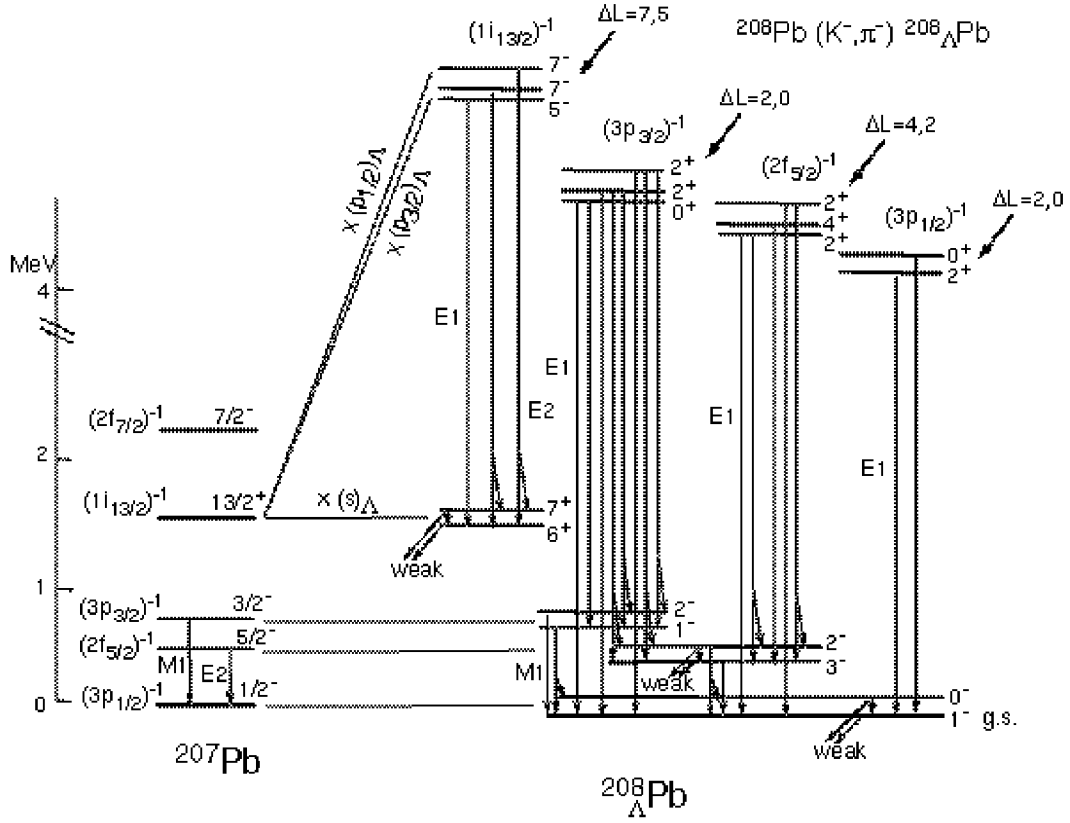

Figure 27: Expected level scheme and γ transitions of $^{208}_{\Lambda}$Pb. Only the non-spin-flip states are shown for the p_Λ states.

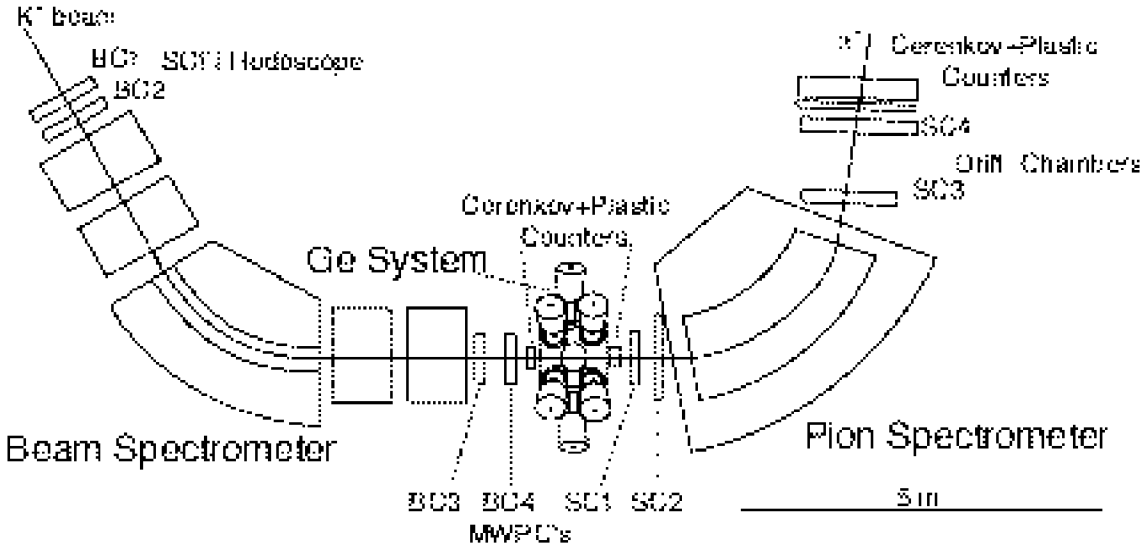

Figure 28: Setup for hypernuclear γ-spectroscopy experiments with the (K^-,π^-) reaction at K1.1 beamline.

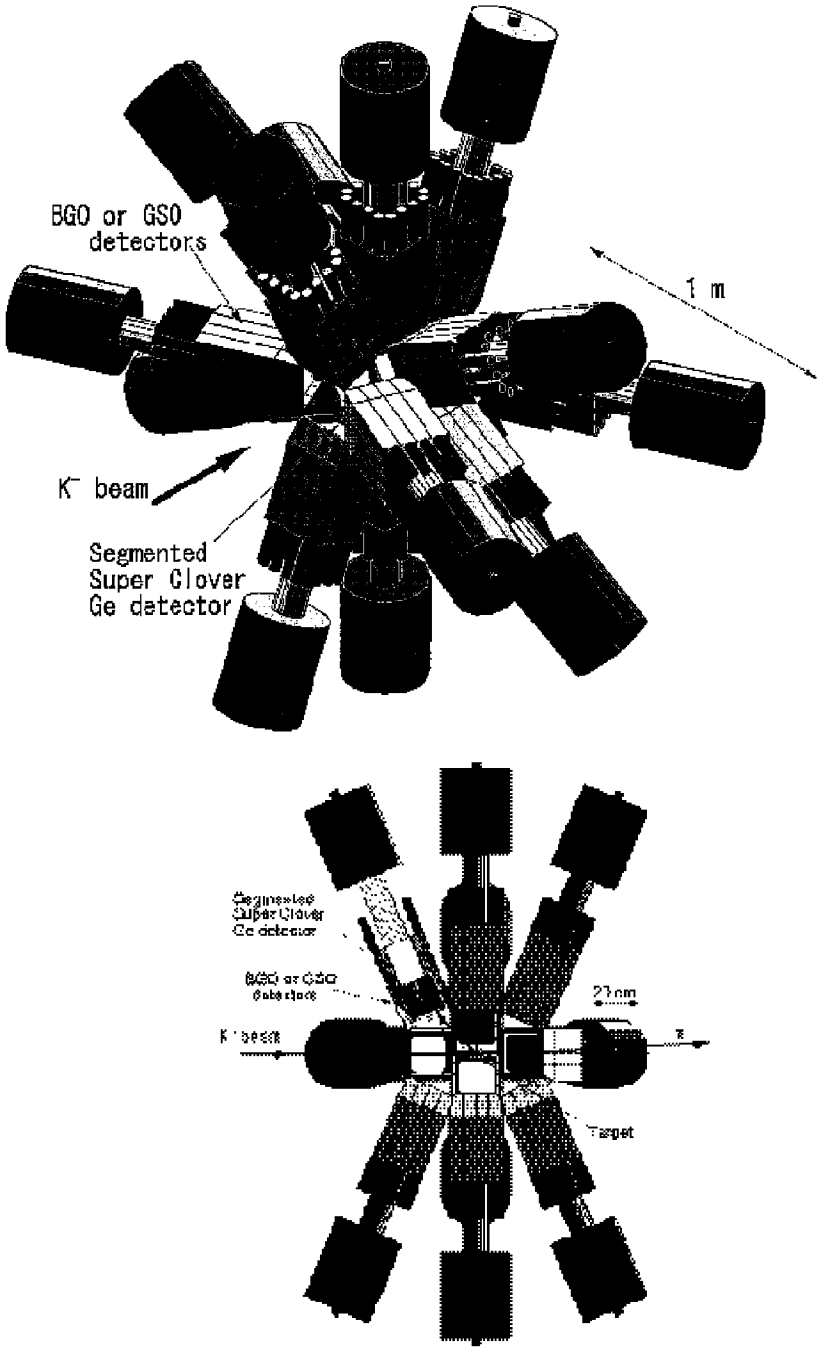

Figure 29: Ge detector system for hypernuclear γ spectroscopy.

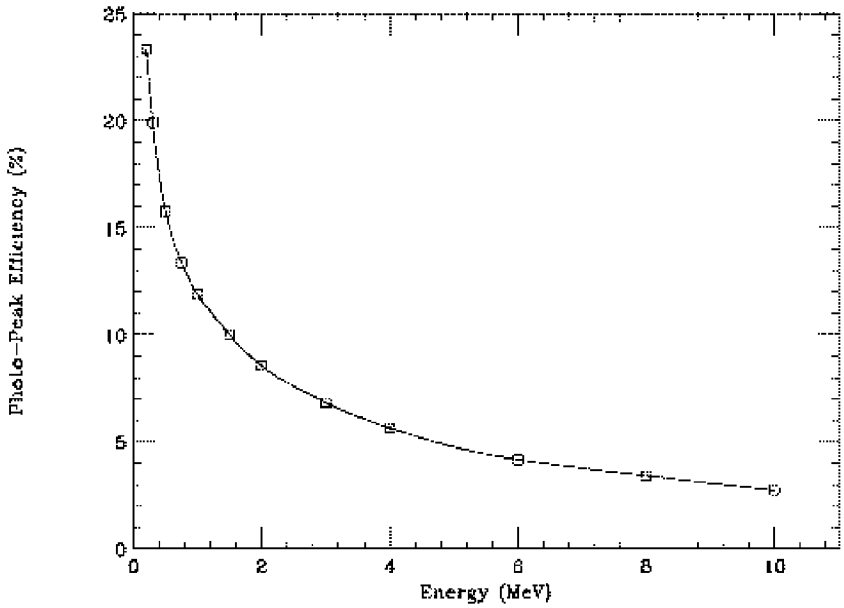

Figure 30: Absolute photo-peak efficiency of the Ge detector system which consists of 14 sets of Segmented Super Clover Ge detectors.

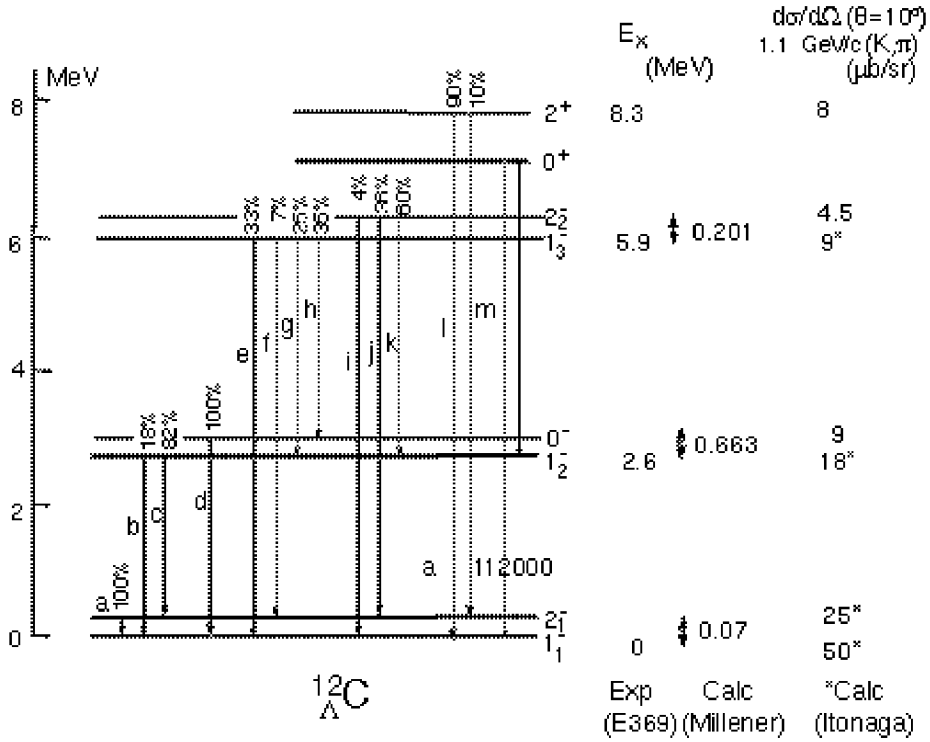

Expected Yield (5 days)

single				γγ coincidnece					
				with a		with c		with d	
		h	1700	c	1900	a	1900	h	55
b	2600	i	64	f	50	g	39		
c	12000	j	580	g	150	k	50		
d	7500	k	1400	j	94				
e	1100	l	2000	k	170				
f	240	m	230	m	31				
g	1300								

Figure 31: Top: Expected level energies and γ transitions of $^{12}_{\Lambda}$C used in the simulation. Bottom: Expected yields of γ transitions of $^{12}_{\Lambda}$C for 5 days' run. Yields of γ-γ coincidence events are also shown.

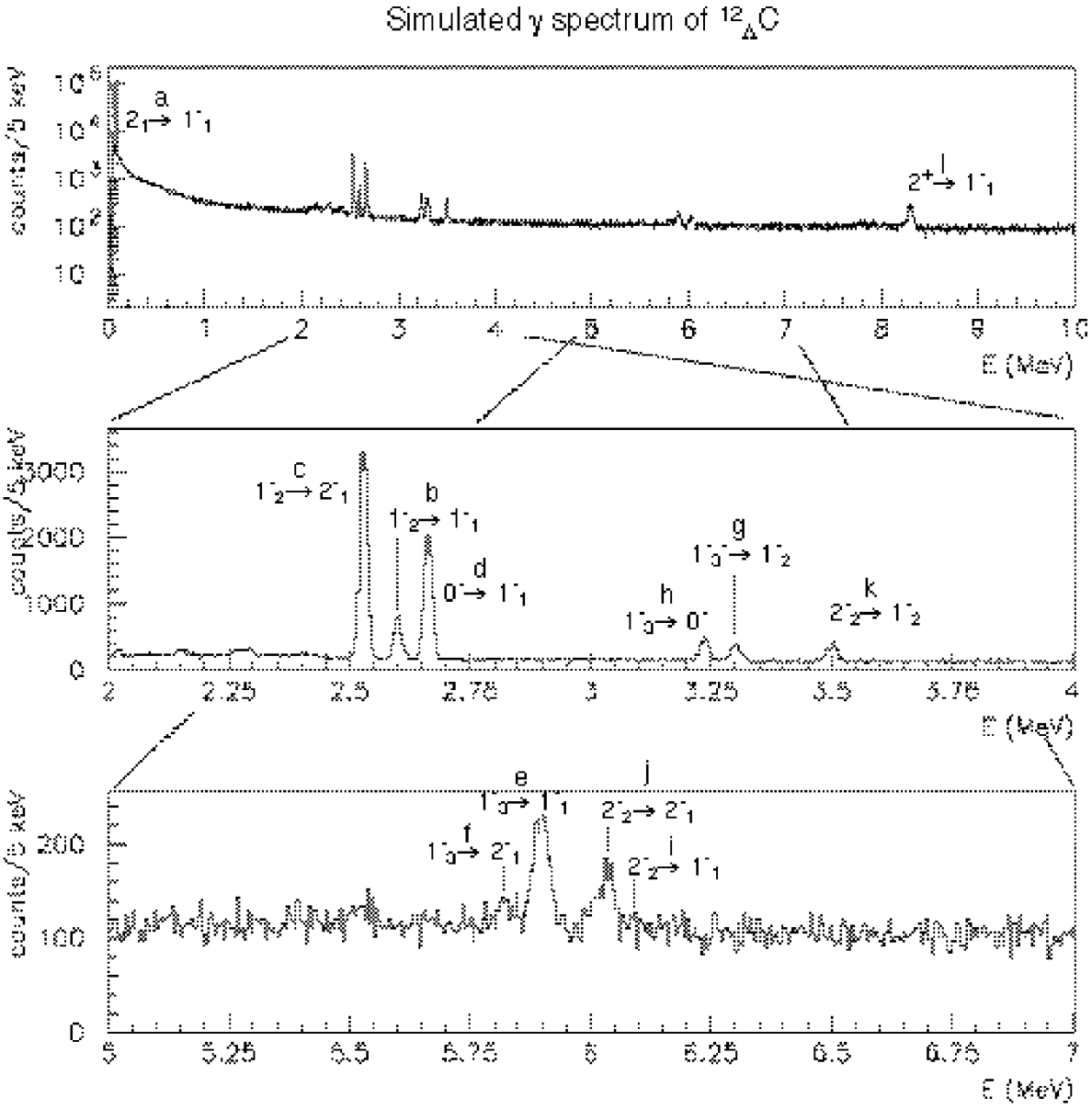

Figure 32: Simulated spectrum of $^{12}_{\Lambda}$C γ rays for 5 days' run with the (K^-,π^-) reaction at 1.1 GeV/c at the 50 GeV PS. Compton/π^0 suppression and Doppler-shift correction are applied.

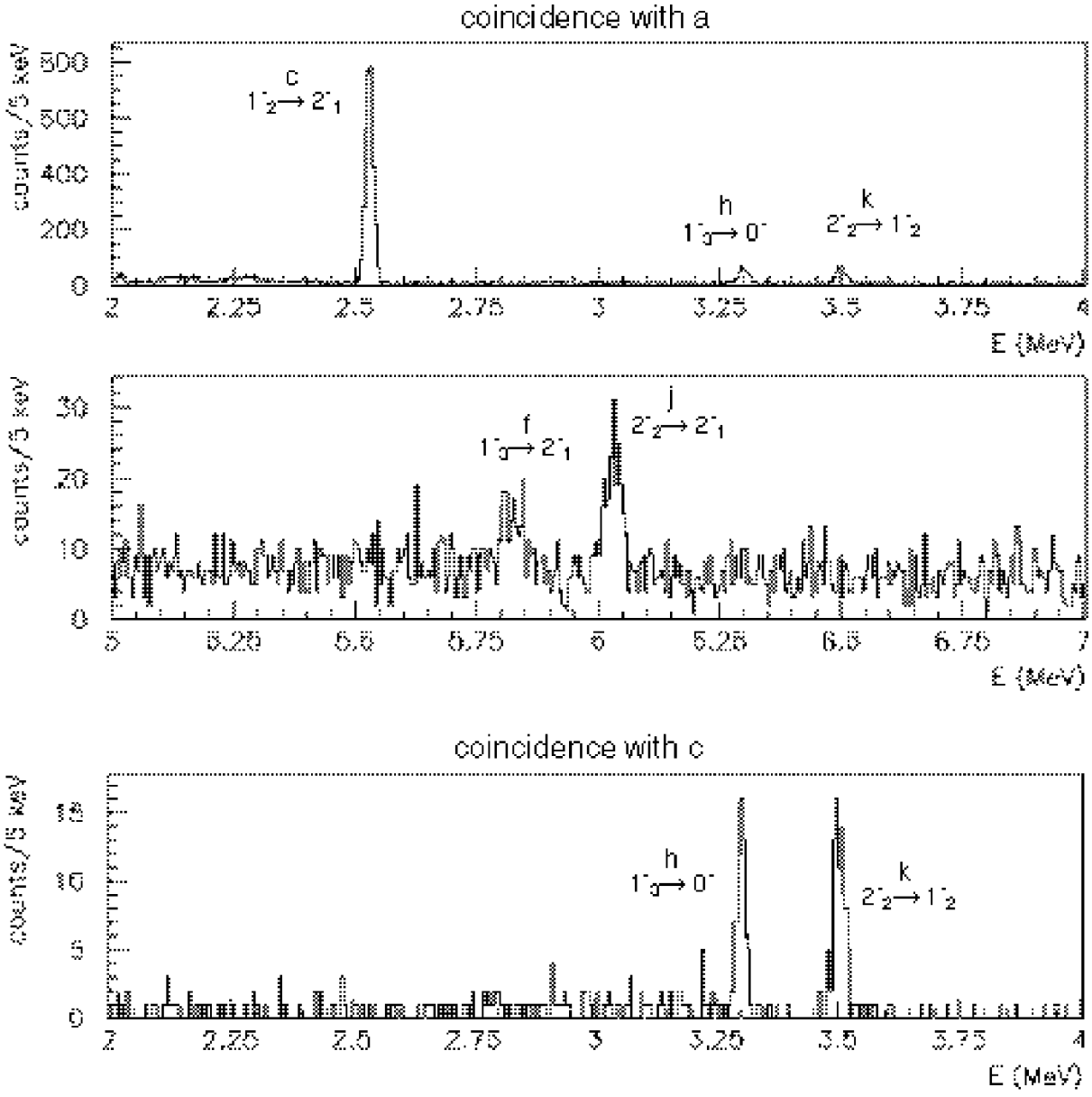

Figure 33: Simulated γ-γ coincidence spectrum of $^{12}_{\Lambda}$C. Top two: coincidence with γ-ray "a" ($1^-_2 \rightarrow 1^-_1$). Bottom: coincidence with γ-ray "c" ($1^-_2 \rightarrow 2^-_1$).

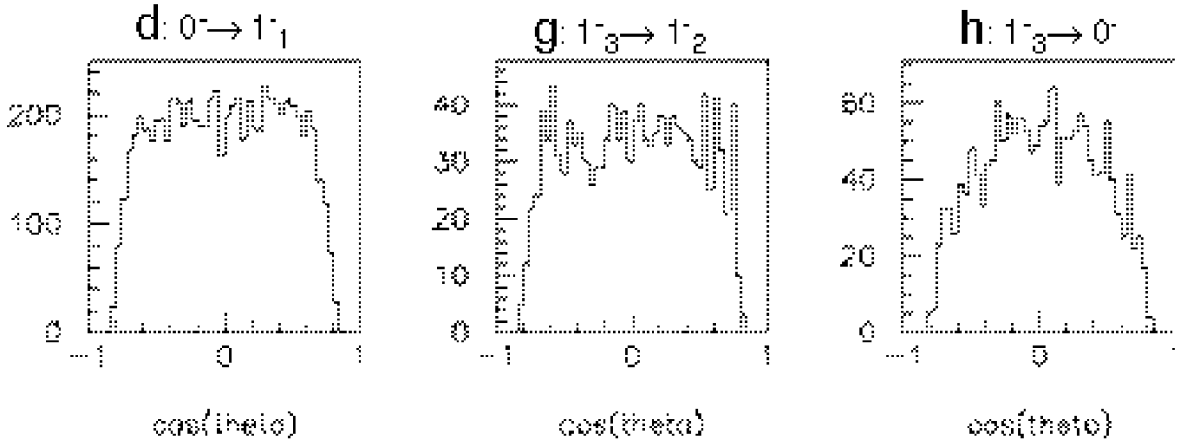

Figure 34: Angular distributions between γ and π^- for some ${}^{12}_{\Lambda}$C transitions (simulated in the same condition as the previous figures).

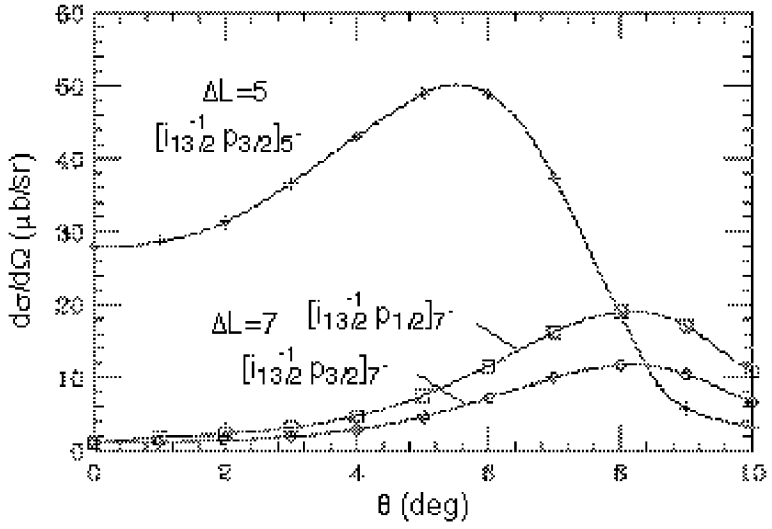

Figure 35: Calculated cross sections for the $\Delta L = 7$ transitions and for the $\Delta L = 5$ transition in the 1.8 GeV/c (K^-,π^-) reaction [20].

4.3 "Impurity Nuclear Physics" – Nuclear Structure Change Induced by Λ

4.3.1 Motivations

In KEK E419, we measured the lifetime of the $\frac{5}{2}^+$ state of ${}^{7}_{\Lambda}$Li with the Doppler-shift attenuation method and derived $B(E2;\frac{5}{2}^+ \rightarrow \frac{1}{2}^+)$ [3]. By comparing it with the $B(E2)$ of the core ^{6}Li nucleus, $B(E2;3^+ \rightarrow 1^+)$, the nuclear size was found to be contracted by 19$\pm$4% by the presence of a Λ, as predicted by Motoba *et al.* [22, 23]. Such a nuclear structure change induced by a Λ may appear in various hypernuclei. Here we propose to study two interesting hypernuclei, ${}^{7}_{\Lambda}$He and ${}^{20}_{\Lambda}$Ne, in which drastic changes of the nuclear structure are expected.

${}^{7}_{\Lambda}$He

When a Λ is added to an unstable nucleus with a nucleon halo or skin, the Λ makes the system more bound and the halo or the skin structure may disappear. ^{6}He is a neutron-rich nucleus having a two-neutron skin. The first excited state of 2^+ is observed as an unbound resonance state (see Fig. 36), but its structure is not well known; the $B(E2;2^+ \rightarrow 0^+)$ has not been experimentally obtained.

Figure 36 shows the expected level scheme and the density distribution of valence neutrons of ^{6}He(2^+) and ${}^{7}_{\Lambda}$He calculated by Hiyama with a cluster model of $\alpha + n + n$ and ${}^{5}_{\Lambda}$He$+n+n$ [24, 25]. When a Λ is added to ^{6}He, the neutron skin in the ground state is expected to shrink. The ^{6}He(2^+)$+s_\Lambda$ state, which has widely-spread two valence neutrons, becomes bound, and the core E2 transition ($\frac{5}{2}^+,\frac{3}{2}^+ \rightarrow \frac{1}{2}^+$) is observed. $B(E2)$ of ^{6}He($2^+ \rightarrow 0^+$) is calculated to be $0.58e^2$fm^4, while the corresponding $B(E2)$ of ${}^{7}_{\Lambda}$He is calculated to be 0.068 and 0.059 e^2fm^4 for $\frac{5}{2}^+ \rightarrow \frac{1}{2}^+$ and $\frac{3}{2}^+ \rightarrow \frac{1}{2}^+$, respectively [25]. The predicted change of $B(E2)$ is caused by a drastic change of valence neutrons in ^{6}He induced by a Λ.

In the present case, these E2 transitions are competing against weak decay. If we assume the weak decay rate of these states to be (200 ps)$^{-1}$, then their lifetimes are 140 ps and 170 ps, and the branching ratios for the E2 γ-transitions are 42% and 17%. We will directly measure the lifetimes of these excited states with weak-decay particles (π^- and proton). Combined with the branching ratios of those E2 transitions, the $B(E2)$'s can be derived.

${}^{20}_{\Lambda}$Ne

${}^{20}_{\Lambda}$Ne is an particularly interesting hypernuclei, because it is presicted that an addition of a Λ changes the ground-state parity from positive to negative.

Figure 37 shows expected relevant low-lying levels and transitions of ${}^{20}_{\Lambda}$Ne. The left part of Fig. 37 is expected from a naive picture, where energies of (0^+,1^+) and 1^- states are

taken from a shell-model calculation [5]. The right part shows a result of the cluster model calculation by Sakuda and Bando [26]. Here the negative-parity states of which structure is ${}^{16}_{\Lambda}$O(p-hole state) + ^{4}He have much lower energies than the 0^+ and 1^+ doublet of the ^{16}O + ${}^{4}_{\Lambda}$He structure. It is because the negative-parity states in ^{19}Ne having a well-clusterized structure of ^{15}O(p-hole state of ^{16}O) + ^{4}He shrinks when a Λ is added, while the positive parity states having ^{16}O + ^{3}He structure is not well-clusterized but rather spherical and thus shrinkage by a Λ is expected to be smaller, as illustrated in Fig. 38.

As shown in Fig. 37, expected γ transitions in each case are completely different from each other. In the latter case, the γ transitions stem mainly from the population of the 2^+ state which has a sizable cross section in the (K^-,π^-) reaction. As shown in Fig. 37, the cross section of ${}^{20}_{\Lambda}$Ne was assumed to be the same as that of ${}^{18}_{\Lambda}$O, which was calculated for 0.8 GeV/c (K^-,π^-) reaction by Yamada *et al.* [27]. By observing all the transitions shown in Fig. 37 we can reconstruct the level scheme and assign spin parities in the same way as the ${}^{12}_{\Lambda}$C example in the previous section, and determine weather the ground state parity is positive or negative.

In addition, the structure of ${}^{20}_{\Lambda}$Ne, particularly its ground-state doublet, will give us information on the effective ΛN spin-dependent interactions in the *sd*-shell region, which will then be theoretically discussed in relation to the spin-dependent interactions derived from *p*-shell hypernuclei.

4.3.2 ${}^{7}_{\Lambda}$He – Setup and Yields

We use the ^{7}Li(K^-,π^0) reaction with 0.8 GeV/c K$^-$ beam from the K1.1 beam line. We use the π^0 spectrometer explained in Section 4.2.4. For this experiment, the spectrometer should have a better energy resolution of 1.5 MeV FWHM at 0.7 GeV/c, in order to separately identify production peaks for the $\frac{5}{2}^+$+$\frac{3}{2}^+$ states and the $\frac{1}{2}^+$ states which are 1.7 MeV apart from each other.

In order to measure the lifetime of the excited states with weak-decay particles, we install the "decay arm" counter system which consists of fast plastic counters and a stack of plastic counters as described in Section 4.4.2. The yields of weak-decay particles and γ rays are estimated by assuming the following conditions.

· K^- beam intensity: 2.2×10^6 /spill(2×10^{14}ppp)
· PS cycle: 3.4 sec
· Target: 10 g/cm^2 /7 ×6×10^{23}
· Cross section: $d\sigma/d\Omega(\frac{5}{2}^+, T=1) \sim 25$ μb/sr at 10^0

· Branching ratio for E2 γ ray: 42%[4]
· Spectrometer solid angle: $\Omega_{eff} = 0.01$ sr
· Spectrometer tracking efficiency: $\epsilon_{sp} = 0.4$
· Ge detector efficiency : $\epsilon_{Ge} = 0.09/2$ at 1.7 MeV
· Ge detector live time: $\epsilon_{Ge\ live} = 0.6$
· Efficiency for weak decay particle: $\epsilon_{weak} = 0.1$

We expect 1700 events for weak decay particles and 330 events for the E2 γ rays in 10 days' beamtime. Statistical accuracy for $B(E2)$ will be better than 10%, although it may have a systematic error from decomposition of the $\frac{5}{2}^+, T = 1$ peak from the $\frac{1}{2}^+, T = 1$ peak in the (K^-,π^0) spectrum. The resolution of the π^0 spectrometer is a key issue.

4.3.3 $^{20}_{\Lambda}$Ne – Setup and Yields

We use the (K^-,π^-) reaction at 1.1 GeV/c or at 0.8 GeV/c with the K1.1 beam line. The spectrometer system is the same as that used in the $^{12}_{\Lambda}$C experiment in the previous section. The yields of γ rays are estimated as shown in Table 5. All the E1 and M1 transitions shown in Fig. 37 can be easily identified, and the level scheme can be reconstructed from $\gamma\gamma$ coincidence in a few days beamtime.

[4]Roughly estimated from calculated ΔL=1 states of $^{12}_{\Lambda}$C at 0.8 GeV/c and calculated $^{12}_{\Lambda}$C and $^{7}_{\Lambda}$Li states at different conditions [18, 28].

Table 5: Yield estimation of γ-transitions of $^{20}_{\Lambda}$Ne for the two cases of level energies predicted by Millener *et al.* [5] and by Sakuda-Bando [26]. We used cross sections for the (K^-,π^-) reaction at 0.8 GeV/c and θ=10^0.

Hypernuclei	$^{20}_{\Lambda}$Ne(Millener *et al.*)		$^{20}_{\Lambda}$Ne(Sakuda-Bando)	
Transition	$1^- \rightarrow 0^+, 1^+_{gsd}$	$1^+ \rightarrow 0^+$	$2^+ \rightarrow 2^-, 1^-_2, 1^-_1$	$1^-_2 \rightarrow 1^-_1, 0^-_{gsd} etc.$
	E1	spin-flip M1	E1	M1
γ energy (MeV)	0.70, 0.45	0.25 [a]	1.72, 1.47, 1.34	0.38, 0.25,..
K^- beam/spill	2.2×10^6 K^-			
$d\sigma/d\Omega$	200 μb/sr [a]		45 μb/sr [b]	
γ branching ratio	0.65, 0.35	0.35	??	??
Target	10 g/cm^2 / 20 $\times6\times10^{23}$			
Effective solid angle Ω_{eff}	0.03 sr			
Tracking eff. ϵ_{sp}	0.4			
Ge eff. ϵ_{Ge}	0.17, 0.21	0.27	0.12	$\sim$0.20
Ge live time $\epsilon_{Ge\ live}$	0.6			
	$\times60\times60/3.4$ spills$\times24$ hours			
Yield/24 hours	2700, 1800	2300	660 (E1 total)	??

[a] Estimated by Millener *et al.* [5]

[b] Estimated by Motoba [28].

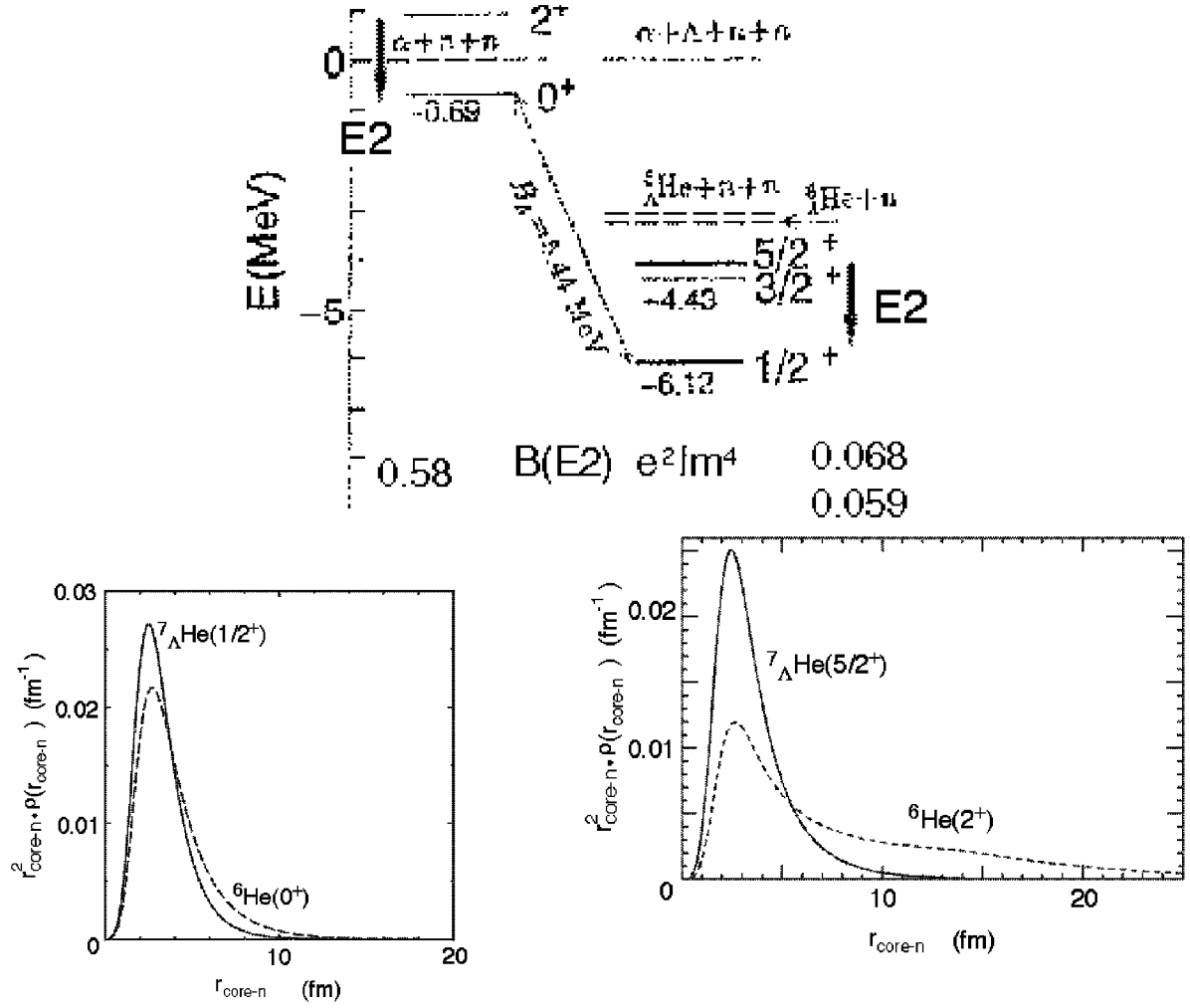

Figure 36: Top: Expected level scheme of ${}^{7}_{\Lambda}$He and $B(E2)$ calculated by Hiyama *et al.* with a 3-body (α (${}^{5}_{\Lambda}$He) $+n+n$) cluster model [24]. Bottom: Calculated density distribution of valence neutrons are compared for ^{6}He(0^+) and in ${}^{7}_{\Lambda}$He($\frac{1}{2}^+$) and for ^{6}He(2^+) and in ${}^{7}_{\Lambda}$He($\frac{5}{2}^+$) [25].

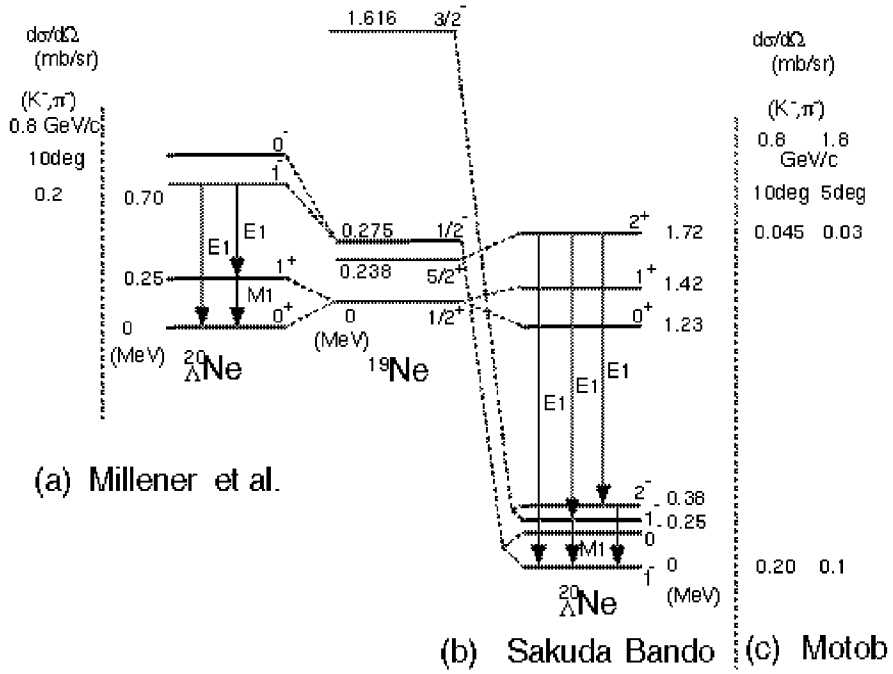

Figure 37: Level scheme and transitions of ${}^{20}_{\Lambda}$Ne. The expected level scheme and the cross section are calculated by Millener *et al.* with the shell model (left part) [5] and with the cluster model by Sakuda and Bando (right part) [26]. (c) shows estimated cross sections by Motoba [28] from calculated ${}^{18}_{\Lambda}$O cross sections by Yamada *et al.* [27]

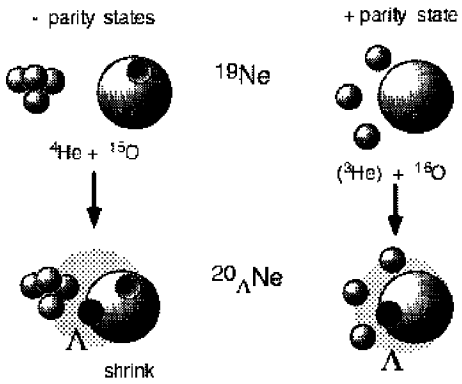

Figure 38: Cluster-model prediction of shrinking effect of ${}^{20}_{\Lambda}$Ne. When a Λ is added, the negative-parity states having the α-^{15}O cluster structure shrinks more than the positive-parity states having a compact (shell-like) structure.

4.4 $B(M1)$ Measurement — g-Factor of Λ in Nuclear Matter

4.4.1 Motivation

Measurement of magnetic moments of a Λ in nuclear matter is an interesting subject. If the size of a baryon is changed in a nucleus by possible partial deconfinement of quarks, the magnetic moment of the baryon may be changed in a nucleus. A Λ particle in a hypernucleus is the best probe to see such an effect. Possible effects are estimated with the quark cluster model [29]. In addition, we can extract effects of the meson-exchange current between a Λ and a nucleon, which may be totally different from the NN case because one-pion exchange is forbidden in the ΛN interaction but $\Lambda\Sigma$ coupling makes another effect, sa calculated by Saito *et al.* [30]. However, measurement of magnetic moments of Λ hypernuclei is extremely difficult with meson beams, and a new approach using heavy ion beams is being proposed.

On the other hand, we propose here to measure probabilities of the spin-flip M1 transition ($B(M1_{sf})$) between the ground-state doublet for various hypernuclei. The doublet states are expected to have almost the same nuclear structure except for the spin direction of the Λ, and thus the $B(M1_{sf})$ is related to the g-factor of Λ as [4]:

$$B(M1_{sf}) \propto | < \phi_{lo}|\mu|\phi_{up} > |^2 = | < \phi_{lo}|g_N\mathbf{J}_N + g_\Lambda\mathbf{J}_\Lambda|\phi_{up} > |^2 \propto (g_N - g_\Lambda)^2$$

where g_N and g_Λ denote effective g-factors of the core nucleus and the Λ, and $\mathbf{J}_N$ and $\mathbf{J}_\Lambda$ denote their spins, respectively. Here the space components of the wavefunctions of the lower and upper states of the doublet (ϕ_{lo}, ϕ_{up}) are assumed to be identical.

4.4.2 Methods – Doppler Shift Attenuation Method and γ-Weak Coincidence Method

In order to measure γ-transition probabilities such as $B(M1)$ and $B(E2)$, we need to know a lifetime of the excited state which undergoes the transition. If the excited state also has other decay branches such as weak decay or other γ-transitions, we also need to measure the branching ratio of the particular transition.

Here we proposal two different methods of the $B(M1)/B(E2)$ measurement, depending on the lifetime of the upper state. Figure 39 shows lifetime ranges to which these methods can be applied, together with the E1/M1/E2 lifetimes for one Weisskopf unit as a function of the transition energy. When the lifetime is $10^{-12} \sim 10^{-11}$ sec, Doppler-shift attenuation method is used to measure the lifetime. When it is comparable to the weak decay lifetime of Λ ($\sim 10^{-10}$ sec), we propose to use the "γ-weak coincidence" method. For shorter lifetimes than 10^{-13} sec, Coulomb excitation may be used in some cases using a "hypernuclear beam" produced from ion beams in the projectile rapidity region.

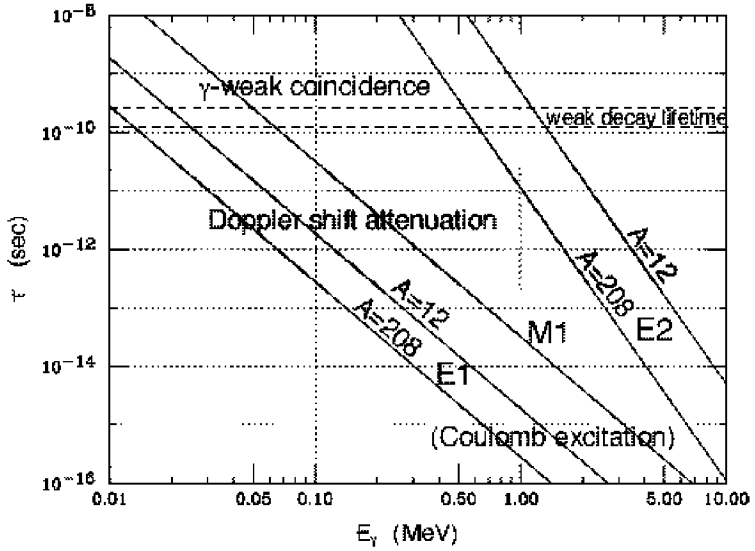

Figure 39: Lifetime ranges to which Doppler-shift attenuation method and γ-weak coincidence method can be applied for transition probability measurement of hypernuclei, shown together with the E1/M1/E2 lifetimes for Weisskopf unit as a function of the transition energy.

In the fist case, we need to choose the optimum reaction (the velocity of recoil hypernucleus) and the target density so that the lifetime of the excited state and the stopping time in the target shall be comparable. The γ-ray peak shape which is partly-broadened by Doppler shift gives lifetime of the state, as we did in the $B(E2)$ measurement of ${}^{7}_{\Lambda}$Li in E419.

In the second case, as explained in Fig. 40, we measure the lifetime of the upper state B directly from the time difference of hypernucleus production and the emission of weak decay particles (protons or π^-) in coincidence with γ-transitions of $B \to A$. The time spectrum of weak-decay particles measured in coincidence with the $B \to A$ γ ray is expressed as:

$$P^{B\to A}(t) = \frac{\lambda_A \lambda_B}{\lambda_B - \lambda_A}\, m\, N_B^0\, (e^{-\lambda_A t} - e^{-\lambda_B t}),$$

where λ_B and λ_A denote the total decay rates of B and A, N_B^0 denotes the initial population of the state B, and m is the branching ratio of the $B \to A$ transition. From this growth-decay function, we can determine λ_B and λ_A.

In order to obtain the $B(M1; B \to A)$ value, we also need to know the branching ratio m. It is measured from the γ-ray yield of $B \to A$ in coincidence with the $C \to B$ transition. If there are no γ transitions like $C \to B$ from upper state, we need to separate B and A in the (K^-,π) spectrum production, which is usually almost impossible for spin doublet states.

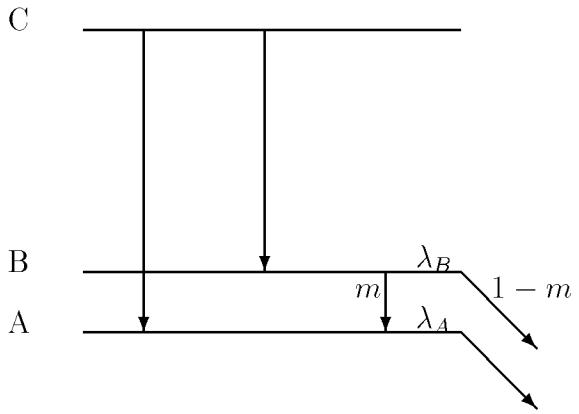

Figure 40: Method of $B(M1)$ measurement from coincidence events of γ-ray and weak-decay particles.

It is noted that when the $B \to A$ γ transition is much slower than the weak decay and this transition is suppressed, the number of γ-weak coincidence events decreases and thus the sensitivity for λ_B deteriorates. In such a case, however, λ_B can be determined from the time spectrum of weak-decay particles in coincidence with C$\to$B γ rays, which is approximately a single exponential decay with λ_B. In general, the time spectrum measured in coincindece with the γ ray (C$\to$B) is:

$$P^{C\to B}(t) = \lambda_B \; N_B^0 \; [\; (1 - m\frac{\lambda_B}{\lambda_B - \lambda_A}) \; e^{-\lambda_B t} + m\frac{\lambda_A}{\lambda_B - \lambda_A} \; e^{-\lambda_A t}].$$

By measuring both of $P^{B\to A}(t)$ and $P^{C\to B}(t)$ and fitting them together to the equations above, we can precisely determine λ_B for a wide range of λ_B. The sensitivity of the $B(M1)$ measurement is discussed in the following sections.

4.4.3 Setup for γ-Weak Coincidence Method

The setup for the γ-weak coincidence measurement is shown in Fig. 41. A half of the Ge detectors in Fig. 29 are replaced by two sets of "decay arm" similar to those used in our previous experiment of hypernuclear lifetime measurement (KEK E307) [31]. The solid angle for the decay particles is about 30% of 4π sr.

Just upstream of the target we install fine-segmented fast plastic scintillation counters which give start-timing signals. In the decay arm, fast scintillators for stop-timing signals are installed as close as possible to the target, and then silicon strip detectors (SSD) are installed to track the decay particles. Behind them are a stack of scintillation counters for dE/dx and range measurements. Protons and pions are identified and their velocities are measured

from the range, dE/dx, and TOF information. According to our previous experience (E307), we can achieve 200 ps FWHM as the overall time resolution of the hypernuclear lifetime. Considering the emission rate of energetic protons or π^- used for lifetime measurement, the efficiency for weak-decay particles will be about 10%.

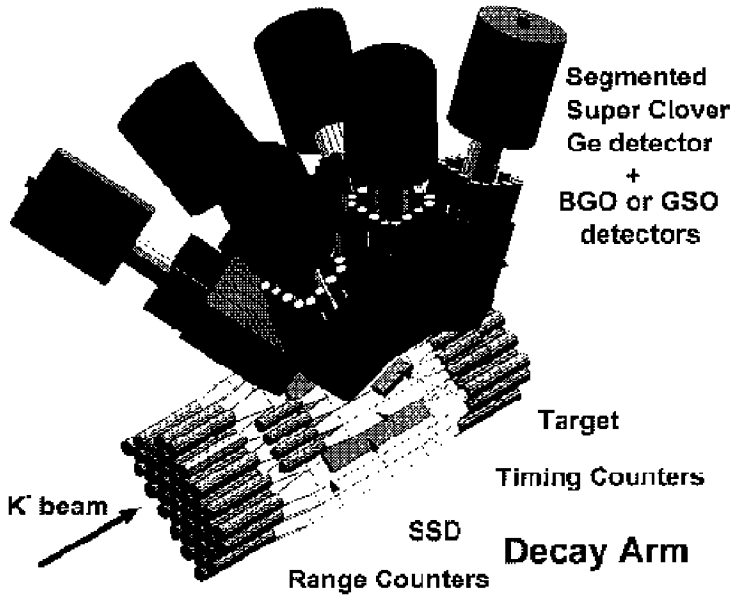

Figure 41: A half side of the setup for the weak-γ coincidence experiments to measure $B(M1)/B(E2)$ using the lifetime measurement with weak-decay particles.

4.4.4 Expected Results – $^{12}_{\Lambda}$C Case

We consider the case of $^{12}_{\Lambda}$C for example. According to the Millener's latest calculation with the new parameter set of the ΛN spin-dependent interactions from our E419 result, the ground-state doublet spacing of $^{12}_{\Lambda}$C is predicted to be 0.071 MeV. The $B(M1)$ of this transition is predicted to be 0.44 μ_N^2 [4], which corresponds to the decay rate of (360 ps)$^{-1}$ for 0.071 MeV. By assuming that the weak decay rate of the upper (2^-) state is the same as that of the ground (1^-) state, (228 ps)$^{-1}$, we estimate the branching ratio of the γ transition to be m=0.39.

We use the 1.1 GeV/c (K^-, π^-) reaction to efficiently populate the 2^- state. We assume the same beam/spectrometer conditions and use the cross sections and γ-ray branching ratios in Fig. 31. We also assume the following conditions:

· K^- beam intensity: 1.9×10^7 /spill(2×10^{14}ppp)
· PS cycle: 3.4 sec
· Target: 10 g/cm^2 / A $\times6\times10^{23}$
· Cross section $\times$ branching ratio: $d\sigma/d\Omega(1^-)_{total} = 47\mu$b/sr at 10^0
· Effective spectrometer solid angle: $\Omega_{eff} = 0.03$ sr
· Spectrometer tracking efficiency: $\epsilon_{sp} = 0.4$
· Ge detector efficiency : $\epsilon_{Ge} = 0.10$ at 0.071 MeV
· Ge detector live time: $\epsilon_{Ge\ live} = 0.6$
· Efficiency for weak decay particle: $\epsilon_{weak} = 0.1$

Then we expect 15000 γ-weak coincidence events in 400 hours' run for m=1. Here, those events in which the 2^- state is populated via γ-ray cascade from upper excited states are included, because all those preceding trasitions are M1 or E1 with high energies ($>$ 2 MeV), being thus much faster than the 0.07 MeV spin-flip M1 transition, and does not affect the time distribution of the weak decay after the spin-flip M1 transition.

In order to estimate accuracy of the $B(M1)$ measurement, we made a simulation of λ_B measurement for the case of $^{12}_{\Lambda}$C. Figure 42shows simulated time spectra of the weak-decay particles in coincidence with the spin-flip M1($2^- \rightarrow 1^-$) transition and in coincidence with the upper $1^-_2 \rightarrow 2^-$ transition, for various cases of the spin-flip transition rate. Figure 43 shows sensitivity of $B(M1)$ determination in the present conditions. Only statistical errors are included. The beamtime of 400 hours allows us to measure the $B(M1)$ within 5% statistical error for a wide range of $B(M1)$ = 0.1–10 μ_N. Although there may exist systematic errors of $\sim$5% in the branching ratio (m) and the lifetime (λ_B), we can determine $B(M1)$ within 10% error in total.

4.5 Further Possibilities

4.5.1 Spectroscopy of Double Λ Hypernuclei — $\Lambda\Lambda$ Interactions

The γ-ray spectroscopy of double Λ hypernuclei is one of the most important subjects to be pursued at the 50 GeV PS. Level structures of double Λ hypernuclei give us information on the $\Lambda\Lambda$ interaction not only for the central force but also the spin-orbit force between two Λ's. They also provide information on the $\Lambda\Lambda$-ΞN coupling and a possible H-dibaryon-like correlation between two Λ's in a nucleus.

${}^{4}_{\Lambda\Lambda}$H

As an example, we take ${}^{4}_{\Lambda\Lambda}$H, where nucleon spin-flip M1 transition, $0^+ \to 1^+$, can be observed around 3 MeV if both states are particle bound. ${}^{4}_{\Lambda\Lambda}$H are produced as a hyperfragment from the Li(K^-, K^+) reaction. We assume the following conditions to estimate the γ-ray yield:

· K^- beam intensity: 3.8×10^7 /spill(2×10^{14}ppp)
· PS cycle: 3.4 sec
· Beam time: 10 days
· Target: 20 g/cm^2 / 7 $\times6\times10^{23}$
· Effective spectrometer solid angle: $\Omega_{eff} = 0.10$ sr
· Spectrometer tracking efficiency: $\epsilon_{sp} = 0.4$
· Ge detector efficiency: $\epsilon_{Ge} = 0.065$ at 3 MeV
· Ge detector live time: $\epsilon_{Ge\ live} = 0.6$

Here we use the intense K$^-$ beam from the K1.8 beamline. We assume using the SKS spectrometer having the acceptance ~ 0.10 sr for K^+ detection. The cross section for the quasi-free production of Ξ^- is taken to be 81 μb/sr, derived from ^{12}C data (99 μb/sr) and mass dependence ($A^{0.38}$) [14]. The formation probability of ${}^{4}_{\Lambda\Lambda}$H(0^+) state for quasi-free Ξ^- production events is assumed to be 0.06% using a theoretical estimate of the production rate for a double-Λ compound nucleus with ^{12}C target (0.3%) [32] and assuming the decay branching ratio of the compound nucleus to the ${}^{4}_{\Lambda\Lambda}$H(0^+) state of 20%.

With those assumptions, the expected yield for the γ-transition is 3100 counts. The background level is estimated to be 3×10^4 counts/100 keV using the same estimation method as described in Section 4.2.3 with the number of quasi-free Ξ^- production events (2×10^8). Thus the γ-ray peak would be clearly observed.

It is easy to identify the observed γ-ray peak as the one from the $M1(0^+ \to 1^+)$ transition in ${}^{4}_{\Lambda\Lambda}$H. From the double charge exchange Li(K^-, K^+) reaction only $Z = 0$ and $Z = 1$ fragments can be produced. With this condition, very limited (hyper-)nuclear species can be produced, among which only ${}^{4}_{\Lambda}$H and ${}^{4}_{\Lambda\Lambda}$H are expected to emit γ-rays. As we know the γ-ray energy of ${}^{4}_{\Lambda}$H is 1.04 MeV, we can safely assign the 3 MeV γ-ray to the $M1(0^+ \to 1^+)$ transition in ${}^{4}_{\Lambda\Lambda}$H. It is noted that when we take into account weak decays of (double-)Λ hypernuclei, single-Λ hypernuclei of $Z = 2$ and normal nuclei of $Z = 2$ and 3 can also be produced, but all possible γ-transitions in those (hyper-)nuclei are known.

Furthermore, this γ-ray assignment can be supported by taking γ-γ coincidence. The

ground state of ${}^{4}_{\Lambda\Lambda}$H (1^+) is expected to decay by

$$ {}^{4}_{\Lambda\Lambda}\mathrm{H} \rightarrow {}^{4}_{\Lambda}\mathrm{H}({}^{4}_{\Lambda}\mathrm{He}) + \pi^0(\pi^-) $$

with large branching ratios (~ 0.5 in total). Here, the excited states (1^+) of ${}^{4}_{\Lambda}$H(${}^{4}_{\Lambda}$He) are favorably populated over the ground states (0^+), because the spin non-flip amplitude is much larger than the spin-flip amplitude in the mesonic weak decay [33]. Therefore, we can detect 1.1 MeV γ-rays from ${}^{4}_{\Lambda}$H(${}^{4}_{\Lambda}$He) in coincidence with the ${}^{4}_{\Lambda\Lambda}$H γ-rays. Using the branching ratio above and the γ-ray detection efficiency in Fig. 30, we expect 110 counts for the γ-γ coincidence events.

${}^{13}_{\Lambda\Lambda}$B

One of the most important experiments for double Λ hypernuclei is to detect E1($p_\Lambda \rightarrow s_\Lambda$) transitions of ${}^{13}_{\Lambda\Lambda}$B. The energy difference of E1 γ transitions of $p_{3/2\ \Lambda}s_\Lambda \rightarrow s_\Lambda s_\Lambda$ and $p_{1/2\ \Lambda}s_\Lambda \rightarrow s_\Lambda s_\Lambda$ provides valuable information on the spin-orbit force between two Λ's. ${}^{13}_{\Lambda\Lambda}$B was produced in the KEK E176 experiment from Ξ^- absortion in emulsion (probablly on ^{14}N), although another assignment to ${}^{10}_{\Lambda\Lambda}$Be cannot be excluded for this double hypernuclear event [34]. According to the E176 result, the yield of ${}^{13}_{\Lambda\Lambda}$B, including the π^- mesonic decay branching ratio, may be of the order of one out of 78 stopped Ξ^- from about 800 events of the quasi-free Ξ^- prodiction in the (K^-,K^+) reaction. This corresponds to the E1($p_\Lambda \rightarrow s_\Lambda$) gamma-ray yield of the order of 100 in 10 days' beamtime at the 50 GeV PS. So this experiment seems to be feasible, although more information on the production and decay of ${}^{13}_{\Lambda\Lambda}$B is necessary.

4.5.2 Spectroscopy of Neutron-Rich Λ Hypernuclei

As described for ${}^{7}_{\Lambda}$He, halo and skin structures of neutron-rich nuclei are expected to be drastically changed when a Λ is added. By using the (K^-,π^+) 2-step reaction, we can produce neutron-rich hypernuclei such as ${}^{9}_{\Lambda}$He, ${}^{11}_{\Lambda}$Li, ${}^{12}_{\Lambda}$Be, ${}^{13}_{\Lambda}$Be, etc. and investigate their structures with γ spectroscopy. Thier level scheme and $B(E2)$'s will give us information of neutron halo structures and their response by a Λ. Particularly interesting is the ${}^{11}_{\Lambda}$Li case, where the core ^{10}Li is unbound but an addition of a Λ will make a few states bound.

Although the cross sections of the (K^-,π^+) reaction seems to be a few orders of magnitude lower than the (K^-,π^0), (K^-,π^-) reactions, those neutron-rich hypernuclei may be possibly produced with high-intensity K$^-$ beam from the 50 GeV PS.

References

[1] H. Tamura, Nucl. Phys. **A639** (1998) 83c.

[2] H. Tamura *et al.*, Phys. Rev. Lett **84** (2000) 5963.

[3] K. Tanida *et al.*, Proc. Int. Symp. on Strangeness Nuclear Physics, February 1999, Seoul; K. Tanida, Ph.D thesis, Univ. of Tokyo (2000); to be published.

[4] R.H. Dalitz and A. Gal, Ann. Phys. **116** (1978) 167; J. Phys. G 6 (1978) 889.

[5] D.J. Millener, A. Gal, C.B. Dover, R.H. Dalitz, Phys. Rev. **C31** (1985) 499.

[6] B. F. Gibson, I. R. Afnan, J. A. Carlson and D. R. Lehman, Prog. Theor. Phys. Suppl. **117** (1994) 339.

[7] V. Fetisov, Proc. APCTP workshop on Strangeness Nuclear Physics (SNP'99), ed. I. T. Cheon, S. W. Hong and T. Motoba, (World Scientific Publishing Singapore), in press.

[8] R. H. Dalitz, R. C. Herndon and Y. C. Tang, Nucl. Phys. **B47** (1972) 109.

[9] Y. Akaishi, Proc. APCTP workshop on Strangeness Nuclear Physics (SNP'99), ed. I. T. Cheon, S. W. Hong and T. Motoba, (World Scientific Publishing Singapore), in press.

[10] R. Bertini *et al.*, Phys. Lett. **83B** (1979) 306.

[11] M. Bedjidian *et al.*, Phys. Lett. **62B** (1976) 467; ibid. 83B (1979) 252.

[12] M. M. Nagels, T. A. Rijken and J. J. de Swart, Ann. Phys. **79** (1973) 338; Phys. Rev. **D12** (1975) 744; ibid. **D15** (1977) 2547; ibid. **D20** (1979) 1633.

[13] A. R. Bodmar and Q. N. Usmani, Phys. Rev. **C31** (1985) 1400.

[14] T. Iijima *et al.*, Nucl. Phys. **A546** (1992) 588.

[15] H. Hotchi, Ph.D thesis, University of Tokyo (2000).

[16] T. Motoba, Nucl. Phys. **A639** (1998) 135c.

[17] T. Hasegawa *et al.*, Phys. Rev. **C 53** (1996) 1210.

[18] K. Itonaga *et al.*, Prog. Theor. Phys. Suppl. **117** (1994) 17.

[19] D.J. Millener, Proc. Int. Conf. on "Hypernuclear Physics with Electromagnetic Probes" (HYPJLAB99), Hampton (1999).

[20] D.J. Millener, private communication (1999).

[21] V.N. Fetisov, L. Majling, J. Žofka and R.A. Eramzhyan, Z. Phys. **A339** (1991) 399.

[22] T. Motoba, H. Bandō and K. Ikeda, Prog. Theor. Phys. **80** (1983) 189.

[23] E. Hiyama, M. Kamimura, K. Miyazaki and T. Motoba, Phys. Rev. **C59** (1999) 2351.

[24] E. Hiyama, *et al.*, Phys. Rev. **C 53** (1996) 2075.

[25] E. Hiyama, private communication (2000).

[26] T. Sakuda and H. Bando, Prog. Theor. Phys. **78** (1987) 1317.

[27] T. Yamada, T. Motoba, K. Ikeda and H. Bando, Prog. Theor. Phys. Suppl. **81** (1985) 104.

[28] T. Motoba, private communication (1995,1996,1999).

[29] T. Takeuchi, K. Shimizu, K. Yazaki, Nucl. Phys. **A481** (1988) 693.

[30] K. Saito, M. Oka, T. Suzuki, Nucl. Phys. **A625** (1997) 95.

[31] H. Bhang *et al.*, Phys. Rev. Lett. **81** (1998) 4321.

[32] Y. Yamamoto, M. Wakai, T. Fukuda, M. Sano, Prog. Theor. Phys. **88** (1992) 1163.

[33] T. Motoba and K. Itonaga, Prog. Theor. Phys. Suppl. **117** (1994) 477.

[34] S. Aoki *et al.*, Prog. Theor. Phys. **85** (1991) 951; K. Imai, Nucl. Phys. A547 (1992) 199.

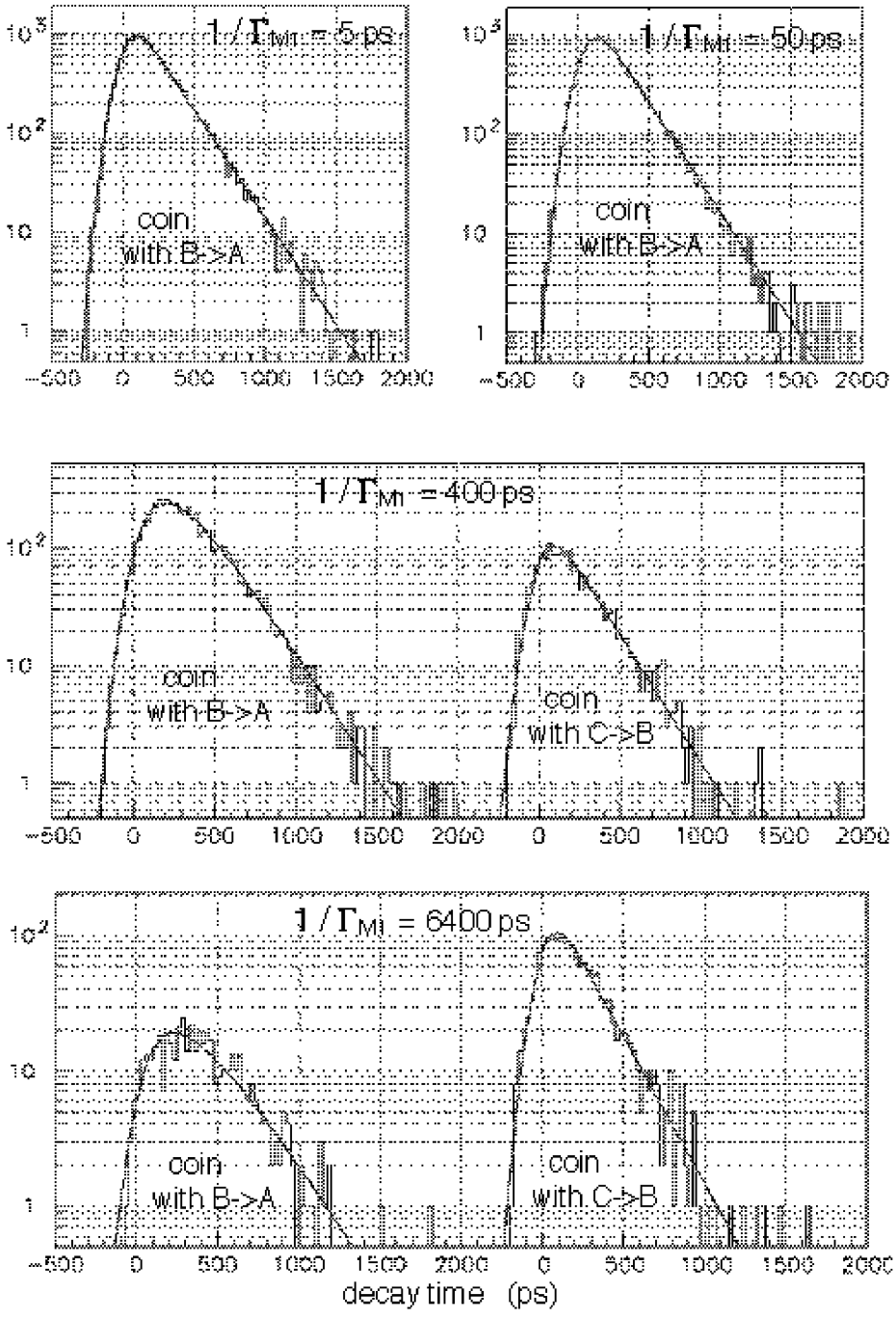

Figure 42: Simulated time spectrum of weak-decay particles of ${}^{12}_{\Lambda}$C measured in coincidence with B$\rightarrow$A (the spin-flip M1($2^- \rightarrow 1^-$) transition) and with C$\rightarrow$B (the $1^-_1 \rightarrow 1^-$ transition) for various values of the B$\rightarrow$A (spin-flip M1) transition rate (Γ_{M1}). A time resolution of 200 ps FWHM is folded. By fitting these two histograms simultaneously to the expected functions (see text), both decay rates λ_A and λ_B can be determined within 5% statistical errors.

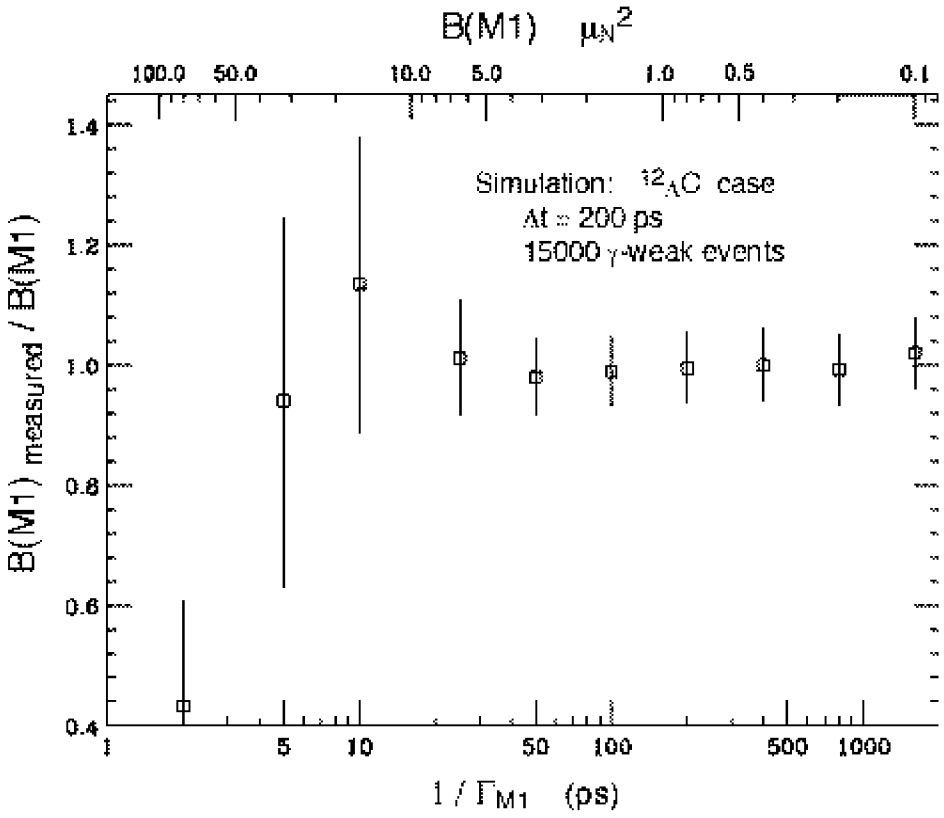

Figure 43: Sensitivity of $B(M1)$ measurement for the $^{12}_{\Lambda}$C case. See text for the conditions of the simulation.

5 High-Resolution Reaction Spectroscopy of S=−1 Hypernuclei

H. Noumi
KEK, Tsukuba, Ibaraki 305-0801, Japan
O. Hashimoto, T. Takahashi, Y. Fujii
Tohoku University, Sendai, Miyagi 980-8578, Japan

High-resolution hypernuclear spectroscopy opens a new frontier in hypernuclear physics. Recent progress provided by the super-conducting kaon spectrometer SKS should be particularly remarkable. In fact, SKS demonstrated a lot of new features of hypernuclei with its high resolution of better than 2 MeV in FWHM, and brought new unsolved problems (Appendix A). We therefore propose **a high-resolution beam line** in order to proceed further high-resolution hypernuclear spectroscopy. This beam line enables us to reach **a few hundred keV** in resolution, which is almost one order of magnitude better than that obtained with SKS. Design of the beam line has already been reported elsewhere [1], however the specification is summarized in appendix B. In the beam line, we could expect not only to resolve open problems but also to proceed new spectroscopic investigations on hypernuclei.

Here, it should be noted on advantages of the present high-resolution reaction spectroscopy;
1) high production rate of hypernuclei enables a series of systematic measurements in reasonably short period.
2) Particularly, hyperon-binding energies of the ground and excited states including particle-unbound states or ones with small production cross section could be directly measured.
One may mind spectroscopy with germanium gamma-ray detector. There is no doubt that its superior performance in resolution is quite powerful in many (hyper)nuclear spectroscopic investigations, as proposed in another part of this letter of intent. However, it is not always mighty. It usually requires to produce large amount of hypernuclei in order to compensate its low detection efficiency. In principle, it is not useful for the stable state against gamma decays. Therefore, the high-resolution reaction spectroscopy is necessary and plays a complimentary role of high-resolution gamma-ray spectroscopy with germanium detectors.

Below, we introduce some typical experimental programs to show the feasibility of the high-resolution spectroscopy with proposed high-resolution beam line. A prospect of the high-resolution spectroscopy to be proceeded in JHF will be mentioned at the end.

5.1 Experimental Programs

5.1.1 Fine structure of Λ-single particle potential

Motivation

It is one of main purposes in hypernuclear physics to know details of the mean field potentials of nuclear matter with hyperons. We know the magic number of ordinary nuclei is characterized by the spin-orbit potential. In lambda hypernuclei, however, the magnitude of the spin-orbit potential is still unclear. In the p-shell hypernuclei, it is suggested that the ΛN spin-orbit interaction is much (a several times) smaller than the NN one. On the other hand, fairly large splitting was observed in the Λ-shell orbital state of ${}^{89}_{\Lambda}$Y. If the splitting is due to the Λ-spin-orbit potential, there is a discrepancy on the spin-orbit interactions in light and heavy system. In the spectrum, one can see sizable strength around the splitting states, which could be significant contributions from Λ states coupled to deeper neutron-hole states. In order to obtain the conclusive result, **further decomposition of the spin-orbit splitting states** from the core-excited states is necessary. Namely, much higher-resolution spectroscopy is required to resolve fine structure of the spectrum. The high-resolution beam line is thus indispensable.

Expected spectrum

Fig. 44 shows a simulated excitation energy spectrum produced via the (π^+, K^+) reaction on ${}^{90}_{\Lambda}$Zr, based on the theoretical calculation with Wood-Saxon + S.O. type one-body potential. Here, the momentum resolutions for the beam line and the spectrometer are assumed to be both 10^{-4}. The energy straggling effect is taken into account due to the finite target thickness, 1mm(0.653g/cm^2) of zirconium. The energy resolution of **300 keV** in FWHM is achievable. The spin-orbit splitting states for f_Λ and d_Λ are clearly separated. Even for p_Λ may be decomposed. The core-excited states are expected to be broader due to their intrinsic widths, thus could be distinguished.

Yield estimation

According to the measurement for ${}^{89}_{\Lambda}$Y [2], the ground state of ${}^{90}_{\Lambda}$Zr is expected to be 0.6 μb/sr. It is well agreed with the theoretical calculation [3]. Below is shown estimated production rate for the ground state in second:

$$\begin{aligned} \text{Rate(cps)} &= I_{Beam}(\text{cps}) \times N_t(\text{cm}^{-2}) \times \frac{d\sigma}{d\Omega}(\mu\text{b/sr}) \times \Delta\Omega(\text{sr}) \times 10^{-30}(\text{cm}^2/\mu\text{b}) \times \varepsilon_{K^+} \\ &= 10^9 \times \frac{0.1 \cdot 6.53}{90} \cdot 6.022 \times 10^{23} \times 0.016 \times 0.6 \times 10^{-30} \times 0.1 \end{aligned}$$

$$= \quad 0.004,$$

where I_{Beam} and N_t are beam intensity per second and the number of target, respectively. $\Delta\Omega$ and ε_{K^+} are the solid angle of the kaon spectrometer and the kaon survival rate with respect to the kaon flight length of 12.4m, being 16 msr and 0.1, respectively. The kaon spectrometer requires the tracking devices only at the focal plane. Thus, their efficiency should be taken into account, which is expected to be 0.8. Kaon identification may be one of the key issue in the present system. The most probable and usual way is to reconstruct the mass from measured momentum and beta (time of flight). In the case, the mass resolution is determined almost only by the resolution of beta. Taking the time resolution of 0.2ns, we estimate expected mass resolution to be as good as 20 MeV/c^2, even when the flight length is set to be 1m. Taking 3σ for the kaon mass gate width, the contamination would be outside of 10σ. Thus, sufficiently good resolution is expected to separate kaons from pions and protons. However, measurement of the time of flight must be done behind the focal place, which sacrifices the kaon survival rate. In case of 1m flight path, another 20% of kaon would be lost.

After all, we have to take into accout the kaon detection and identification efficiency of 0.8^3=0.5, where another factor of 0.8 for DAQ live time is assumed in addition.

In summary, we expect **170 counts/day** for the ${}^{90}_{\Lambda}$Zr ground state (0.6μb/sr). This is surprisingly high count rate. Thus, systematic measurements of heavy Λ-hypernuclear structure can be done with high precision in a short period.

5.1.2 Precision spectroscopy of light hypernuclei

Motivation

In 1995, core-excited states in ${}^{12}_{\Lambda}$C produced by the (π^+, K^+) reaction were discovered at KEK[4]; two small peaks inbetween well-known two prominent peaks were found. Among two small peaks, for higher one in excitation energy, it is pointed out that a simple configuration of a Λ coupled to a core-nucleus state does not seem to reproduce the excitation energies. Further microscopic treatment in theoretical calculations is required. Recently, an idea of **inter-shell mixed configuration** to describe core excited states is proposed by Motoba *et al.*[5]. In this model, core-nucleus excited states with different parity coupled to the different Λ-orbits can be contributed to describe $1\hbar\omega$ excited configurations (Fig. 45).

If it is true, a several states with different spin-parity may be populated as core-excited states. In fact, the observed peak looks broader than experimental resolution so that it can be decomposed into two states in peak fitting. Further fine structure of the core-excited states have to be clarified.

Yield estimation

In case of (π^+, K^+) on 0.2 g/cm^2 ^{12}C, for the state with the production cross section of 0.1μb/sr, one can accumulate **100 counts within a day**. Fine structure of different spin-parity states can be investigated very efficiently.

5.1.3 Spectroscopy of neutron-halo Λ hypernuclei

Motivation

Mean field potential for Λ in different nuclear density is of much interest. Precision spectroscopy of Λ **hypernuclei with neutron halos** would provide information on the **Λ-neutron and Λ-neutron-matter interactions**. Properties of neutron-halos may be modified to the embedding of a Λ hyperon. D. E. Lanskoy and his co-workers examined the response of neutron-single particle energy in ${}^{12}_{\Lambda}$Be with different ΛN interactions [6]. They found the level scheme of neutron-single particle energy is dependent on the strength of ΛNN force, as shown in Fig. 46.

However, two step reaction process must be required to reach neutron-halo Λ hypernuclei. The high-resolution and high-sensitivity is required to investigate such hypernuclei. The high-resolution beam line is thus best-suited for the present purpose.

Feasibility

Let us consider the case of ^{12}C$(\pi^-, K^+)^{12}_{\Lambda}$Be. Production cross section could be approximately estimated by taking a product of two single-step cross sections:

$$\begin{aligned} d\sigma/d\Omega|_{(\pi^-,K+)} &= \sigma(\pi^-,\pi^0)/(\pi R^2) \times d\sigma/d\Omega|_{(\pi^0,K^+)} \\ &\sim 0.3(\mathrm{mb})/300(\mathrm{mb}) \times 0.01(\mathrm{mb/sr}) = 10(\mathrm{nb/sr}). \end{aligned}$$

Here, πR^2 represents the cross section of the target nucleus seen by the intermediate π^0. Another two-step process, $(\pi^-, K^0) \rightarrow (K^0, K^+)$, could contribute to the production and is expected to be the same order of magnitude. Using 0.6g/cm^2 thick carbon target, about **20 counts/day** could be observed.

5.1.4 Spectroscopy of Σ hypernuclei

Motivation

The spectroscopic study of Λ hypernuclei have been relatively being in progress. Particularly, recent high-precision hypernuclear spectroscopy with a high-resolution magnetic spectrometer and/or a germanium gamma-ray detector array made it possible to resolve the states

split by the ΛN spin-dependent interaction, such as the spin-orbit and spin-spin forces, which were too small to observe before. On the other hand, the study of Σ-hypernuclei is still at the very beginning stage. In other words, our knowledge of the Σ-nucleus potential, even in its size, is quite primitive.

In order to understand the baryon-baryon interactions not only in free space but also in baryonic matter in extended flavor space, it is necessary to investigate nuclei including other octet-strange baryon(s) like Σ, $\Xi(\Lambda\Lambda)$, and so on. In particular, The ΣN interaction is important and closely related to the ΛN interaction through mixing since Σ's mass differs only 80 MeV from Λ's. We wish to proceed the Σ-hypernuclear study as well as the Λ-hypernuclear study in order to understand the baryon-baryon interaction further more.

In addition, recently, it becomes one of hot subjects to see a role of strangeness in high-density nuclear matter which might be realized in neutron stars or supernovas. Namely, in **a neutron star with hyperons** such as Λ or Σ^-, K^-, and/or strange-quark matter may have **different mass and radius** from that without strangeness. This may change a formation scenario of a neutron star and blackhole and the thermal and structural evolution of a neutron star. In this regards, it is of particular importance to investigate the Σ-nucleus potential through spectroscopic study of Σ hypernuclei.

Σ-hypernuclear bound state

Owing to the repulsive nature of the Σ-nucleus potential at the nuclear surface (Fig. 47-left), one may observe the narrow peak structure of the **Coulomb-Assisted Hybrid Σ-hypernuclear Bound States (CAHBS)**. Fig. 47-right shows calculated ${}^{208}_{\Sigma^-}$Hg spectrum produced by the (π^-, K^+) reaction [7]. According to theoretical calculation, the ${}^{208}_{\Sigma^-}$Hg $[p^{-1}_{h11/2}, \Sigma_{1h}]$ an $[p^{-1}_{h11/2}, \Sigma_{1i}]$ states may be populated by the (π^-, K^+) reaction, which are 2 MeV apart from each other and have the widths of 1.6 MeV and 0.2 MeV, respectively. Utilizing the high-resolution beam line, these states can be seen. Detailed information on the Σ-nucleus potential could be extracted.

Yield estimation

The cross section of CAHBS is expected to be as small as 0.1μb/sr. Since the wave function of the state is defusing out of the nucleus, the overlapping of the wave with the nuclear core becomes small. This causes the state width deu to absorption small but also makes the production cross section small.

Expected yield is estimated to be about **10 counts/day**, for the lead target of 0.6g/cm^2. This count rate is sufficiently high, and hence, the experiment could be carried out within

reasonably short period.

5.2 Impact for Other Facilities in the World

At present, there is no facility, other than TJNAF, which has and demonstrates any hypernuclear production systems with high-resolution at the level of sub-MeV. TJNAF-CEBAF provides high-quality electron beam up to 6 GeV, and hence, enables to carry out high-resolution spectroscopic investigations via the $(e, e'K^+)$ reactions.

Since the $(e, e'K^+)$ reaction involves the charge transfer of ΔZ=-1, neutron-rich Λ hypernuclei can be produced. Using the nuclear target of isospin equal to 0, one can investigate mirror hypernuclei of those obtained via the ΔZ=0 reaction like (π^+, K^+). Therefore, TJNAF plays **a complimental role** to JHF in hypernuclear studies.

Intense primary electron beam compensates small cross section of the $(e, e'K^+)$ reaction. It is, however, practically limited to increase beam current since the accidental rate increases deu to bremsstrahlung. As the same reason, it is hard to go to heavy target for precision hypernuclear spectroscopy. Hadron-induced reaction is therefore much advantageous to produce hypernuclei efficiently.

5.3 A Prospect for High-Precision Hypernuclear Spectroscopy

The high-intensity pion beam allows us to carry out **hypernuclear decay spectroscopy with high precision**. In this beam line, the differential decay widths ($\mathrm{d}\Gamma/\mathrm{d}E$ and $\mathrm{d}\Gamma/\mathrm{d}\theta$, energy and angular distributions) in addition to Γ can be measured very precisely, based on high statistics.

The **nonmesonic decay mechanism** of hypernuclei has yet to be revealed. There exists a discrepancy between theory and experiment on the decay branching ratios in nonmesonic process. However, available data seem poor in quality. Recently, new observables, the asymmetry of nonmesonic decay has been measured. A further accumulation of data with better quality is necessary. Precise measurements of the decay observables will improve the situation.

Mesonic decay in heavy hypernuclei is sensitive to pion propagation in the nucleus, which reflects the dynamics of hadrons in the nuclear medium. **Exotic decay**, such as positive pion emission, is interesting since it is sensitive to the $\Lambda\Sigma$ mixing effect. The sensitivity for the branching ratios of these decays will be as high as $\mathbf{10^{-3}}$ in the present beam line.

Various contributions to the weak decay mechanism will be clarified through the high-statistics, high-sensitivity hypernuclear decay spectroscopy.

The **hypernuclear magnetic moment** is quite sensitive to the details of the hyperon-nucleon interaction in the nuclear medium. Particularly, the isospin dependence is interesting since it would reflect the structure of the exchange current, *e.g.*, the contributions of kaon exchange and/or Σ excitation. It has been an ambitious dream to measure the hypernuclear magnetic moment. This dream may come true at the present facility.

Appendix A: Brief Description on Hypernuclear Spectroscopy with SKS

Recent progress on hypernuclear investigations provided by the super-conducting kaon spectrometer SKS shows importance of high-precision spectroscopy for hypernuclear physics. Here, we describe briefly what we learned with SKS.

First, the single-particle nature of Λ hypernuclei was clearly shown by Λ-major shell structures measured by the (π^+, K^+) reactions. A series of Λ-major shell orbital states from the ground to highly-excited states were clearly observed even in heavy hypernuclei of the mass number up to 208, owing not only to the selectivity of the (π^+, K^+) reaction but also to the high resolution. Observed Λ-major shell orbital states in ${}^{89}_{\Lambda}$Y were found to be decomposed into two peaks (Fig. 48-right). These states were first claimed to be Λ spin-orbit splitting states This result seemed to indicate the large spin-orbit term in Λ-single particle potential, in contrary to the other suggestion in light hypernuclear system where small ΛN spin-orbit interaction is favored. The configuration of the observed states is still unclear since significant contribution from hole states of the core nucleus has to be taken into account.

Second, SKS found unique quantum states in hypernuclei. Supersymmetric states were observed in ${}^{9}_{\Lambda}$Be, in which a Λ hyperon can occupied a unique orbital configuration since Λ is free from Pauli exclusion principle of the nucleon. A discovery of core-excited states in ${}^{12}_{\Lambda}$C was surprisingly provided since their excitation energies were never reproduced with a naive picture of a Λ coupled to core-^{11}C excited states (Fig. 48-left). A unique adea of configuration-mixed states is proposed to solve the problem. The mode allows a mixture of different Λ-major orbital states coupled to core-^{11}C excited states.

Appendix B: High-Resolution GeV-Pion Beam line

The main proton synchrotron of the Japan Hadron Facility (JHF) will deliver a high-power beam of 50 GeV and 15 μA. By taking advantage of the low-emittance primary beam (4.1π mm·mrad), a **High-Intensity, High-Resolution GeV-Pion Beam Line** can be

designed.The beam line will provide a pion intensity as high as $\mathbf{10}^9$ per second and a momentum resolution as good as $\mathbf{10}^{-4}$, which are respectively 1000-times more and 10-times better than those realized at K6 of the KEK 12-GeV PS [8]

The present beam-line facility will enable us to increase the production rate of hypernuclei drastically, and will provide us a so-called hypernuclear factory with the (π, K^+) reaction. The (π, K^+) reaction has unique features; 1)it favors to populate stretched states, 2)can produce polarized hypernuclei, and 3)is a background-free reaction. The (π, K^+) reaction plays a complementary role on the hypernuclear study to the (K^-, π) reaction. Thus, the pion beam line should be constructed. Utilizing the present facility, next-generation hypernuclear studies with high precision will be proceeded at JHF, where **high resolution, high statistics, and high sensitivity** will be key issues.

A layout of the proposed beam line is illustrated in Fig. 49, together with a kaon spectrometer. The beam line consists of two halves. The first half is from PP to MS and for separating pions from the other secondary particles with an electrostatic separator. Since no tracking devices are available, due to the high counting rate, the beam momentum must be determined by measuring the reaction point where the beam position is strongly correlated with its momentum. Thus, the second half is from MS to FF and for making the beam dispersive vertically at FF. The dispersion and vertical magnification at FF are to be $\mathbf{\sim 10cm/\%}$ and $\mathbf{-0.4}$, respectively. A momentum resolution of $\mathbf{10}^{-4}$ can be achieved when the source size (production target) is smaller than 2.5mm.

The total length and acceptance of the beam line are **35m** and **4msr·%**. According to the Sanford-Wang formula [9] the π^+ intensity is estimated to be more than $\mathbf{10}^9$ per second with a platinum production target 6cm long.

The kaon spectrometer in the figure is designed to be a resolution as good as $\mathbf{10}^{-4}$ to match with the pion beam line. This is obviously optimized for the resolution, compromising with the acceptance and kaon survival rate. The specifications of the kaon spectrometer should be changed, if necessary, so that the resolution, acceptance, maximum central momentum, total length, cost, and so on, will have to meet experimental requests.

The design concept of the kaon spectrometer is summarized as follows.

1. The kaon momentum is determined by the hit position at the focal plane. The resolution is almost determined by the horizontal beam size at the experimental target.

2. The vertical vertex point can be reconstructed from the vertical position and divergence at the focal plane. The vertex resolution of less than 1mm is thus required so that the beam momentum resolution is to be 10^{-4}, which is predominantly determined by the primary beam size at the production target.

3. Satisfying items 1 and 2, we could remove any vertex detectors at around the target, where the counting rate is expected to be too high to drive counters.

We could design a kaon spectrometer to meet above conditions. The horizontal magnification and dispersion are –0.851 and 8.327 cm/%, respectively. The vertical magnification ($R33$) is –3.08. Since the spectrometer has a vertical focus, the vertex resolution is determined by Y_O=$Y_I/R33\sim$0.5mm/3.08$\sim$0.16mm$\ll$1mm, where Y_O and Y_I represent the vertex resolution (object size) and position resolution (image size) at the focal plane, respectively.

Specifications of the pion beam line and kaon spectrometer are summarized in Table 6.

Table 6: Specifications of the pion beam line and kaon spectrometer. [a] Corrections for higher order aberrations are required.

	π Beam Line	K Spectrometer
Max. Central Momentum(GeV/c)	1.5	1.5
Total Length(m)	34.738	12.4
Horizontal Acceptance(mrad)	$\pm$50	$\pm$100
Vertical Acceptance(mrad)	$\pm$10	$\pm$40
Momentum acceptance(%)	$\pm$1	$\pm$5
Horizontal Magnification	0.773	–0.851
Vertical Magnification	–0.409	–3.084
Dispersion(cm/%)	10.614	8.327
Momentum Resolution($\Delta P/P$)	10^{-4}	10^{-4} [a]

References

[1] H. Noumi, Nucl. Phys. **A639**, 117c(1998).

[2] H. Hotchi, Doctor Thesis, University of Tokyo, (2000).

[3] T. Motoba, H. Bandō, R. Wünsch, and J. Žofka, Phys. Rev. **C38**, 1322(1988).

[4] T. Hasegawa *et al.*, Phys. Rev. Lett. **74**, 224(1995).

[5] T. Motoba, Nucl. Phys. **A639**, 135c(1998).

[6] D. E. Lanskoy, Nucl. Phys. **A639**, 157c(1998).

[7] S. Tadokoro and Y. Akaishi, Phys. Lett. **B282**, 19(1992).

[8] The K6-SKS spectrometer system has realized about 50 events of the ${}^{12}_{\Lambda}$C(g.s.) production per hour with a graphite target 1.8g/cm^2 thick.

[9] J. R. Sanford and C. L. Wang, BNL 11279 and BNL 11479 (1967); C. L. Wang, Phys. Rev. Lett., **25**, 1068 (1970).

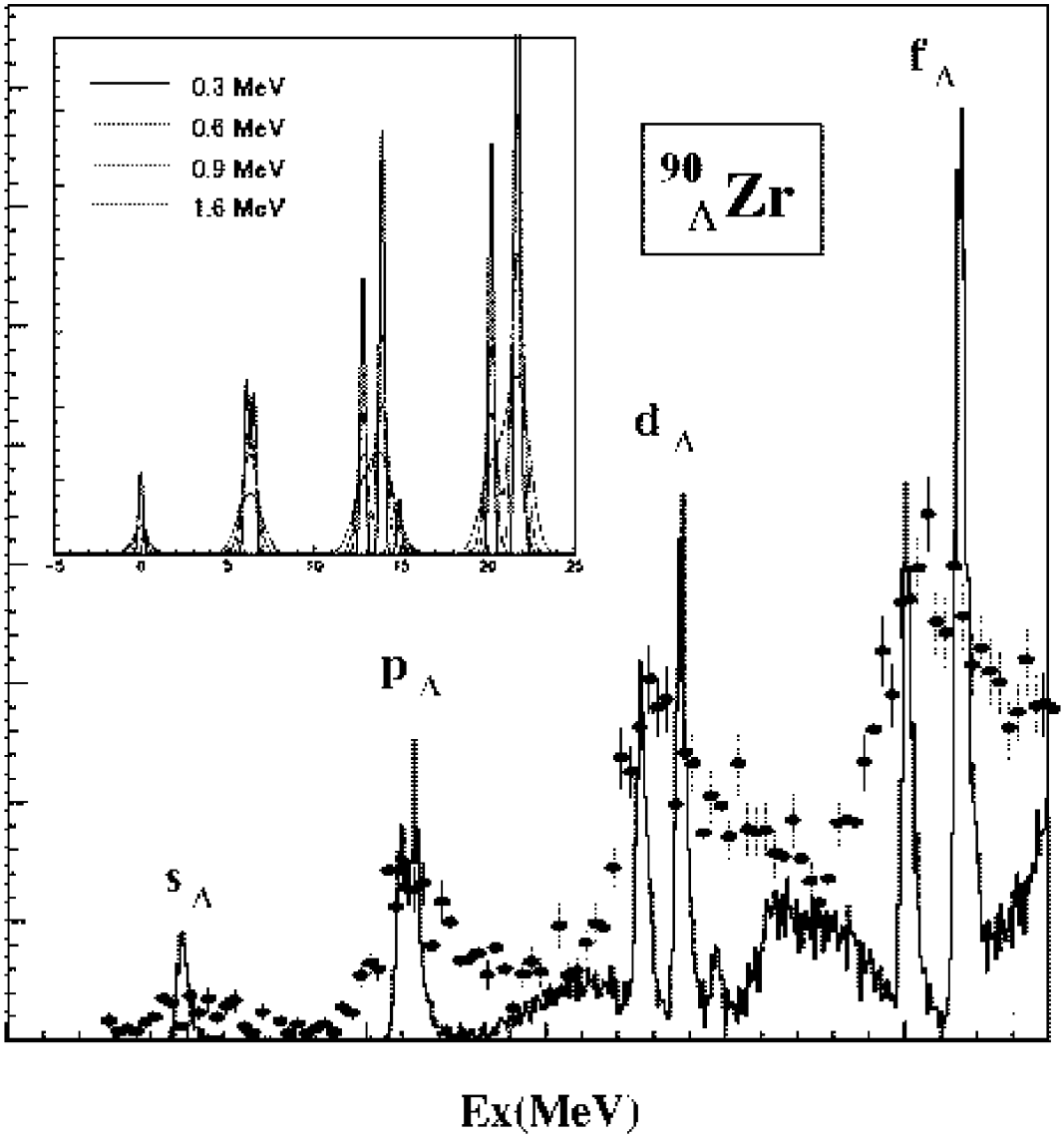

Figure 44: Simulated excitation energy spectrum for ${}^{90}_{\Lambda}$Zr (histogram), together with the measured spectrum for ${}^{89}_{\Lambda}$Y(plot with closed circles). More realistic simulation was made with the Zr target of 1mm thichness, assuming the beam line and spectrometer resolution of 10^{-4} each. Change of the spectrum shape with respect to the energy resolution is also displayed at the up-left corner.

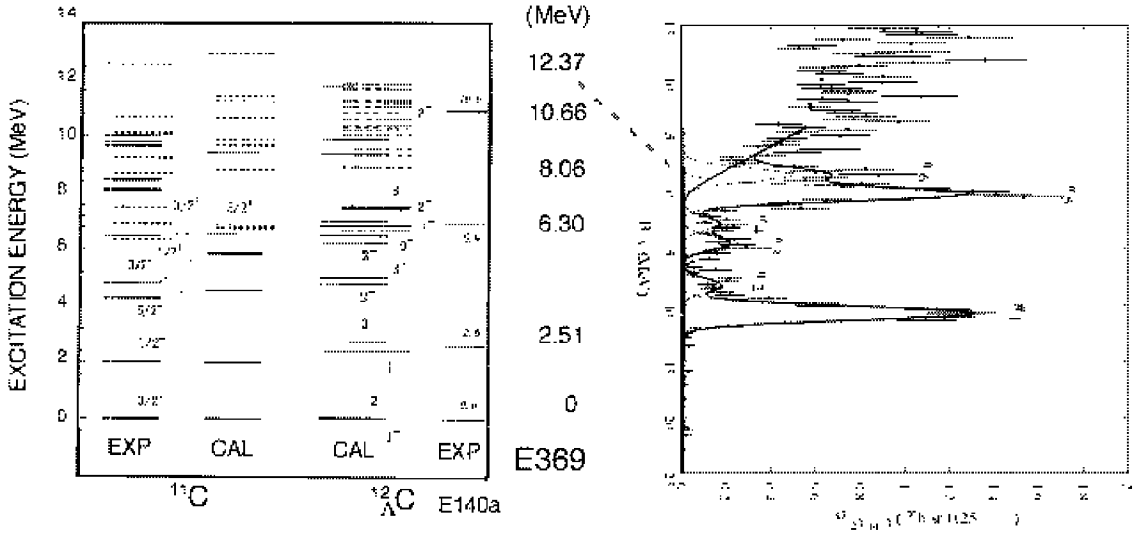

Figure 45: $^{12}_{\Lambda}$C level scheme calculated with an extended model of inter-shell mixed configuration, shown together with the measured spectrum.

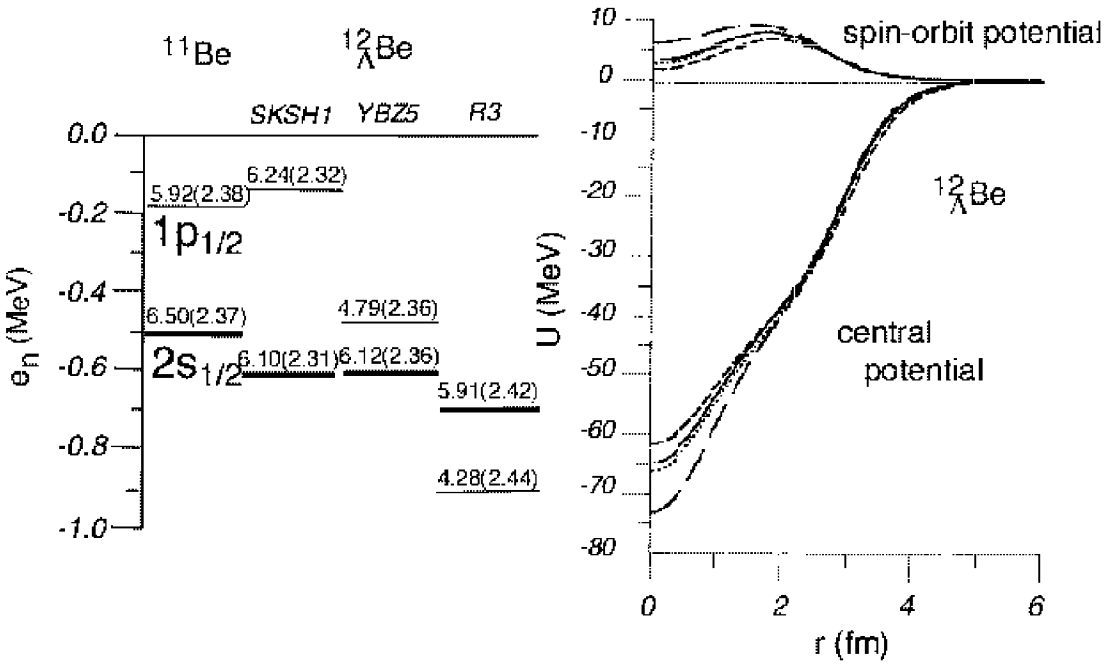

Figure 46: Neutron-single particle energy (left) and potentials (right) calculated with three different sets of ΛN interaction presented by D. E. Lanskoy [6].

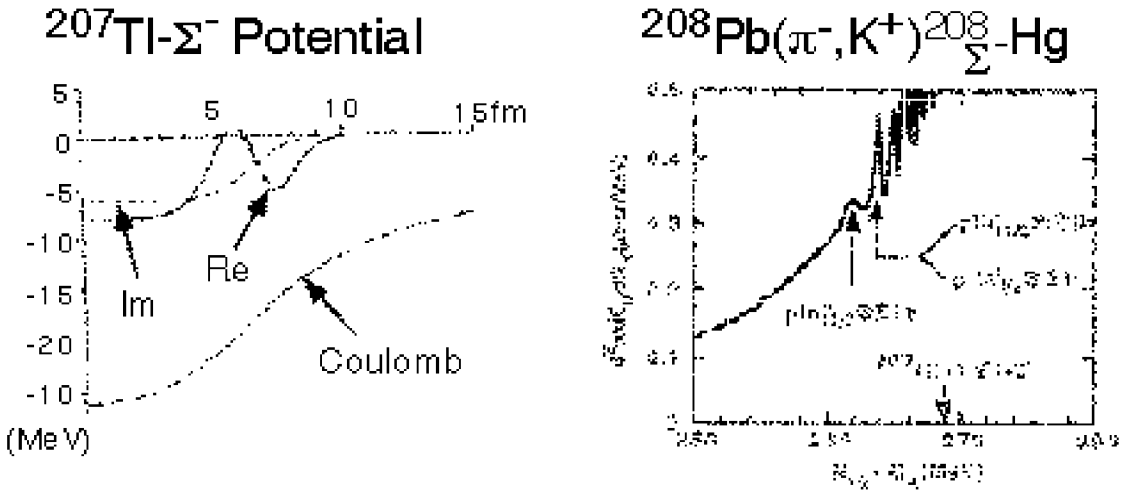

Figure 47: (left) Calculated Σ-Tl potential and (right) $^{208}_{\Sigma^-}$Hg spectrum produced by the (π^-, K^+) reaction.

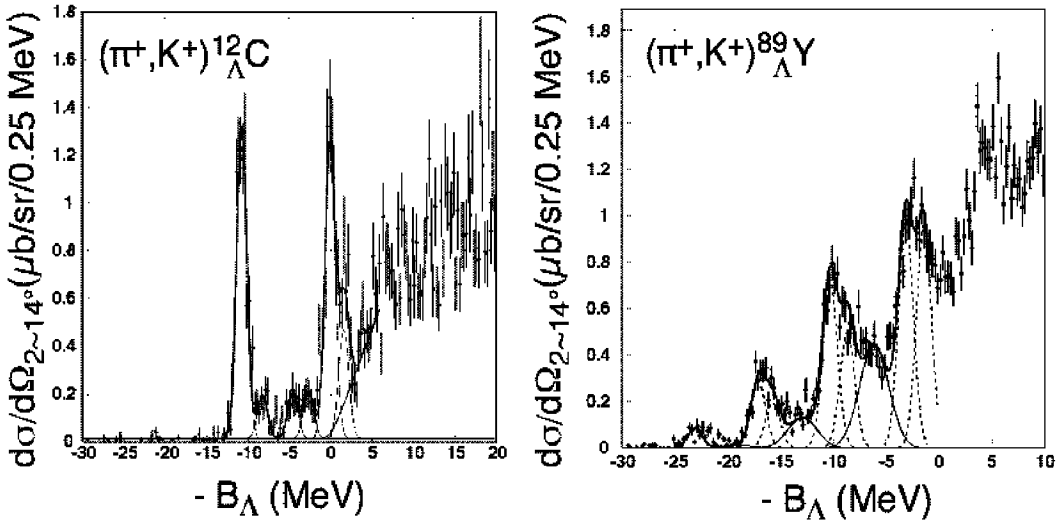

Figure 48: $^{12}_{\Lambda}$C (left) and $^{89}_{\Lambda}$Y (right) spectra produced by the (π^+, K^+) reactions, observed with SKS.

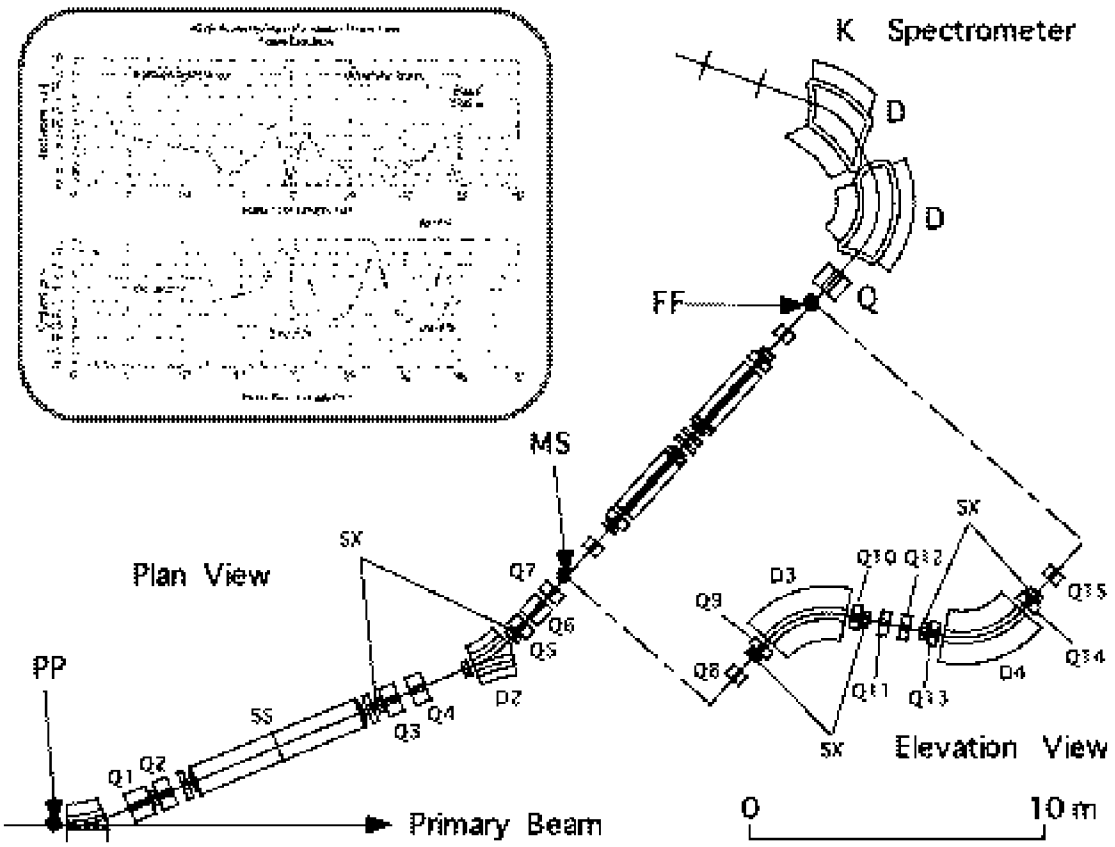

Figure 49: High-intensity, high-resolution pion beam line and kaon spectrometer.

6 Study of Dense Nuclear Matter with Strangeness

T. Kishimoto
Osaka University, Japan
H. Noumi
KEK, Tsukuba, Ibaraki 305-0801, Japan

6.1 Strangeness for high density nuclear matter

Nuclei are made up of nucleons by the strong interaction. The strong interaction among quarks is well described by QCD although the strong interaction between hadrons are so complex that one is forced to use effective theories. The effective theories, however, reproduce well properties of nuclei with reasonable precision. The effective nucleon-nucleon (NN) interaction has been constructed by NN scattering data with theoretical models which extrapolate the NN interaction in free space to that in nuclei. There are many models of effective NN interaction based on meson exchange model.

Recently high density nuclear matter is under intense discussion due primarily to current interest to neutron stars. The neutron stars have the highest baryon density in nature and they are in an almost lowest energy state. We do not know whether it is baryon matter, meson baryon matter or quark matter although it is believed that strangeness is playing a vital role. Strangeness has quite unique feature because of its marginal mass of s-quark. Fermi energy becomes compatible to the mass difference between strange- and non-strange particles at high density where strange particles start to appear. The density is strongly affected by their mutual interaction and its density dependence.

Precise knowledge of the hyperon-nucleon (YN) and kaon-nucleon (KN) interaction at the normal nuclear density is a key to know the equation of state (EOS) at high density. Hypernuclei have strange hyperons in a nucleus. They are therefore primary source of the interaction. However, only Λ hypernuclei are studied in detail. It is argued that Σ-nucleon interaction is of particular importance in the neutron star because Σ^- is the lightest negatively charged baryon which reduces degeneracy pressure of electrons. The Σ hypernuclei are ideal source of information on the ΣN interaction although little has been known experimentally.

The KN interaction is of another primarily importance. If it turns out to be strongly attractive as suggested by many theories, Bose-Einstein condensation of kaon (so-called kaon condensation) may take place in neutron stars. It is particularly important to study kaonic nuclei which directly gives us KN interaction. In this letter of intent we propose series of experiments to study KN and ΣN interactions by using low energy kaon beams.

6.2 Kaonic nuclei and Kaon Condensation in neutron stars

The KN interaction at low energy region is particularly important nowadays because of the current interest in neutron stars where the so-called kaon condensed state may be achieved by a strong attractive interaction [1, 2]. The existence of the kaon condensed state softens the EOS of nuclear matter in the neutron stars and reduces their calculated maximum mass above which the neutron stars become black holes. The observed mass distribution of the neutron stars agrees with the calculation with this softening [3]. The introduction of strange hyperons in the EOS gives a similar softening. Hyperons may also play a vital role although quantitative understanding of the EOS requires a knowledge of both the KN and YN interactions at high density [4]. The KN interaction, in particular, is known much less than YN interaction.

Recently, effective kaon mass in dense nuclear matter has been derived by the Chiral SU(3) effective Lagrangian including $\bar{K}N$, $\pi\Sigma$, $\pi\Lambda$ systems[5]. Such a theoretical model reproduces well the $\Lambda(1405)$ as a $\bar{K}N$ bound state due to the strong $\bar{K}N$ attractive interaction [5, 6]. The $\bar{K}N$ interaction makes the K^- feel a strong attractive potential in nuclei which consequently leads to the existence of deeply bound kaonic nuclei. The $\Lambda(1405)$, however, can also be interpreted as a three-quark state with $\ell = 1$ excitation. In this case no attractive $\bar{K}N$ interaction is relevant and the deeply bound kaonic nuclei do not necessary exist.

Experimental data of K^- optical potential mostly come from kaonic atoms. Recent extensive analysis of kaonic X-ray data concludes that the potential is strongly attractive [7]. The derived depth is around -200 MeV which opens a possibility of kaon condensation at around three times normal nuclear density. Derivation of the optical potential from the kaonic atom data is, however, subtle since the atomic state is sensitive only to the phase shift of K^- wave function at the nuclear surface. The phase shift alone cannot determine the depth of the potential since the K^- wave function has an ambiguity in number of nodes in the nucleus especially when the potential depth is quite deep. The strong imaginary part of the potential further obscures the nodes. Earlier studies with a different treatment of the nuclear surface gave much shallower potentials of -80 to -90 MeV [7] which tend to exclude the kaon condensation in the neutron stars.

If $\bar{K}$-nuclear potential is as attractive as derived from the kaonic atom studies suggest [7], then deeply-bound kaonic nuclei should exist. The observation of kaonic nuclei gives directly the K^- optical potential and gives decisive information on the existence of kaon condensation in neutron stars. We show the general properties of the kaonic nuclei and that the (K^-, N) reaction can excite them with cross section experimentally measurable.

The lowest energy state of the kaonic nuclei appears at around $\frac{3}{2}\hbar\omega_K - V_0$ MeV. If the

potential is as deep as -200 MeV as suggested by kaonic atom, naive argument gives the $\hbar\omega = \sqrt{8}40A^{-1/3}$ reflecting facts that the potential depth is 4 times deeper and nucleon mass is 2 times heavier than kaon. The $1s$ state of ${}^{28}_{K}$Si appears at around -140 MeV bound which the deepest bound state ever observed in nuclear physics. The width is estimated as narrow as around 10 MeV [5, 7]. The narrow width is understandable since dominant conversion channels like $KN \to \pi\Sigma$ or $KN \to \pi\Lambda$ are energetically almost closed. It is likely that the estimate has an error for such a deeply bound kaonic state which is also highly excited as a hyperon and nucleon state. Even a couple of times wider $1s$ state should be seen well separated since the next excited state ($1p$) is expected to appear 40 MeV higher.

The (K^-, N) reaction where a nucleon (N) is either a proton or a neutron is shown schematically in Fig. 50. The nucleon is knocked out in the forward direction leaving a kaon scattered backward in the vertex where the $K + N \to K + N$ takes place. This reaction can thus provide a virtual K^- or $\bar{K}^0$ beam which excites kaonic nuclei. This feature is quite different from other strangeness transfer reactions like (K^-, π), $(\pi^\pm, K^+)$ and (γ, K^+) extensively used so far. They primarily produce hyperons and thus are sensitive to states mostly composed of a hyperon and a nucleus.

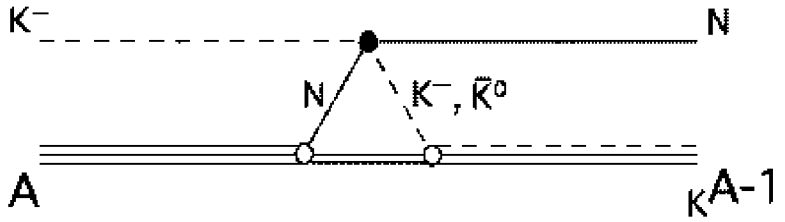

Figure 50: Diagram for the formation of kaonic nuclei via the (K^-, N) reaction. The kaon, the nucleon, and the nucleus are denoted by the dashed, thin solid and multiple lines, respectively. The kaonic nucleus is denoted by the multiple lines with the dashed line. The filled circle is the $KN \to KN$ amplitude while the open circles are the nuclear vertices. The bubbles represent distortion.

The momentum transfer, which characterizes the reaction, is shown in Fig. 51. We are interested in states well bound in a nucleus (BE = 100 ~150 MeV). The momentum transfer for the states is fairly large ($q = 0.3 \sim 0.4$ GeV/c) and depends little on the incident kaon momentum for $P_K = 0.5 \sim 1.5$ GeV/c, where intense kaon beams are available. The momentum transfer a little beyond the Fermi momentum makes the reaction similar to the (π^+, K^+) reaction for hypernuclear production where so-called stretched states are preferentially excited [13].

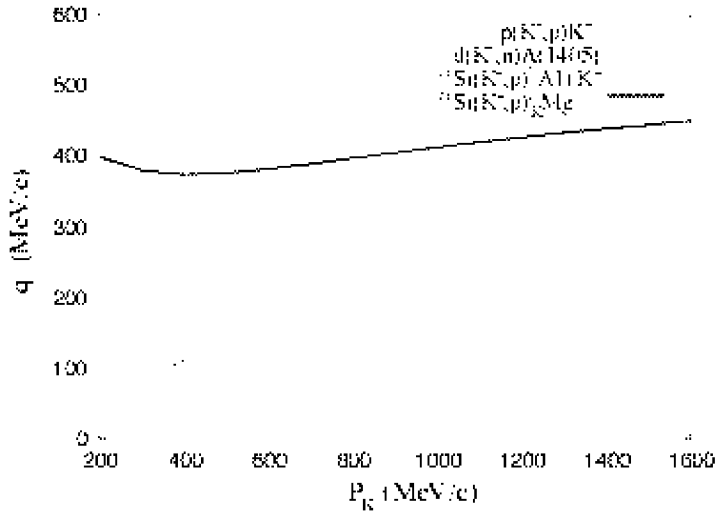

Figure 51: The momentum transfer of the (K^-, N) reaction at 0 degrees is shown for four reactions. Here binding energy of kaonic nucleus $^{27}_{K}$Mg is taken to be -150 MeV.

The (K^-, N) reaction on deuteron studies the $\bar{K}N$ component of excited hyperons. The $d(K^-, p)$ reaction excites K^-n states which can only have $I = 1$. On the other hand $d(K^-, n)$ reaction excites a K^-p state which can have either $I = 1$ or $I = 0$. Cross sections to the excited hyperons depend on their $\bar{K}N$ component. For instance, the well known $\Lambda(1405$ MeV) should be abundantly excited by the (K^-, n) reaction if it is a $\bar{K}N$ bound state with $I = 0$ as usually believed. The $d(K^-, p)$ reaction, in particular, gives information on the K^-n interaction below the threshold, which plays a decisive role on the kaon condensation in the neutron stars.

The cross section was estimated by the distorted wave impulse approximation (DWIA). The cross section of the elementary reaction was given by the phase shift analysis of available data[15]. The c.m. (center-of-mass) differential cross section of the $K^-n \to K^-n$, $K^-p \to K^-p$ and $K^-p \to \bar{K}^0n$ reactions at 180° are shown in Fig. 52 as a function of incident kaon momentum. For instance, the $K^-p \to K^-p$ reaction has a peak at around 1 GeV/c. We take 1 GeV/c for the incident kaon momentum. Since the target nucleon is moving in a nucleus, Fermi averaging has to be made for the two body cross section which smears the fine momentum dependence. The c.m. cross section is reduced by 20 to 30 % depending on models for this averaging. We take ∼1.3 mb/sr as the c.m. cross section at 1 GeV/c. The calculated cross section for the kaonic nuclear $1s$ states are shown in table 7. Here we take ^{12}C and ^{28}Si for the present study.

The calculated cross sections turn out to be fairly large which can compensate for a

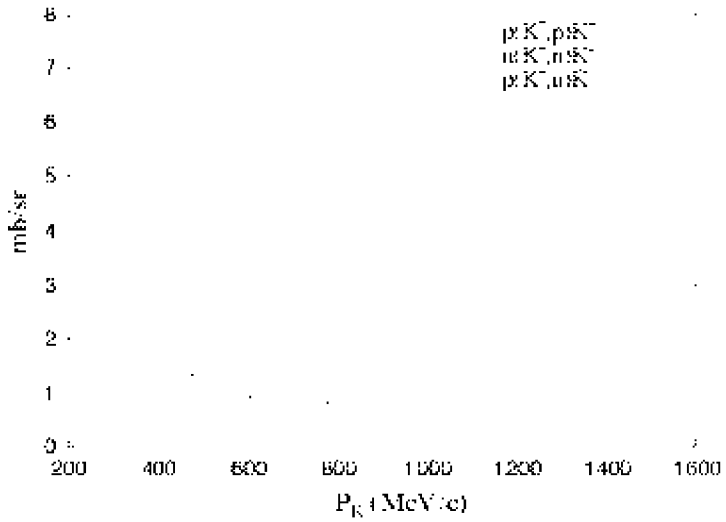

Figure 52: The c.m. differential cross sections of the three reactions are shown as a function of incident kaon lab momentum.

nucleus	N_{eff}^{pw}	D_{eik}	$d\sigma/d\Omega$ μb/sr
^{12}C	0.055$\sim$0.26	0.25	100$\sim$490
^{28}Si	0.029$\sim$0.15	0.16	35$\sim$180

Table 7: Calculated laboratory differential cross sections of the $1s$ states excited by the (K^-, p) reactions at P_K=1 GeV/c for the ^{12}C and ^{28}Si targets. Range of values corresponds to the b parameter (see text).

low intensity kaon beam. Backgrounds may obscure the clear observation of kaonic nuclei. Nucleons from knock-out reactions are not a problem since the nucleons associated with the deeply-bound kaonic nuclei are much more energetic. Kaon absorption by two nucleons in nuclei can generate energetic nucleons. The process has to involve another nucleon in addition to the (K^-, N) reaction. Thus one expects the process gives smaller cross section than that of the (K^-, N) reaction. The process can be interpreted as a spreading width of the kaonic nuclei. A Λ produced in the forward direction by the quasifree (K^-, π) reaction provides an energetic nucleon. It would not be a serious background since no peak structure is expected.

Backgrounds and signals are further separated by observing incident momentum dependence of the cross section. We would like to measure the (K^-, N) reaction at 1.0, 1.2 and 1.5 GeV/c. The low cross sections at 1.2 and 1.5 GeV/c require intense kaon beam. The (K^-, p) and (K^-, n) reactions are ideal for the study of the kaonic nuclei. A study of the reaction

requires intense low energy kaon beam for which 50 GeV JHF is particularly suitable.

6.3 Hyperon-nucleon and hyperon-hyperon interactions

It is believed that hyperons become important in the high density matter where Fermi energy become compatible to the mass difference of hyperons and nucleons. The lightest hyperon is a Λ hyperon. A Λ is another type of neutron which has no Pauli blocking thus occupies the lowest energy level. Fortunately Λ N interaction is relatively well known at normal nuclear density since we have so many Λ hypernuclear data. The abundance of Λ at high density is derived by the theoretical density dependence with ΛN interaction. It is known that abundance of Λ is already appreciable at $\sim 3\rho_N$.

However, what is particularly important is the Σ^-N interaction. The Σ^- is the lightest negatively charged hyperon. The degeneracy pressure of electrons suppress strongly the existence of protons in the neutron star. Existence of negatively charge particle allow the existence of protons. The increase of proton abundance could compensate the mass difference of Σ^- and Λ. This situation can be found in a chemical potential of charged particles.

The Σ^-N interaction is unfortunately not so well known. The only Σ hypernuclei observed so far is ${}^{4}_{\Sigma}$He. Bound state is observed in T=1/2 channel which suggests slightly attractive interaction for T=1/2 channel. The strong isopsin dependent interaction (Lane term) makes the ${}^{4}_{\Sigma}$He (T=1/2 state) exist. On the other hand no bound T=3/2 state is found so far. Studies of other Σ^- hypernuclei have been quite inconclusive due primarily to conversion process ($\Sigma N \to \Lambda N$) possible in a nucleus. We have little information of ΣN interaction which forbid us to predict the abundance of Σ hyperon in the neutron star. It has been pointed out that attraction by Coulomb interaction may make a bound state exist even the ΣN interaction is weak or even repulsive. Furthermore the repulsive nature of the interaction reduces the width of the state which makes the state seen easily. Observation of the so-called Coulomb assisted state will give us clear information of the ΣN interaction.

6.3.1 (K^-, π^+) reaction for the study of Coulomb associated Σ hypernuclei

In order to produce the Coulomb assisted state, it is essential to have reaction that has small momentum transfer. The (K^-, π^+) reaction is the unique reaction that can give zero momentum transfer at so-called magic momentum for Λ and Σ production. The magic momentum for the Σ is around $P_K = 400$ MeV/c. It is well known that such low momentum beam has difficulty to overcome the kaon decay in-flight. Beam line has to be as short as possible although certain length is needed to have separated beam. High intensity primarily beam available at JHF is thus essential particularly for such low momentum beam line.

6.4 Beam line and spectrometer

For the study of Σ hypernuclei we need to have low momentum, high intensity and high resolution beam line. The expected K^- beam intensity at JHF is around 10^4/sec at 500 MeV/c and 10^3/sec at 400 MeV/c if we are confined to conventional design of a beam line that has a length of $\sim$25 m. The beam intensity is not enough even at JHF for such a long beam line. We thus propose to have another beam line that is around 17 m in length and momentum resolution of the order of 1/1000. This design is challenging though a little shorter beam line was already proposed at Kaon Factory in Canada. Despite the difficulty of the design work a low momentum short beam line is relatively inexpensive. Furthermore we have the SPECII spectrometer which was used at CERN and just fits to the present purpose.

For the study of (K^-, N) reaction we use the beam line of K1.1 which is already proposed. Therefore we can start the experiment with little additional cost.

References

[1] D. B. Kaplan and A. E. Nelson, Phys. Lett., B175 (1986) 57

[2] G. E. Brown, Nucl Phys A574 (1994)217, G. E. Brown, M. Rho, Phys. Rep. 269 (1996) 333, C. H. Lee, Phys. Rep. 275 (1996) 255

[3] M. Prakash and J.M. Lattimer, Nucl.Phys. A639 (1998)433

[4] P. J. Ellis, R. Knorren, M. Prakash. Phys.Lett.B349 (1995)11

[5] T. Waas, N. Kaiser and W. Weise, Phys. Lett. B379 (1996) 34

[6] P. B. Siegel and W. Weise, Phys. Rev. C, 38 (1998)221

[7] C.J. Batty, E. Friedman, A. Gal. Physics Report 287 (1997) 385

[8] R. Barth at al., Phys. Rev. Lett. 78 4027 (1997)

[9] A. D. Martin, Nucl. Phys. B179 (1981) 33

[10] G.Q. Li, C.H. Lee, and G.E. Brown, Phys.Rev.Lett.79 5214 (1997); G.Q. Li, G.E. Brown, C.H. Lee, Phys.Rev.Lett.81 2177 (1998)

[11] A. Ramos and E. Oset, in Proceedings of XV Int. Conf. on Particles and Nuclei, Uppsala, Sweden, 1999 [Nucl. Phys. A (to be published)]

[12] M. Lutz, Phys. Lett. B 426, 12 (1998)

[13] C. B. Dover, L. Ludeking and G. E. Walker, Phys. Rev. C22 (1980) 2073

[14] T. Yamazaki, et al., Z Phys. A 355, (1996) 219

[15] Gopal et al., Nucl. Phys. B119 (1977) 362